Chapter-4

Synthesis & Application of Roof Shape secondary amines as CSA

Section 1
Effect of additional chirality on molecular recognition

Section 2
Electronic effects on chiral recognition

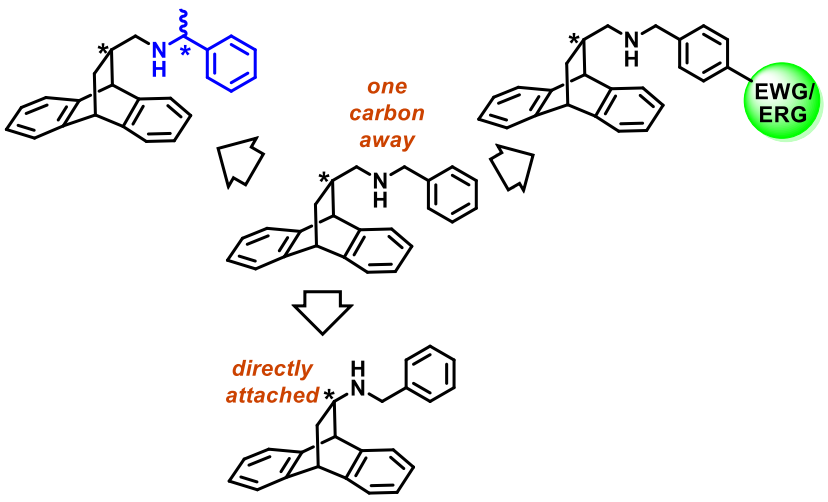

Section 3
Effect of distance of chiral center on chiral recognition

Table of Contents

4.1 Introduction:

Since the discovery of anthrancene in 1833, it has been utilized in a wide range of applications due to its ability to undergo Diels-Alder reaction with suitable dienophiles. Such [4+2] cycloadditions reactions between anthracene and various dienophiles lead to the formation of prototypical class of compounds which possess bulkiness and molecular rigidity due to its basic skeleton along with appropriate functional groups attached to the top ridge or bridge of the molecular architecture. The close resemblance of the shape of these molecules with the shape of a roof of a house has led to term this class of compounds as '*Roof shaped*' compounds. Such chiral molecules possessing unique shapes, sizes and functional groups have found a number of applications in diverse areas of modern chemistry, medicinal chemistry and material science. The relationship of their specific properties and chiral description has also been established by exhaustive study.

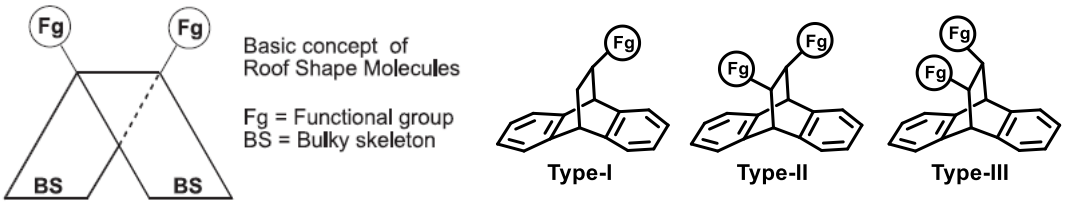

Figure 1 (a) Basic skeleton (b) classification of roof shape molecules

Various substituted roof shape compounds have been known to act as clathrate hosts and have been studied for their inclusion behavior.[1] It was found that the complex formation, stoichiometries and selectivities of the clathrates depend greatly on the structural features of the hosts including the number, nature, flexibility and the geometry of functional groups present. One such example is compound **1** which has been reported to form inclusion complexes with alcohols and acids.[2–5]

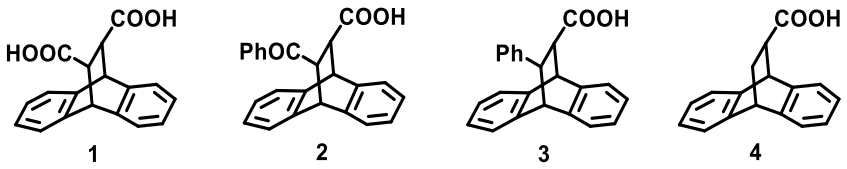

Figure 2 Various roof shape acids reported in literature

However, the retention of one of the –COOH group and modification or omission of the second group leads to the loss of symmetry in the molecule and hence changes their properties. This is demonstrated in **2** and **3**, which showed properties similar to the parent

compound **1**[6] but, an interesting observation was made for **4**. It was utilized for the separation of methanol from ethanol and other higher alcohols due to its selective ability to form inclusion complexes with methanol. Owing to its great applicability, the diacid **1** was optically resolved *via* diastereomeric salt formation with brucine[4] and later using optically active (*S*)-proline[7] giving rise to chiral versions of roof shape compounds.

Later, the diacid was also resolved successfully by crystallizing it with optically pure brucine from which a number of optically active bis-allylamides (Scheme 1) possessing a rigid molecular skeleton were synthesized and utilized as precursors for liquid chromatographic chiral stationary phases. [8,9]

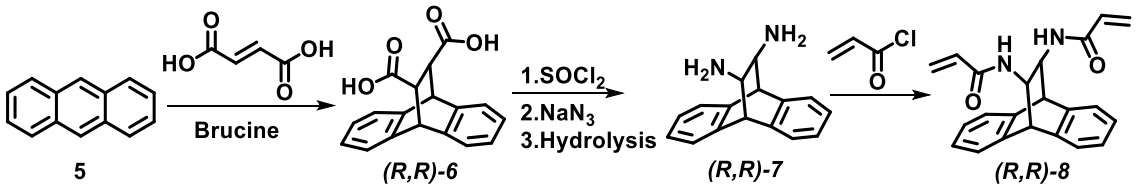

Scheme 1 Synthesis of chiral roof shape bis-allylamides

Roof shape molecules possessing diarylmethanol functional groups **(9-12)** comprising a characteristic rigid framework have been reported and studied as chiral hosts for their inclusion behavior (Figure 3).[10] The comparison between these derivatives revealed that the bi-methanols are largely superior to the mono-methanols, except for the 4-chlorophenyl substituted methanol, which has proved to have equal efficiency.[11] Hence, not only the nature of the functional group, but also the number of functional groups present were important factors affecting the applications of such molecules.

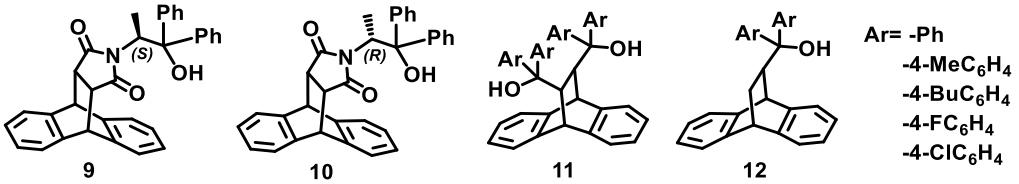

Figure 3 Roof shape diaryl methanol derivatives

Soldevilla *et al* later reported the asymmetric synthesis of roof shape compounds by employing chiral dienophiles. They studied the Diels–Alder reactions between chiral ester derived from acrylic acid and 3-hydroxy-4,4-dimethyl-1-phenyl-2-pyrrolidinone (chiral auxiliary) with anthracene, catalyzed by titanium tetrachloride in good *de*. LiOH-hydrolysis of the adducts derived from esters (*R*)- or (*S*)-**4** gave the corresponding enantiopure acids along with the complete recovery of chiral auxiliary (Scheme 2).[12]

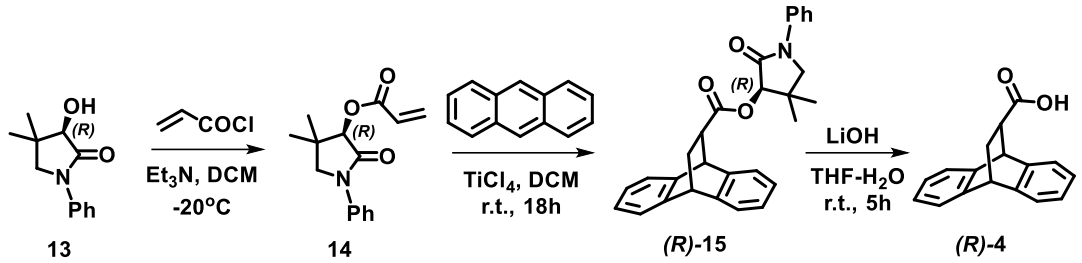

Scheme 2 Asymmetric synthesis of roof shape chiral aicd 4

Wandrey *et al* reduced the roof shape chiral diacid to obtain chiral bis-alcohol **(18)** (Scheme 3) and utilized it as a C_2-symmetric bifunctional ligand which can coordinate to metal atoms forming an effective catalyst system providing effective stereoselectivity. They utilized its complex with titanium for enantioselective addition of Et_2Zn to aldehydes giving excellent enantioselectivities.[13]

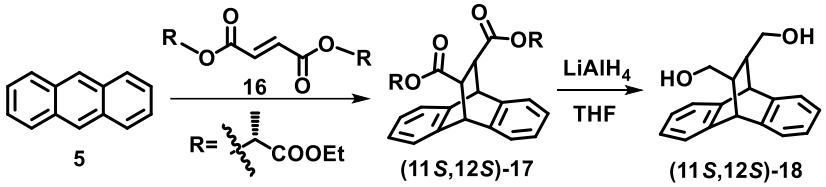

Scheme 3 Synthesis of chiral roof shape bis-alcohol

The *trans* roof shape diol was converted into corresponding diphosphine which was utilized as ligand forming complexes with various metal ions (Scheme 4). The Pd-complex of this ligand has been used for carbonylation of ethylene,[14,15] as well as asymmetric allylic alkylation of α-aryl ketones,[16] whereas its Rh(I) complex was used to carry out asymmetric hydrogenation of prochiral olefinic substrates.[17]

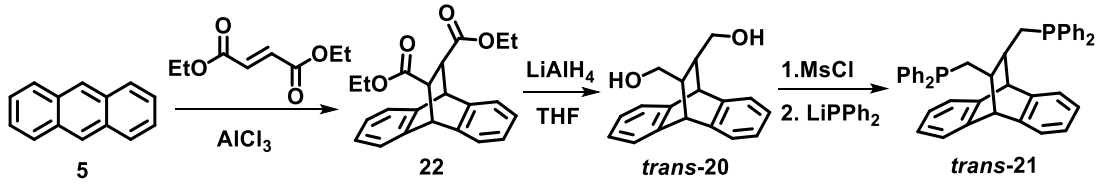

Scheme 4 Synthesis of roof shape *trans*-diphsphine

The chiral auxiliary approach was extended further to synthesize chiral roof shape diacids using chiral menthyl, isomenthyl and bornyl as the chiral auxiliaries. Chiral dienophiles were prepared from a series of acids which were used for asymmetric cycloadditions to anthracene giving high yields and *de* (Scheme 5). Acid catalyzed hydrolysis lead to accessing a valuable synthetic pathway to both enantiomers of the roof shape dicarboxylic acid.[18]

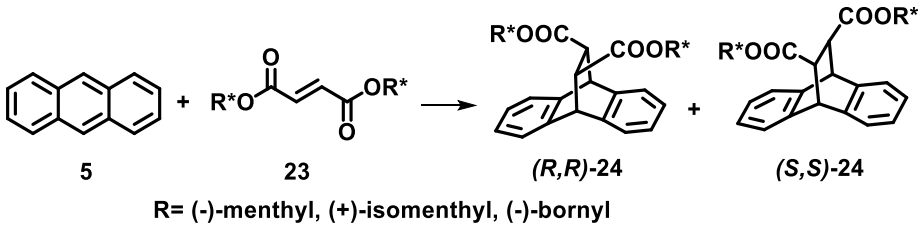

Scheme 5 Asymmetric synthesis of roof shape compounds

Later, fused heterocycles of roof shaped oxazolidinones **(28)** and imidazolidinones **(27)** were reported which were readily synthesized from the Diels-Alder reaction between anthracene and corresponding dienophiles **(25 & 26)** (Scheme 6). They have been utilized as chiral auxiliaries for asymmetric alkylation of amides. The advantage of such chiral derivatives for auxiliaries over the amino acid-derived heterocycles would be their high crystallinity and the steric congestions associated with the conformational rigidity.[19–22]

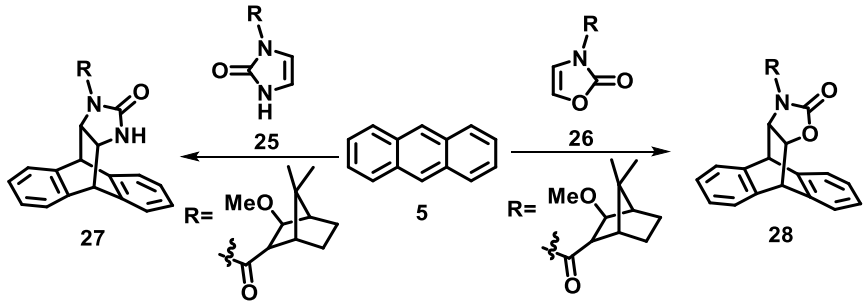

Scheme 6 Synthesis of roof shape oxazolodinones and imidazolidinones

A new class of artificial roof shaped chiral proline catalysts has been reported which was found to be more efficient than proline itself because of its rigid roof-shaped framework for the selective shielding of one side of a catalyst center (Scheme 7). It was utilized in asymmetric three component Mannich reaction giving 56-90% *ee* and yield 56-76%.[23]

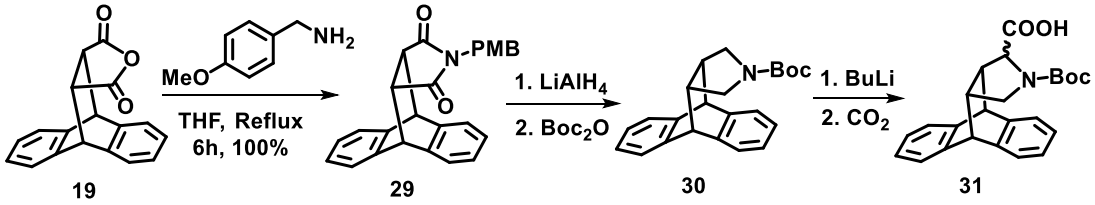

Scheme 7 Synthesis of roof shape proline derivative

Schiff base **(33** & **34)** derived from roof shape diamine unit **(32)** (Figure 4) have shown good reactivity and selectivity for asymmetric additions of isocyanoacetamides to aryl, heteroaryl, alkenyl, and alkyl aldehydes (88-98% *ee*) as compared to some well-established Schiff bases reported in literature.[24]

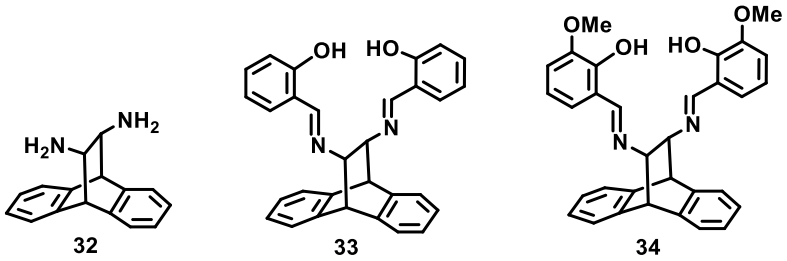

Figure 4 Schiff bases derived from roof shape diamine

Various 9-10-dihydroanthracene derivatives have been reported to possess biological activity and medicinal properties. Meprotiline **(35)** is known to show anti-MDR activity on cancer cell and *P. falciparum*;[25] **36** and **37** possess capabilities to reverse the chloroquine resistance in parasites isolated in vitro and in human malaria[26,27]; **38** and **39** were shown to possess anti-psychotic properties[28] while **40** and **41** were found to be 60 times more potent than Verapamil (Figure 5).[29]

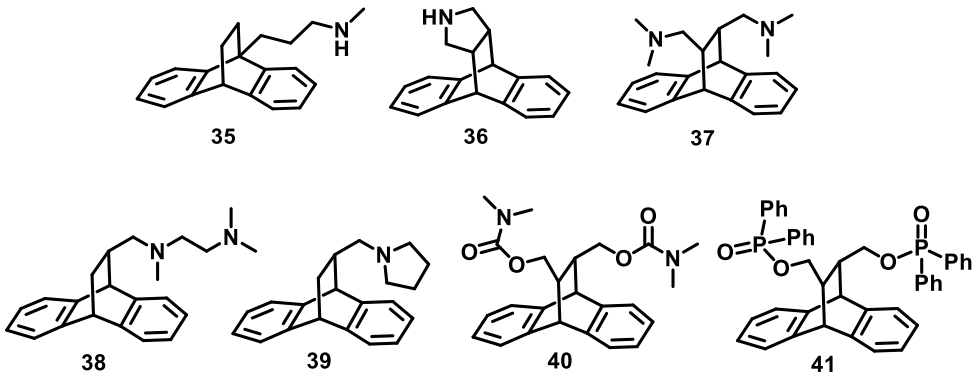

Figure 5 Some of roof shape molecules with application in medicinal chemistry

Earlier our group has reported the resolution of roof shape alcohols **42** & **43** and synthesized various chiral cyclic tertiary amines **44-47** (Figure 6).

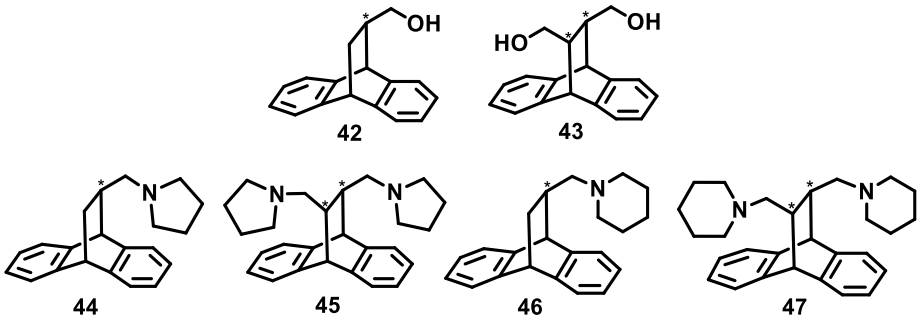

Figure 6 Roof shape chiral alcohols and amines

These cyclic tertiary amines **(44-47)** were scanned as chiral solvating agents for discrimination of the signals of some optically active compounds using NMR

spectroscopy.[30,31] The alcohol **23** was also used as chiral auxiliary for optical enrichment of α-halo acids (Scheme 8).[32]

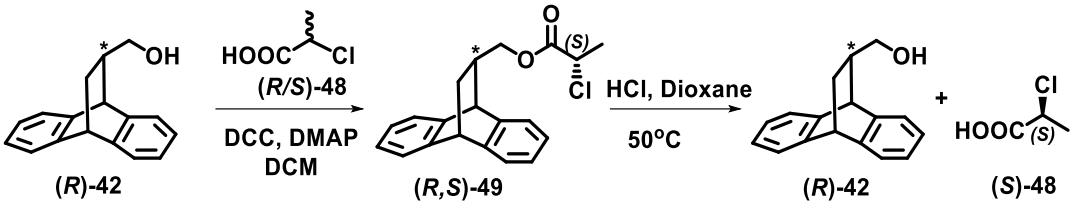

Scheme 8 Diastereoselective ester formation with α-chloro acid and its hydrolysis

4.2 Results and Discussion:

Since the introduction of roof shape molecules by Weber as a structurally diverse motif and its application as clathrate hosts showing inclusion properties, the application of such molecules in different areas ranging from medicinal chemistry to material science has been explored. Roof shape molecules possessing functional groups such as alcohol, amine, acid and acid derivatives have also found applications in medicinal chemistry,[27,29,33] as ligands in catalytic transformations,[34–37] as mediators in organocatalytic reactions[38] and in preparations of functional materials.[39] Our group has been actively involved in the synthesis of such molecules having a tertiary amine pendent group and used as chiral solvating agents for discrimination of the signals of some optically active compounds in NMR spectroscopy.[30,31] Some of these derivatives have also been used as a chiral auxiliary for asymmetric synthesis of α-halo acids.[32]

4.2.1 Roof shape secondary amines possessing additional chirality:

4.2.1.1 Synthesis of the ligands:

Our objective was to synthesize optically pure roof shape secondary amines and evaluate them as chiral solvating agents for the discrimination of signals of chiral acids by NMR spectroscopy. In designing the molecules, we have explored the effect of introducing another aromatic system by choosing to attach benzyl amine with the aim of adding an additional supramolecular interaction in the form of π-stacking.

With this aim, we synthesized the chiral alcohol utilizing the procedure reported in the literature starting from Diels-Alder reaction between anthracene and ethyl acrylate to build the roof shape ester **(50)** in racemic form. For the efficient resolution of this compound, we reduced the ester using $NaBH_4$ and iodine in THF to obtain racemic alcohol **(51)** which was subjected to kinetic resolution utilizing enzymatic transesterification to access optically pure roof shape alcohol **(*R*)-51** (Scheme 9). This enantiomerically pure roof shape alcohol **(*R*)-51** proved to be useful building block for the synthesis of roof shape amines. The ^{1}H NMR spectra for all the synthesized compounds were well in agreement with the reported chemical shift values. The absolute configuration of optically pure alcohol **(*R*)-51** was confirmed by recording its specific optical rotation and comparing it with the literature value. The optical purity of **(*R*)-51** was also confirmed to be >99% by subjecting it to chiral HPLC analysis. The chiral alcohol **(*R*)-51** accessed in the present work was then converted

to mono tosylate **(*R*)-53** derivative to make the nucleophilic attack facile. Further, **(*R*)-53** was then treated with benzyl amine to furnish chiral roof shape secondary amine **(*R*)-54** (Scheme 11). The formation of **(*R*)-54** was confirmed by ^{1}H NMR spectra, showing characteristic peaks of doublet at **δ** 4.38 and triplet at **δ** 4.28 corresponding to the bridge head protons. The benzylic protons appear as two doublets at **δ** 3.80 and 3.72 having a coupling constant of 13.2 Hz due to geminal coupling. A broad singlet at **δ** 2.35 corresponds to –NH proton. This was also confirmed by IR spectra which shows a single peak at 3065 cm^{-1} due to the N-H stretching frequency in secondary amines. The formation of the target molecule was confirmed by recording its HRMS which showed a molecular ion peak at 326.1898 which was comparable to the exact mass of **(*R*)-54**.

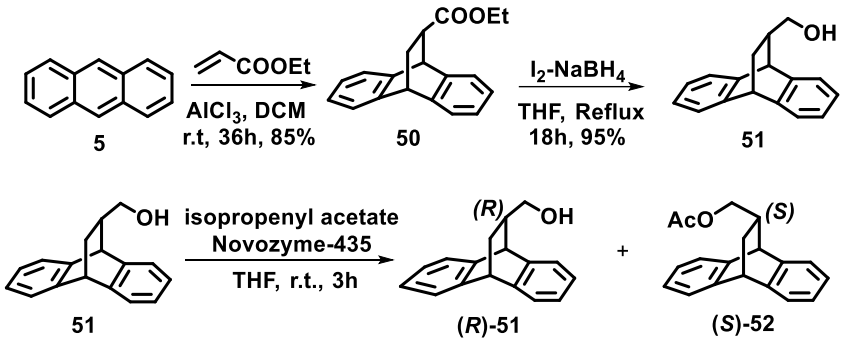

Scheme 9 Synthesis and resolution of roof shape alcohol

In order to study the match-mismatch effect by changing the orientation of the aromatic ring of benzyl amine unit, we further prepared two more derivatives by selecting two enantiomers of the chiral benzyl amine. Roof-shape amine **(*R,R*)-55** was prepared by using (*R*)-α-phenylethylamine, and its diastereomer **(*R,S*)-55** was obtained by using (*S*)-α-phenylethylamine using the same reaction conditions (Scheme 10).

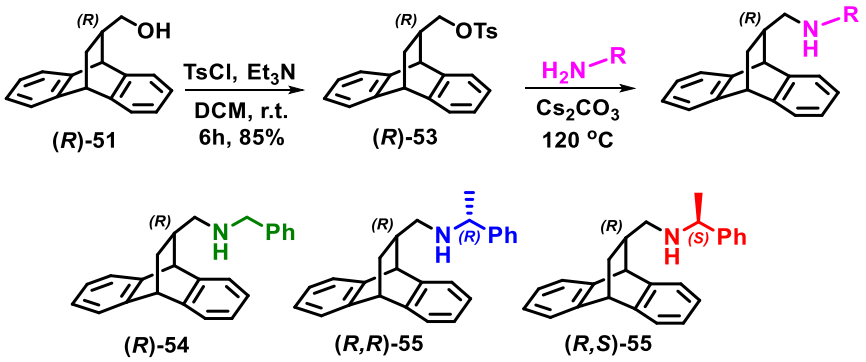

Scheme 10 Synthesis of roof shape chiral secondary amines

The ^{1}H NMR spectra for **(*R,R*)-55** and **(*R,S*)-55** were almost similar with only a minor difference in the chemical shift values for the protons associated with the chiral centers at the α-phenylethyl amine moiety. The proton at chiral centre appears as a quartet at **δ** 3.69 for **(*R,R*)-55** and at **δ** 3.66 for **(*R,S*)-55** whereas, the –C*H*$_3$ protons appear as a doublet at **δ** 1.37 and 1.08 for **(*R,R*)-55** and **(*R,S*)-55** respectively. One of the two aromatic rings of the rigid bicyclic roof shape portion of the CSA, second aromatic ring of the benzyl unit and the second chiral center should control the orientation of its diastereomeric complex with acidic analyte for effective chiral discrimination by molecular recognition.

4.2.1.2 Chiral recognition using NMR Spectroscopy:

Having prepared the three roof-shape secondary amines **(*R*)-54**, **(*R,R*)-55** and **(*R,S*)-55**, we examined different acidic substrates for a possible and detectable discrimination of the NMR signals. The molecular recognition study was conducted in $CDCl_3$ (400 MHz; 20 mM concentration; ratio of 1:1) with (*R/S*)-mandelic acid as the test substrate, targeting the CαH proton of Ph*C*H*(OH)COOH. For such study, the degree of induced chemical shift (Δδ) and nonequivalence (ΔΔδ) on the complex formation with CSA are measured. In this case, the signal of the Cα*H* proton shifted toward the upfield region in all three cases, while for **(*R*)-54** and **(*R,R*)-55** the signals also separated (Figure 7). However, in the case of **(*R,S*)-55** the signals did not resolve and both C$_\alpha$*H* protons of the diastereomeric salt appeared as a singlet (Figure 7 and Table 1, entry 1).

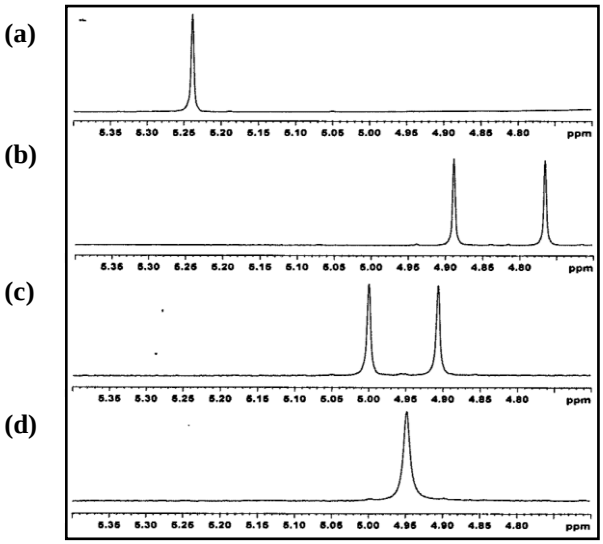

Figure 7 ^{1}H NMR Spectra of α-*H*: (a) (*R/S*)-mandelic acid (b) with **(*R*)-54** (c) with **(*R,R*)-55** (d) with **(*R,S*)-55**

In the case of α-chloropropanoic acid, all three roof-shape amines failed to distinguish the signals (entry 2, Table 1). We also examined derivatives of mandelic acid where the hydroxyl group was blocked by introducing suitable protecting groups. In the case of *O*-acetyl mandelic acid (Figure 8) and *O*-methyl mandelic acid (Figure 9), we observed a similar pattern of selectivity, although the chemical shift nonequivalence (ΔΔδ) was much reduced (entries 3 and 4, Table 1).

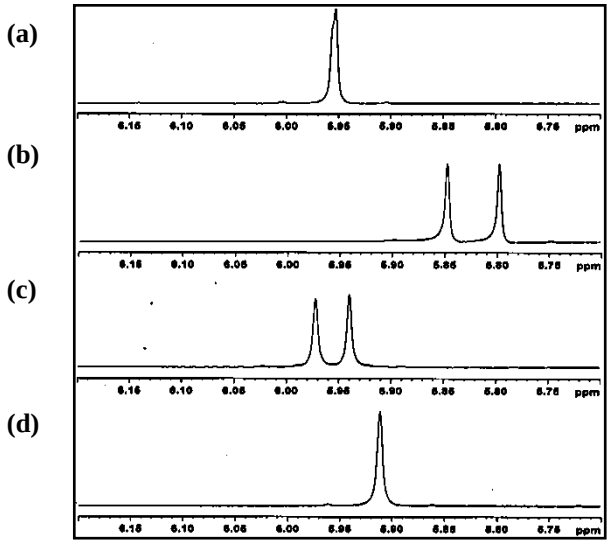

Figure 8 ^{1}H NMR Spectra of α-*H*: (a) (±) *O*-Acetyl mandelic acid (b) with **(*R*)-54** (c) with **(*R,R*)-55** (d) with **(*R,S*)-55**

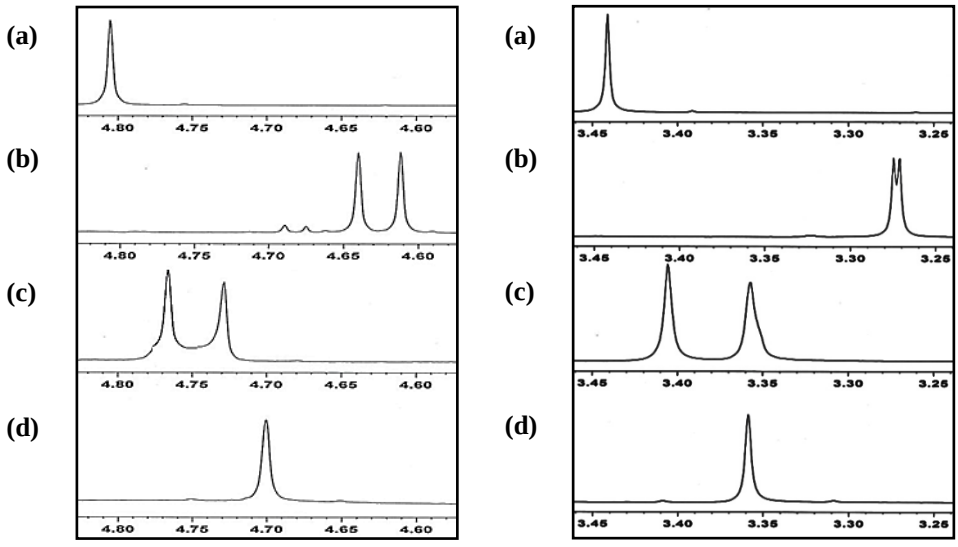

Figure 9 ^{1}H NMR Spectra showing CαC*H*$_3$ (right) and Cα*H* (left) of: (a) (±) *O*-Methyl mandelic acid (b) with **(*R*)-54** (c) with **(*R,R*)-55** (d) with **(*R,S*)-55**

Similar selectivity was seen in the case of α-bromo phenylacetic acid (Figure 10) contrary to α-chloropropanoic acid, indicating the supporting role of aromatic ring in the molecular recognition (entry 5, Table 1).

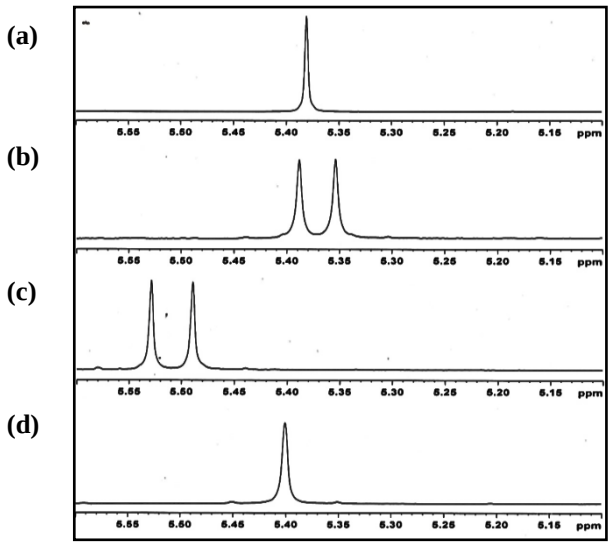

Figure 10 ^{1}H NMR Spectra of α-*H*: (a) (±)-α-Bromo phenylacetic acid (b) with **(*R*)-54** (c) with **(*R,R*)-55** (d) with **(*R,S*)-55**

It is often advantageous to analyze a sample by targeting more than one nuclei to confirm the optical purity. Application of ^{19}F NMR spectra for structural determination has distinct advantages of fewer and sharper peaks compared to ^{1}H NMR. We extended our study for 4-trifluoromethylmandelic acid and compared the separation of signals in ^{1}H NMR for the C*αH* and ^{19}F NMR for CF_3 group (Figure 11) (entry 6, Table 1).

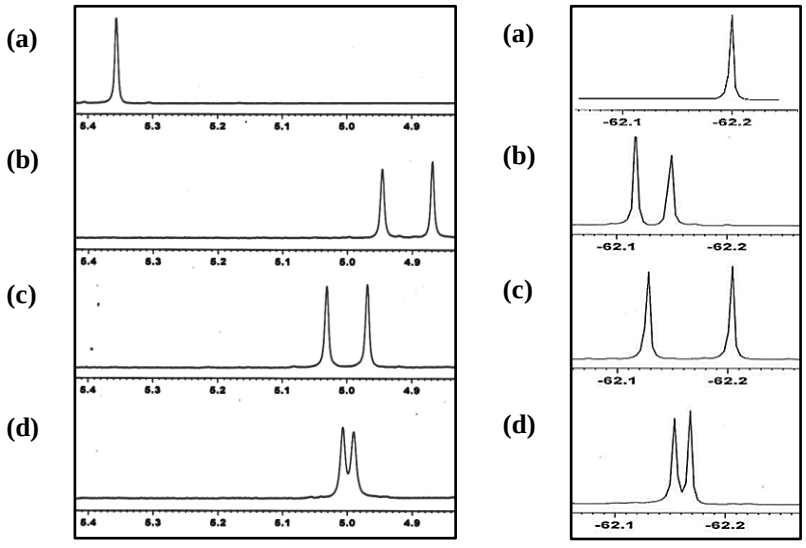

Figure 11 ^{1}H (left) & ^{19}F (right) NMR Spectra of: (a) (±) 4-Trifluoromethyl mandelic acid (b) with **(*R*)-54** (c) with **(*R,R*)-55** (d) with **(*R,S*)-55**

Although CSA **(*R*)-54** and **(*R,R*)-55** were almost equally effective where baseline separation of signals was observed, the CSA **(*R,S*)-55** showed relatively poor resolution.

Optically active natural and artificial amino acids have become an integral part of the design and synthesis of several biologically important molecules. Determination of optical purity of amino acids is becoming an important consideration. Recently, few chiral solvating agents have been studied to measure optical purity of amino acids by NMR analysis.[40,41] We also extended our study of the present CSAs to check the discrimination of the protons of the *N*-Ts derivative of phenyl glycine (entry 7, Table 1). In this case, the signals of the methyl group of *N*-Ts and $C_\alpha H$ showed discrimination in ^1H NMR analysis (Figure 12). Almost similar selectivity was seen, where CSA **(*R,S*)-55** showed comparatively poor separation of both these signals.

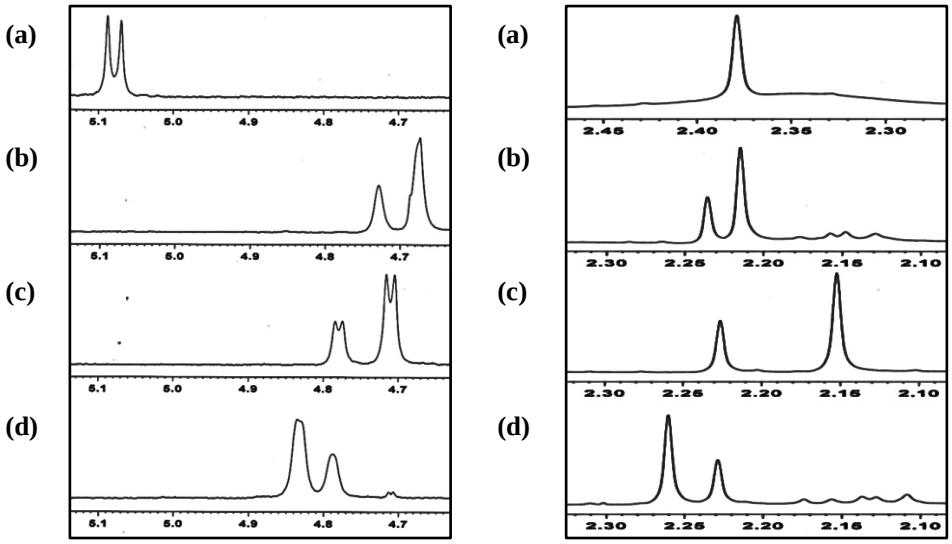

Figure 12 ^1H NMR Spectra of: (a) *N*-Tosylphenyl glycine (*R*:*S* 65:35) (b) with **(*R*)-54** (c) with **(*R,R*)-55** (d) with **(*R,S*)-55**

Next, we examined ibuprofen and naproxen, two commonly used nonsteroidal anti-inflammatory drugs as substrates. The CSA **(*R*)-54** and **(*R,R*)-55** showed the same ability to recognize the isomers of ibuprofen, but the other was quite less effective, while all the three proved incapable of showing separation of signals of naproxen (entries 8 and 9, Table 1). The present system was then examined for relatively bulky 2-hydroxy-3-methoxy-3,3-diphenylpropanoic acid, which is an intermediate for few pharmaceuticals. Signals of $C_\alpha H$ and $C_\beta OCH_3$ of this compound were seen to have been resolved due to the complex formation between this racemic acid and the **(*R,R*)-55**, more than the other two derivatives (entry 10, Table 1).

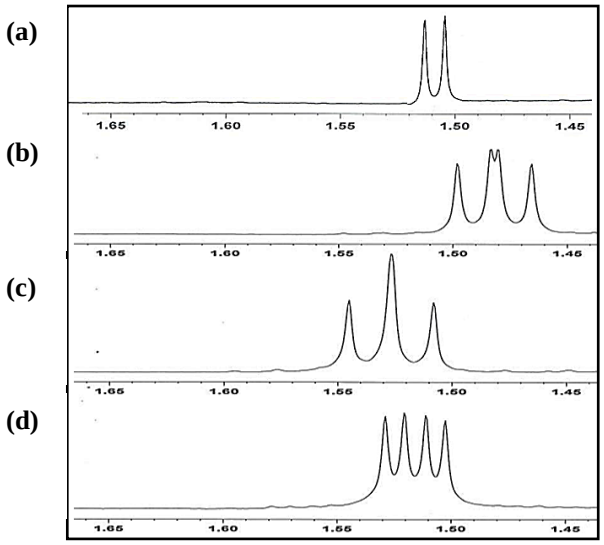

Figure 13 ^{1}H NMR Spectra of: (a) (±) ibuprofen (b) with **(*R*)-54** (c) with **(*R*,*R*)-55** (d) with **(*R*,*S*)-55**

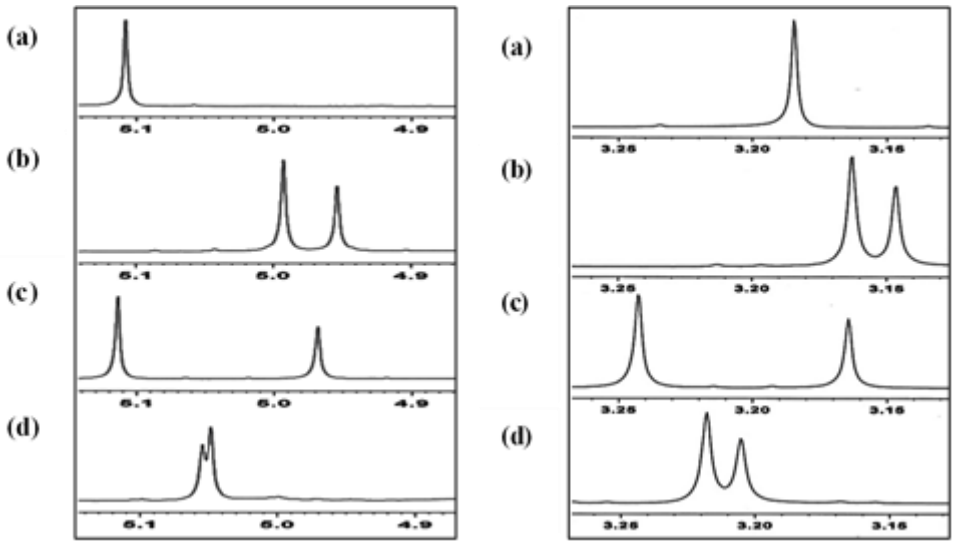

Figure 14 ^{1}H NMR Spectra of: (a) 2-hydroxy-3-methoxy-3,3-diphenyl propanoic acid (*S*:*R* 60:40) (b) with **(*R*)-54** (c) with **(*R*,*R*)-55** (d) with **(*R*,*S*)-55**

Table 1 Comparison of the ability of CSA to discriminate signals of chiral acids

No	Substrates	NMR nucleus	(*R*)-**54**		(*R*,*R*)-**55**		(*R*,*S*)-**55**	
			Δδ[a]	ΔΔδ[b]	Δδ	ΔΔδ	Δδ	ΔΔδ
1	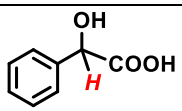	^{1}H	-0.411	0.123	-0.285	0.093	-0.289	--[c]
2	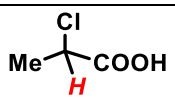	^{1}H	-0.048	--[c]	0.042	--[c]	-0.016	--[c]

3	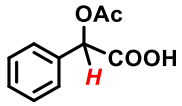	^{1}H	-0.130	0.050	0.003	0.032	-0.041	--[c]
4	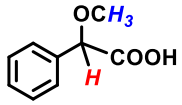	^{1}H (Cα) ^{1}H (CH_3)	-0.179 -0.167	0.028 0.003	-0.055 0.060	0.043 0.049	-0.104 -0.082	--[c] --[c]
5	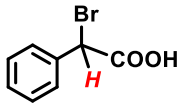	^{1}H	-0.010	0.034	0.128	0.040	0.020	--[c]
6	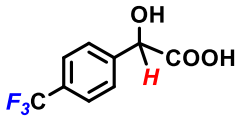	^{1}H ^{19}F	-0.351 -0.127	0.077 0.032	-0.356 -0.094	0.062 0.076	-0.357 -0.099	0.017 0.015
7	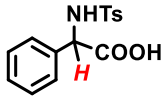	^{1}H (Cα) ^{1}H (CH_3)	-0.165 -0.396	0.055 0.079	-0.201 -0.353	0.070 0.074	-0.146 -0.287	0.049 0.031
8	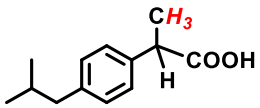	^{1}H	-0.038	0.015	0.007	0.019	-0.004	0.008
9	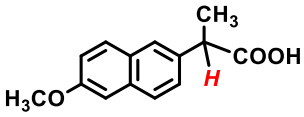	^{1}H	-0.050	--[c]	0.010	--[c]	-0.074	--[c]
10	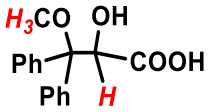	^{1}H (Cα) ^{1}H (OCH_3)	-0.135 -0.029	0.039 0.016	-0.067 0.020	0.146 0.079	-0.056 0.028	0.006 0.013

[a]Induced chemical shift (Δδ); [b]Nonequivalence (ΔΔδ); [c]Signals were not separated.

At this stage, we conclude that **(*R*)-54** and **(*R,R*)-55** were more effective in chiral recognition of mandelic acid and its derivatives compared to **(*R,S*)-55**.

The use of optically pure of 1,1'-binaphthyl-2,2'-diol (BINOL) and its derivatives in asymmetric synthesis and catalysis is now a very important subject.[42] There are only a few reports on the use of chiral solvating agents for establishing optical purity of BINOL and its derivatives in the literature. Even in these reports, BINOL and analogues were converted to their alkoxy derivative before being subjected to the CSA analysis.[43] There is also one other report on the use of quinine as CSA to discriminate signals of isomers of BINOL in ^{1}H NMR.[44] Since our present secondary amine based roof-shape CSAs were expected to be strongly basic in nature, we investigated them for their ability to interact with weakly acidic BINOL or its derivatives. However, for BINOL all three were ineffective in separating the signals (entry 1, Table 2). Structurally similar 2,2',7,7'-tetrahydroxy-1,1'-binaphthyl possessing a C2-symmetric axis is also utilized in asymmetric chemistry.[45,46]

The presence of two more easily accessible hydroxyl groups in this molecule may lead to better interactions with the CSA. This was supported by the observation that the CSAs **(*R*)-54** and **(*R,S*)-55** were able to separate the signal of the most shielded hydrogen attached to the C8 position while CSA **(*R,R*)-55** failed to resolve them (entry 2, Table 2). This hydrogen showed a clear doublet in the most upfield part of the aromatic region (**δ** 6.4), convenient for easy measurement (Figure 15).

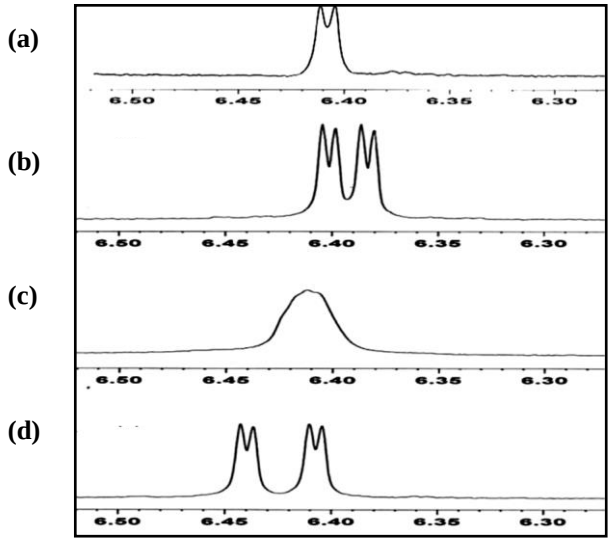

Figure 15 ^{1}H NMR Spectra of: (a) 2,2′,7,7′-tetrahydroxy-1,1′-binaphthyl (b) with **(*R*)-54**; (c) with **(*R,R*)-55**; (d) with **(*R,S*)-55** (20.0 mM, $CDCl_3$, 400 MHz)

This hypothesis was confirmed when poor separations were seen when these two outside hydroxyl groups were either blocked as 7,7'-dimethoxy-2,2'-dihydroxy-1,1'-binaphthyl or in case of 6,6'-dibromo-2,2'-dihydroxy-1,1'-binaphthyl (entries 3 and 4, Table 2).

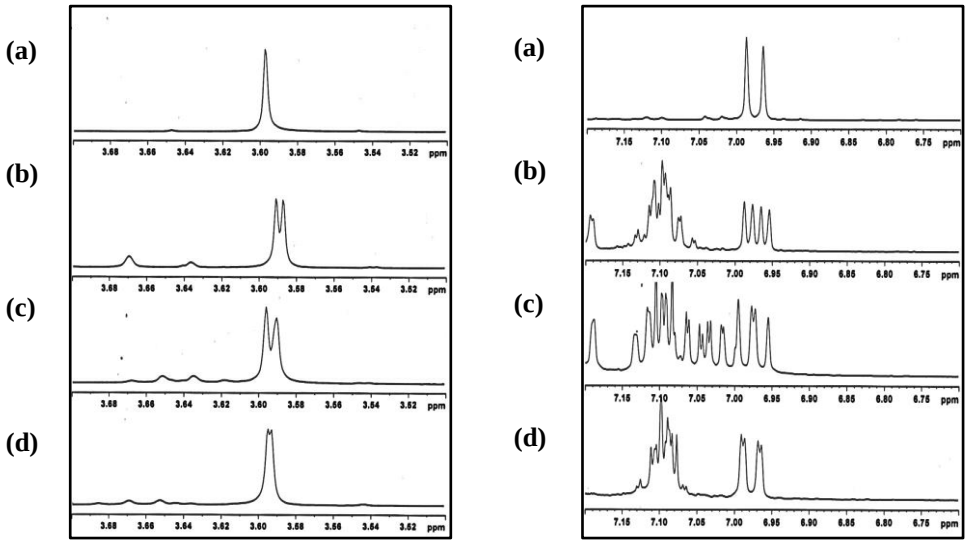

Figure 16 ^{1}H NMR Spectra of: (a) (±) 7,7'-dimethoxy-2,2'-dihydroxy-1,1'-binaphthyl (left) (a) (±) 6,6'-dibromo-2,2'-dihydroxy-1,1'-binaphthyl (right) (b) with ***(R)*-54 (c)** with ***(R,R)*-55** (d) with ***(R,S)*-55**

In another set of experiments, we examined 3,3'-dimethoxy-2,2'-dihydroxy-1,1'-binaphthyl and 3-methoxy-2,2',3'-trihydroxy-1,1'-binaphthyl for the same study. Similar to the above observations, the latter one showed reasonable separation with **(*R,S*)-55** as against the other two (entries 5 and 6, Table 2).

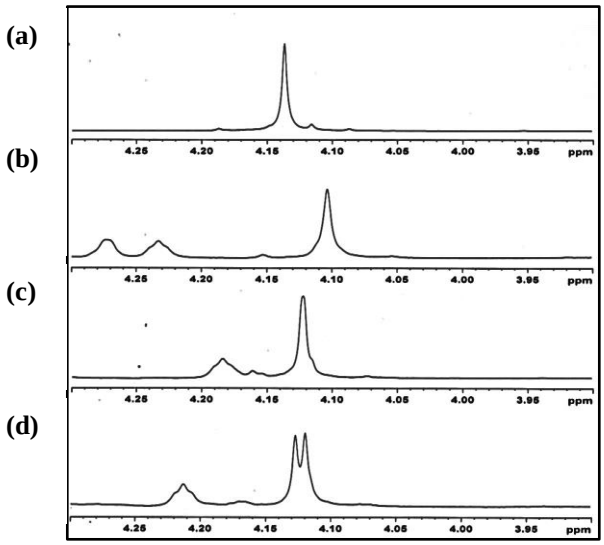

Figure 17 ^{1}H NMR Spectra of: (a) (±) 3-methoxy-2,2',3'-trihydroxy-1,1'-binaphthyl (b) with **(*R*)-54** (c) with **(*R,R*)-55** (d) with **(*R,S*)-55**

Recently, chiral Brønsted acids such as phosphoric acid derivative 1,1'-binaphthyl-2,2'-diyl hydrogen phosphate and its analogues have found wide uses as chiral catalysts.[47] We examined the effect of these CSAs by systematically studying the ^{31}P NMR and concluded the efficiency of **(*R*)-54** and **(*R,S*)-55** to be higher as against **(*R,R*)-55** (entry 7, Table 2).

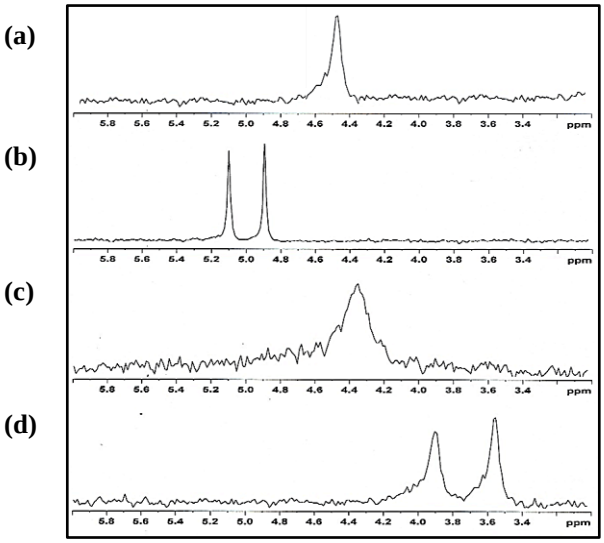

Figure 18 ^{31}P NMR Spectra of: (a) (±) 1,1′-Binaphthyl-2,2′-diyl hydrogen phosphate (b) with ***(R)*-54** (c) with ***(R,R)*-55** (d) with ***(R,S)*-55**

Table 2 Comparison of ability of CSA to discriminate signals of chiral BINOL derivatives

No	Substrates	NMR nucleus	(*R*)-**54**		(*R*,*R*)-**55**		(*R*,*S*)-**55**	
			Δδ[a]	ΔΔδ[b]	Δδ	ΔΔδ	Δδ	ΔΔδ
1	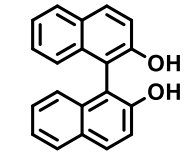	^{1}H	0.007	--[c]	0.010	--[c]	0.011	--[c]
2	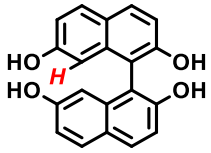	^{1}H	-0.015	0.019	0.005	--[c]	0.017	0.032
3	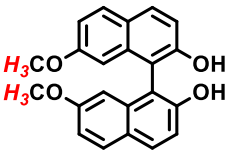	^{1}H	-0.008	0.004	-0.004	0.005	-0.003	0.002
4	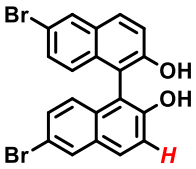	^{1}H	0.005	0.011	0.001	0.018	-0.002	0.005
5	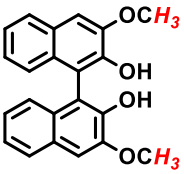	^{1}H	0.002	--[c]	0.001	--[c]	--[d]	--[c]
6	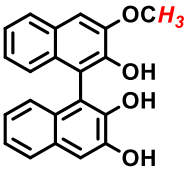	^{1}H	-0.033	--[c]	-0.014	--[c]	-0.014	0.007
7	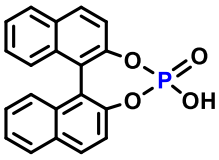	^{31}P	+0.529	0.205	-0.114	--[c]	-0.739	0.341

[a]Induced chemical shift (Δδ); [b]Nonequivalence (ΔΔδ); [c]Signals were not separated; [d]Noshift

In all of the examples investigated in this class of compounds, **(*R*)-54** and **(*R,S*)-55** were more effective. Between them, the latter one **(*R,S*)-55** proved to be slightly superior class of CSA for binaphthyl system, while its diastereomer **(*R,R*)-55** was found more effective in the chiral recognition of derivatives of mandelic acid. Such a match−mismatch effect for controlling supramolecular interactions between diastereomeric chiral solvating agents for molecular recognition is noteworthy.

4.2.1.2 Determination of Accuracy of Analysis:

To demonstrate practical utility of the present CSAs for the quantitative determination of enantiomeric excess (*ee*) of the unknown sample of mandelic acid we performed controlled experiment. A set of samples of known *ee* (optical purity) of mandelic acid with 0, 20, 50, 70 and 90% *ee*, respectively, were prepared. These samples were analyzed with 1.0 equivalence of **(*R,R*)-55** by recording their ^{1}H NMR. The experimental results were in accordance with the theoretical values as can be seen from Figure 19 where a linear relationship between the observed and actual values of % *ee* can be observed. The observed % *ee* values were found to be within acceptable level of actual values, which confirms the accuracy of the analysis and possibility of the practical use in determining enantiomeric excess of sample of unknown optical purity.

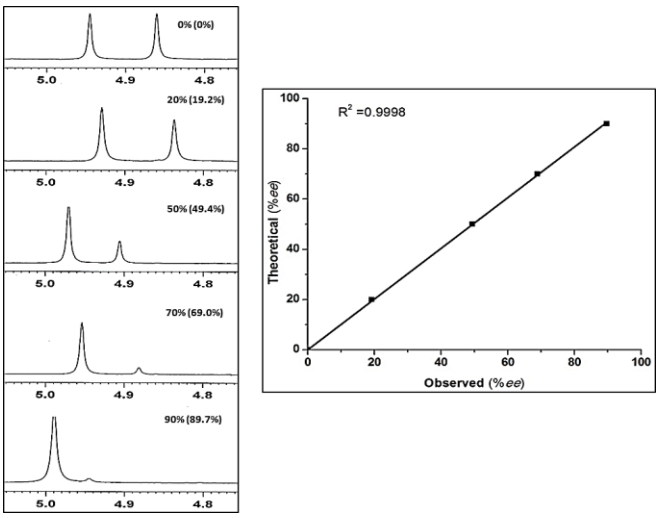

Figure 19 ^{1}H NMR spectra of scalemic mixture of MA in the presence of (*R,R*)-55; values in parentheses are observed by NMR (left) and its correlation between theoretical and observed % *ee* values (right).

4.2.1.4 Determination of Ideal Concentration for Analysis:

A variation in the chemical shift non-equivalence (ΔΔδ) with the concentration of the ligand and substrate was analyzed. Since the stoichiometry of the complex formed between the CSA **(*R,R*)-55** and substrate (mandelic acid) is 1:1, the same ratio was maintained throughout the analysis. The total concentration of sample was varied from 5mM, 10mM, 20mM, 30mM, 40mM to 50mM and the change in the chemical shift non-equivalence (ΔΔδ) was observed. The plot of this shift with change in the molar concentration showed that as the concentration of the sample was increased from 5mM to 10mM, there was a drastic increase in the resolution of the signal for CαH proton which further increased slightly as

the total concentration was increased to 20mM. However, any further increase in the concentration (30mM, 40mM and 50mM) did not cause any considerable change in the resolution of the substrate signals. Hence, 20mM was the concentration of choice to perform all the CSA studies.

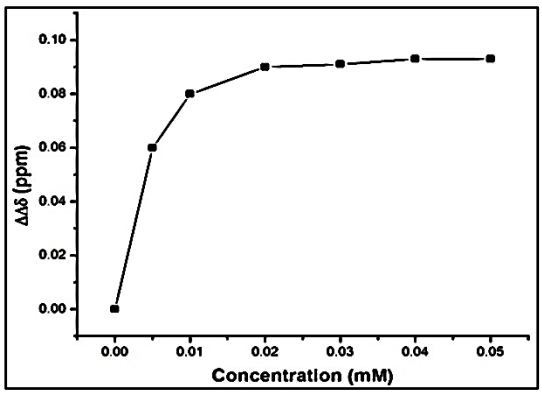

Figure 20 Graph showing change in chemical shift nonequivalence for α-*H* proton of racemic MA at different concentrations having 1:1 molar ratio with (*R,R*)-55

4.2.1.5 Determination of difference in Binding Ability:

An experiment was designed to determine the difference in binding ability of **(*R,R*)-55** with both the isomers of mandelic acid. For a constant concentration of **(*R,R*)-55** (20 mM), a varying amount of (*R*)-MA and (*S*)-MA was added in such a way that the molar ratio varied from 0.2, 0.5, 1.0, and 1.5. The change in the chemical shift (Δδ) value for α-H proton of mandelic acid was plotted against the molar ratio of chiral mandelic acid (Figure 21). The negative values for Δδ suggest an upfield shift of the signal. For both the isomers of MA, a minima is observed at molar ratio of 1.0 indicating maximum shift in **δ** value. However, the shift with (*R*)-MA is much more than that with (*S*)-MA indicating a stronger association of **(*R,R*)-55** with (*R*)-MA as compared to its association with (*S*)-MA.

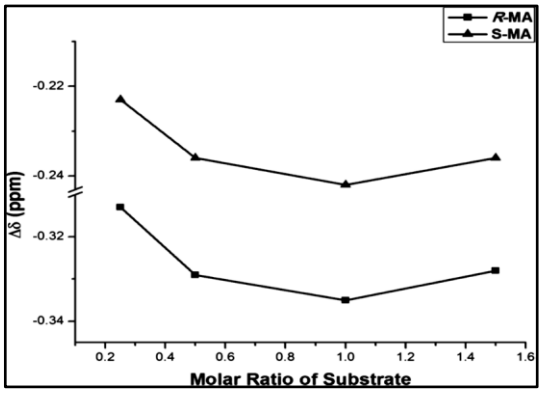

Figure 21 Graph showing the effect of different molar ratios of (*S*)-MA and (*R*)-MA with (*R,R*)-55 upon change in chemical shift for the α-H proton of mandelic acid.

4.2.1.6 Determination of Primary Interaction with Acidic Substrates:

The probable mode of action for the recognition of substrates with amino CSA should involve its protonation followed by its complexation with carboxylate. The formation of the carboxylate anion was confirmed when the carbonyl stretch (1716 cm^{-1} for mandelic acid) disappeared in the FT-IR spectra of its mixture with **(*R*)-54** or **(*R,R*)-55**, and the new strong peaks appeared at 1624 and 1602 cm^{-1} (the COO- stretch).[48] However, in the case of **(*R,S*)-55** all the three peaks were observed, possibly indicating incomplete complex formation.

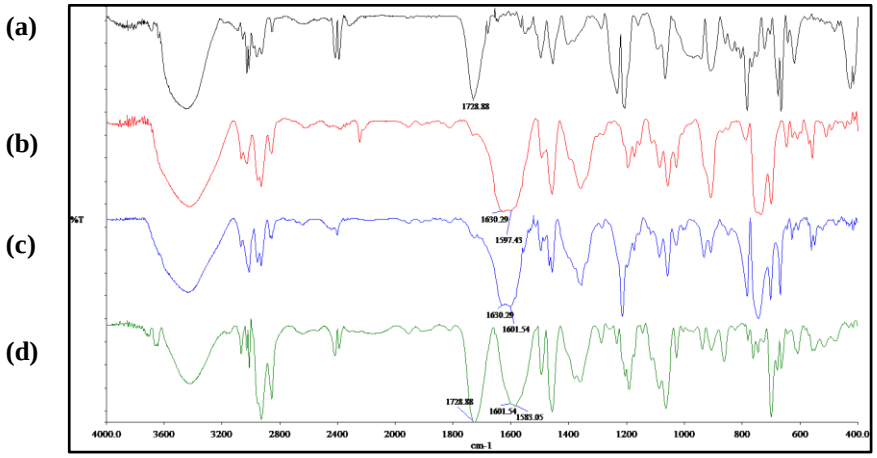

Figure 22 IR Spectra of: (a) (±) Mandelic acid (b) with (*R*)-54 (c) with (*R,R*)-55 (d) with (*R,S*)-55

4.2.1.7 Crystal Structure of Diastereomeric Salts:

Having established the efficacy of the three CSAs and collected information about the match-mismatch effect, we proceeded to understand the supramolecular interactions in depth. First, the experiments were run with nonracemic sample of mandelic acid with one known isomer excess with optically pure **(*R,R*)-55**. The signal of proton attached to the chiral center CαH of (*R*)-mandelic acid [**(*R,R*)-55·*R*-MA**] appeared more upfield. The solution of the equimolar mixture of **(*R,R*)-55** with (*R*)-mandelic acid in acetonitrile was left for slow evaporation, and the crystals obtained were subjected to single crystal X-ray diffraction study. Similarly, a mixture of **(*R,R*)-55** with (*S*)-mandelic acid was allowed to give a crystal of its diastereomeric salt [**(*R,R*)-55·*S*-MA**] for the similar analysis.

The sample of [**(*R,R*)-55·*R*-MA**] crystallized in monoclinic chiral space group $P2_1$. The crystal structure contained one molecule each of **(*R,R*)-55** with (*R*)-mandelic acid along with a molecule of acetonitrile in the asymmetric unit (Figure 23). The hydrogen attached to the chiral carbon of (*R*)-mandelic acid appears to be laying on top of one of the aromatic rings of the roof-shape bicyclic framework. The shortest perpendicular distance between the

plane passing through this ring and the hydrogen is 4.18 Å, and it is observed to be shifting upfield region due its shielding effect in ^{1}H NMR analysis. The C−O bond lengths (~1.24-1.25 Å) in the COOH group show that proton transfer has occurred from *R*-MA to amine moiety of the **(*R,R*)-55**, revealing that the complex is salt. In the crystal structure, the *R*-MA molecules are engaged in the formation of 2_1-screw related helical chain through O-H···O hydrogen bonding interactions (H···O=1.837Å, O···O=2.657Å/ O-H···O=179°) involving hydroxyl H-atom and carbonyl oxygen of the carboxylic group. The **(*R,R*)-55** molecules are associated with the molecular chain of *R*-MA on both sides through strong N-H···O hydrogen bonding interactions involving N-H protons of **(*R,R*)-55** and carboxyl and hydroxyl group of *R*-MA. One N-H proton of **(*R,R*)-55** makes bifurcated H-bonding interactions with carbonyl (H···O=1.916Å, N···O=2.758Å/ O-H···O=144°) and hydroxyl oxygen (H···O=2.179Å, N···O=2.969Å/ O-H···O=138°). The other N-H proton is engaged with second *R*-MA molecule through N-H···O hydrogen bond involving carbonyl oxygen (H···O=1.797Å, N···O=2.746Å/ O-H···O=165°).

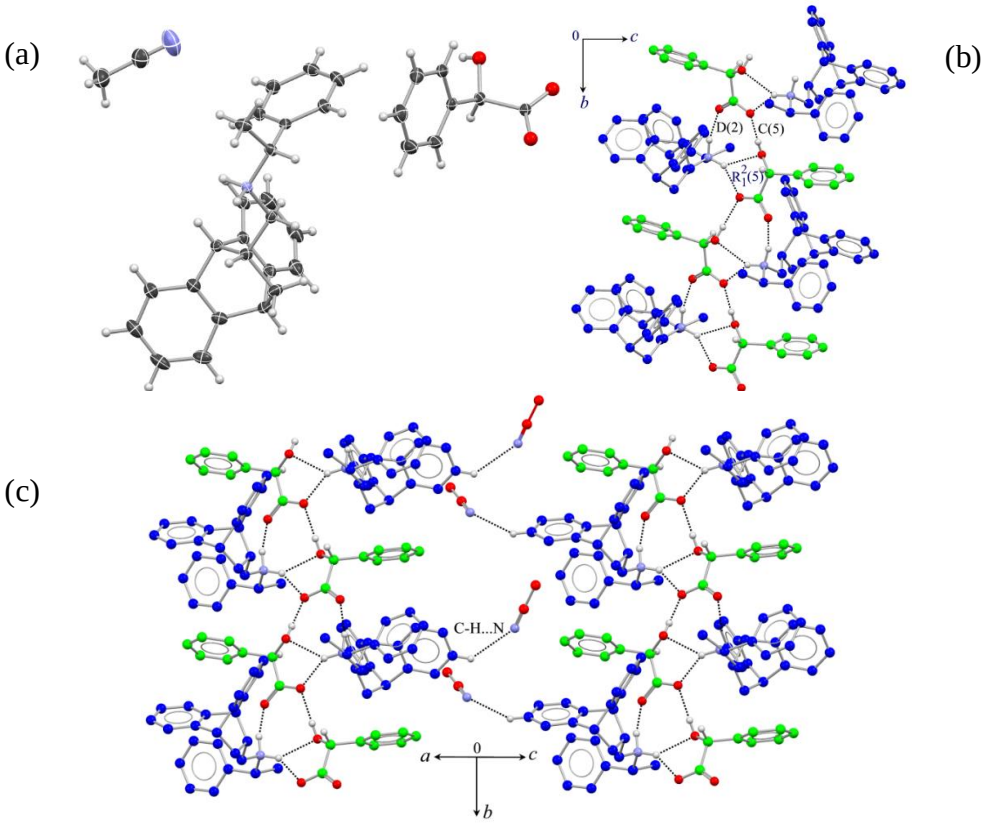

Figure 23 (a) ORTEP diagram of **(*R,R*)-55•*R*-MA** salt (b) Association of **(*R,R*)-55** (blue) molecules to the O-H···O hydrogen bonded helical chain of ***R*-MA** (green) through N-H···O hydrogen bonding interactions generating an extended chain assembly. (c) linking of the neighboring helical chains through acetonitrile molecules via C-H···N interactions.

In general, two molecules of **(*R,R*)-55** linked to the two molecules of *R*-MA through N−H···O hydrogen bonding interactions to generate the tetrameric assembly which formed an extended chain assembly along the b-axis. The neighboring chains along the *bc*-diagonal were linked through acetonitrile molecules via C−H···N interactions (H···N = 2.714Å, N···C = 3.427 Å /C−H···N = 134°) between the N atom of the guest acetonitrile and C−H aromatic proton of the **(*R,R*)-55** moiety and other van der Waals forces between the host and the guest molecules. This reveals that acetonitrile molecules play a vital role in fusing the neighboring helical chains, thereby inducing its crystallization.

The complex [**(*R,R*)-55·*S*-MA**] also crystallized in monoclinic chiral P2_1 space group containing two molecules of each component in the asymmetric unit. The crystal structure of [**(*R,R*)-55·*S*-MA**] (Figure 24) is isostructural to the [**(*R,R*)-55·*R*-MA**] structure. The C−O bond lengths (∼1.24−1.26 Å) in the COOH group show that proton transfer has occurred from *S*-MA to the amine moiety of the **(*R,R*)-55** revealing that the complex is salt. The neighboring symmetry independent *S*-MA molecules generate the helical chain similar to [**(*R,R*)-55•*R*-MA**] through O-H···O hydrogen bond (H···O=1.907Å, O···O=2.720Å/ O-H···O=163^o and H···O=1.598Å, O···O=2.827Å/ O-H···O=155^o) involving hydroxyl H-atom and carbonyl oxygen of the carboxylic group. Both symmetry independent **(*R,R*)-55** molecules are associated with this extended chain on either side through N-H···O hydrogen bonding interactions to generate the layered structure. One of the N-H proton of **(*R,R*)-55** is involved in the bifurcated N-H···O hydrogen bonding interactions with the carbonyl (H···O=1.925Å, N···O=2.739Å/ O-H···O=138^o; H···O=1.901Å, N···O=2.729Å /O-H···O=137^o) and hydroxyl (H···O=2.013Å, N···O=2.818 Å/ O-H···O=138^o; H···O=2.059Å, N···O=2.878Å/ O-H···O=139^o) oxygens of *S*-MA molecules. The other N-H proton forms a N-H···O hydrogen bonding interactions with the carboxyl oxygen of *S*-MA (H···O=1.821Å, N···O=2.788Å /O-H···O=165^o; H···O=1.959Å, N···O=2.916 Å /O-H···O=162^o).Similar to the crystal structure of [**(*R,R*)-55·*R*MA**], two molecules of each *S*-MA and **(*R,R*)-55** constitute a tetrameric structure through hydrogen-bonding interactions, which is extended along the a-axis to generate the chain structure. The neighbouring chains are loosely connected to each other roughly along the b-axis *via* hydrophobic interactions.

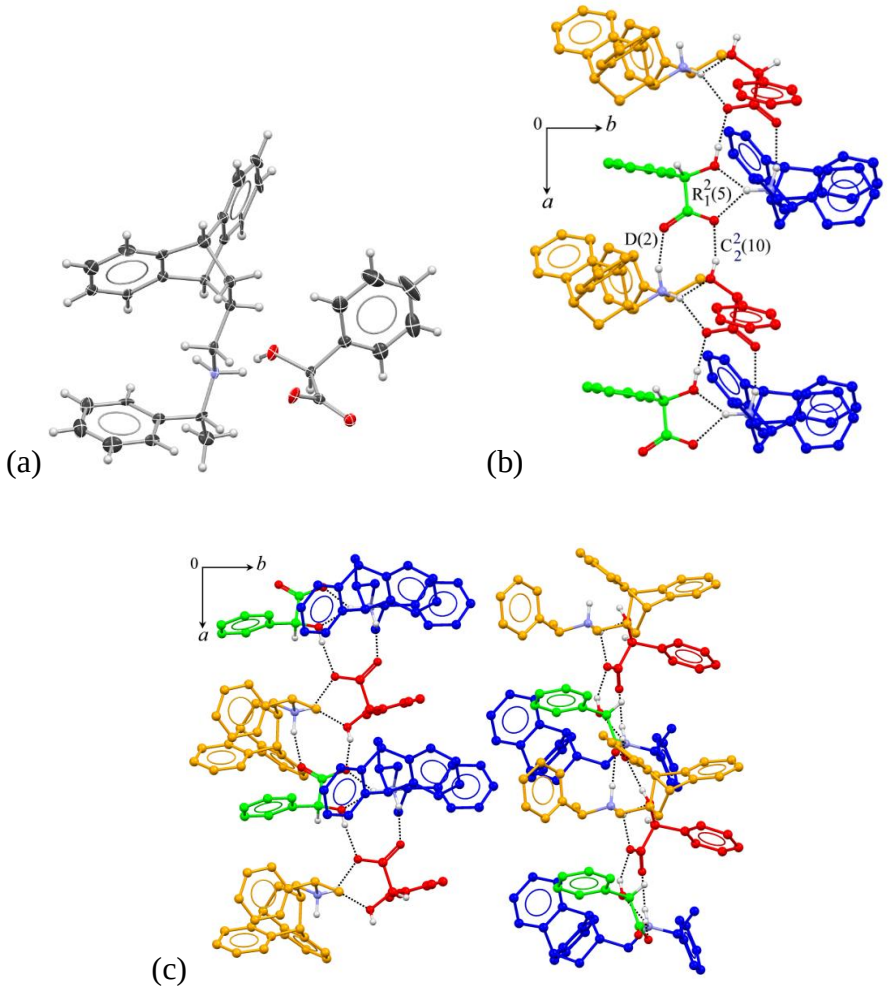

Figure 24 (a) ORTEP view of **(*R,R*)-55•*S*-MA** salt. The displacement ellipsoids are drawn at 40% probability level and H atoms are shown as small spheres of arbitrary radii. (b) Association of the symmetry independent **(*R,R*)-55** molecules to the O-H···O hydrogen bonded helical chain of ***S*-MA** (green and red) through N-H···O hydrogen bonding interactions generating an extended chain assembly. (c) linking of the neighboring helical chains through van der Waals forces.

To the best of our knowledge, there are very few reports on the crystal study of the structure of the salt of test substrate and the CSA to understand the supramolecular interactions.[49] The experimental observations of shielding and deshielding effects in the two pairs in ^{1}H NMR analysis corroborated well with the information obtained from these crystal structures, even though one needs to be cautious in comparing the two.

4.2.1.8 Comparison of CSA activity with literature:

In most of the cases, we found the present roof shape amine to be comparable or better than some of the reported chiral amine based CSAs (Figure 25).

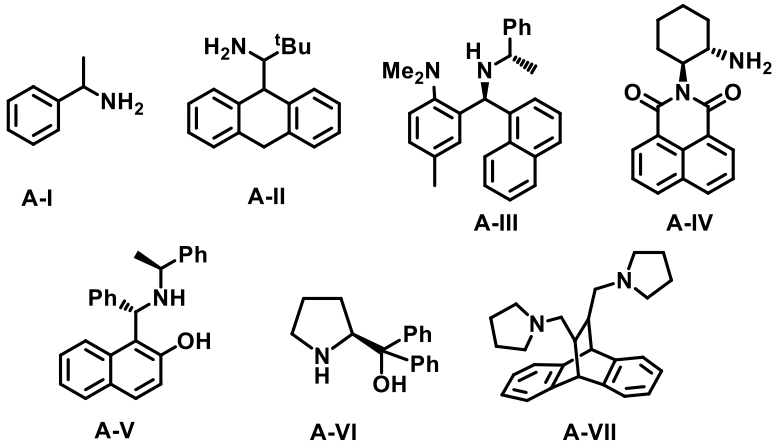

Figure 25 Some chiral amines reported in the literature for their CSA activity

In order to further establish the role of the roof shape part of the secondary amine, we prepared the *N*-methyl derivative of (*R*)-α-phenylethylamine and scanned as CSA for the recognition of (±)-mandelic acid. We observed a small shift in signal (induced chemical shift; $\Delta\delta = -0.066$ ppm) but there was no splitting of the signals ($\Delta\Delta\delta = 0$ ppm).

Table 3 Table shows a comparison of the literature values of induced chemical shift for some of the substrates with our CSAs

No.	Substrate	Our Best CSA	ΔΔδ	Reported CSA	ΔΔδ
1.	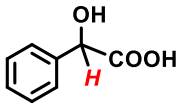	*R*-**54**	0.123	A-**1**[50]	0.035
				A-**3**[50]	0.085
				A-**5**[51]	0.025
				A-**6**[52]	0.062
				A-**7**[53]	0.071
2.	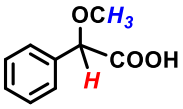	*R,R*-**55**	0.043 (αH) 0.049 (CH_3)	A-**2**[54]	0.014 (αH)
				A-**3**[50]	0.021 (CH_3)
				A-**4**[40]	0.051 (αH)
				A-**6**[52]	0.023 (αH)
					0.003 (CH_3)
3.	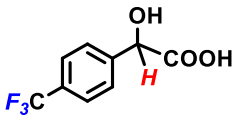	*R*-**54**	0.077	A-**5**[51]	0.056
4.	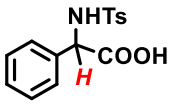	*R,R*-**55**	0.070	A-**1**[50]	0.031
5.	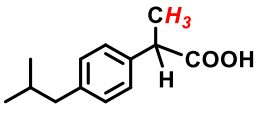	*R,R*-**55**	0.019	A-**2**[54]	0.005

4.2.2 Electronic effects of Roof shape secondary amines on chiral recognition:

4.2.2.1 Synthesis of the ligands:

The strategy for the synthesis of chiral secondary amines involving nucleophilic substitution reaction on the activated site, suffers a major disadvantage which limits its applicability. This method could be applied effectively only when the nucleophilic amines were readily available. Hence, to overcome this limitation, Mignonac[55] developed the reductive amination methodology which has proved to be an important route towards synthesis of α-chiral amines in organic as well as pharmaceutical industries. The main advantages of employing this strategy is that it is an efficient stepwise methodology involving two steps. The first step is the imine formation between the carbonyl compound and the amine reagent followed by its reduction using a hydride source. However, this methodology also has some disadvantages like formation of alcohol as a by-product due to reduction of aldehyde or ketone group resulting in lower yield and over alkylation of the amine were secondary amine was desired. The most common strategies in reductive amination can be subdivided into three main strategies: (1) use of molecular hydrogen with heterogeneous catalysts (palladium, platinum or nickel catalysts) for reduction of imine which is environmentally friendly but incompatible with various functional groups such as nitro, cyano and C-C multiple bonds[56] (2) transfer hydrogenation utilizing formic acid or one of its derivative (Leuckart-Wallach type)[57] (3) use of hydride reductants *e.g.* $NaBH_3CN$,[58] $LiBH_3CN$,[59] $NaBH_3CN$-$ZnCl_2$,[60] $NaBH_4$[61] etc. Recently chiral phosphoric acid and its derivatives have been employed as organocatalysts in reductive amination utilizing Hantzsch esters or silanes as hydride sources.[62]

So we employed this strategy to compare the synthetic yield obtained from both the processes as well as to propose an alternate route towards accessing optically pure roof shape secondary amines. The synthesized tosylate **(*R*)-53** was converted to azide **(*R*)-56**, by treatment with sodium azide in DMF, which on hydrogenation gave amine **(*R*)-57**.

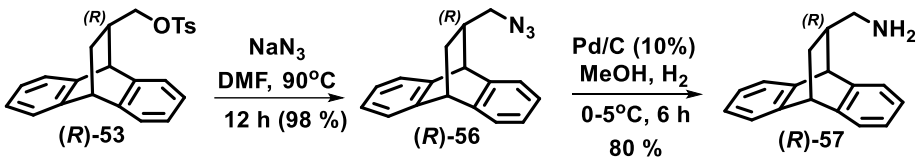

Scheme 11 Synthesis of chiral roof shape amine (*R*)-57

The amine **(*R*)-57** was condensed with benzaldehyde and the Schiff base formed was reduced *in situ* to the corresponding **(*R*)-54** (Scheme 12). The overall yield of this three step procedure was slightly better than one step method developed earlier (55%).

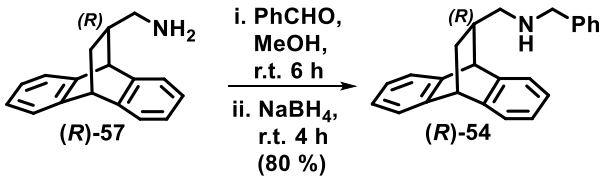

Scheme 12 Alternate synthesis of (*R*)-54 using reductive amination method

The phenomena of molecular recognition depends upon a number of factors. It has been reported in the literature that the change in electronic effects in a molecule due to presence of various electron withdrawing or releasing substituents, is the prime factor causing a change in the polarizability of the molecule. Depending upon the strength of the substituent, the binding affinity is increased or decreased, affecting the phenomena of molecular recognition.[63] The introduction of electron withdrawing or releasing substituents on the aromatic ring of the benzyl unit of roof shape chiral secondary amines, can lead to change in the aromatic interactions which are known to play a significant role in stabilizing the diastereomeric complexes formed *in situ* during CSA study. Hence the design of such systems with varying groups is important in understanding the interactions like edge to face and face to face interactions which play a vital role during molecular recognition. The effect of substituent highly depends on the inductive effect due to the electronegativity of the atoms for groups such as $-NO_2$, -F, -OH, -CN, $-NH_2$, $-OCH_3$ *etc*. and the resonance effect.[64,65] Since the electron accepting strength of $-NO_2$ group and electron donating strength of $-OCH_3$ group is one of the strongest, we selected these substituents to occupy 4-position of the benzyl moiety. Since these substituents also possess ability to undergo hydrogen bonding, the detail study of the changes in the crystal packing due to introduction of these groups will be beneficial towards gaining a deeper insight into the mode of molecular recognition.

Following the reductive amination protocol, two more derivatives, **(*R*)-58** and **(*R*)-59**, were synthesized using 4-nitrobenzaldehyde and 4-methoxylbenzaldehyde condensed with roof shape chiral amine **(*R*)-57**, respectively followed by the reduction of imine *in situ* using $NaBH_4$ (Scheme 13).

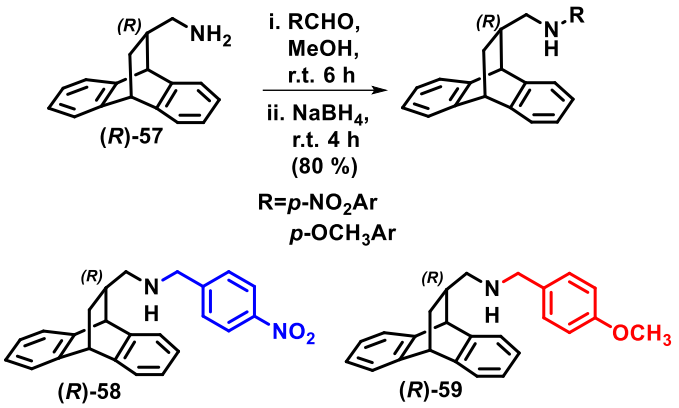

Scheme 13 **Synthesis of chiral roof shape amines using reductive amination method**

The two derivatives were chosen to introduce electron withdrawing and electron releasing group, in order to change the electronic effect and study the behaviour in molecular recognition as CSA.

4.2.2.2 Chiral recognition using NMR Spectroscopy:

The synthesized roof shape amines were then screened to compare their ability of molecular recognition of chiral acids. The degree of discrimination was evaluated by recording ^{1}H NMR of equimolar mixture of CSA and test acid in $CDCl_3$ (400 MHz; 20 mmol). In the initial study we scanned α-substituted phenylacetic acids, such as mandelic acid (**A-1**). In this case the signal for C$_\alpha$*H* proton of ArC*H*(OH)COOH was observed to have shifted towards the upfield region, for all three roof shape CSAs.

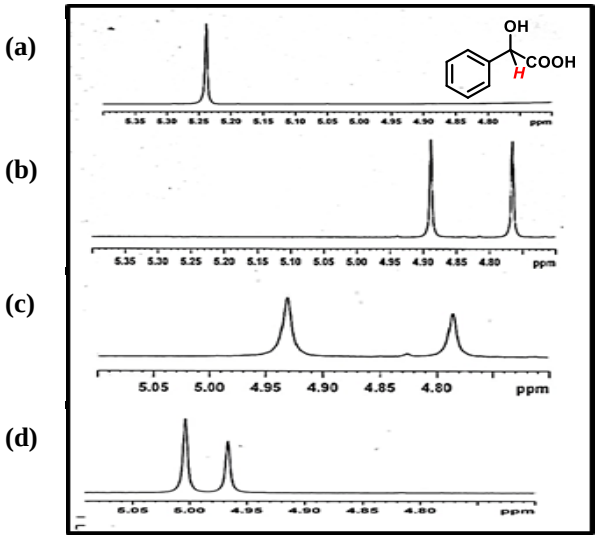

Figure 26 Separation of C$_\alpha$H of (a) (*R/S*)-mandelic acid; (b) with (*R*)-**54**; (c) with (*R*)-**58**; (d) with (*R*)-**59**

For mandelic acid, **A-1**, the C$_\alpha$*H* proton shifted from blank value of 5.238 ppm to 4.808, 4.859 and 4.986 ppm respectively for (*R*)-**54**, (*R*)-**58** and (*R*)-**59** (Table 3, entry 1), which can also be quantified as -0.431, -0.379 and -0.253 ppm (Δδ). For effective chiral discrimination, the two isomers of **A-1** need to shift with different proportion, which is established by measuring the non-equivalence (ΔΔδ) or gap between the two signals. For mandelic acid **A-1**, the CSAs showed 0.123, 0.146 and 0.037 ppm respectively for (*R*)-**54**, (*R*)-**58** and (*R*)-**59**. This observation is consistent with electronic effect due to introduction of substituent on the aromatic ring of benzyl amine, where strongly withdrawing one in (*R*)-**58** showed maximum separation (Figure 26).

To understand the interactions we also made similar changes in mandelic acid, prepared 4-nitromandelic acid (**A-II**) and scanned for the three CSAs. Although the shift in position of C$_\alpha$*H* proton was observed for all the three, CSAs, (*R*)-**54** failed to register any non-equivalence (ΔΔδ), while other two, (*R*)-**58** and (*R*)-**59**, showed discrimination to small extent (Table 3, entry 2). However, the discrimination for 4-trifluoromethylmandelic acid (**A-III**), was moderate with all the three derivatives (Figure 27) (Table 3, entry 3).

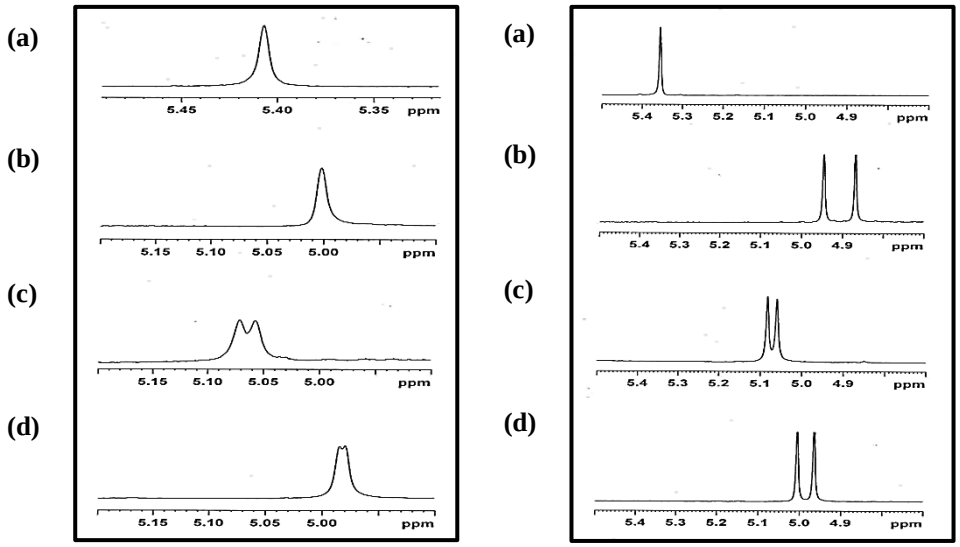

Figure 27 ^{1}H NMR Spectra of: (left) (a) (±) 4-Nitro mandelic acid, (right) (a) (±) 4-Trifluoromethyl mandelic acid, (b) with *(R)*-**54**, (c) with *(R)*-**58**, (d) with *(R)*-**59**

The effectiveness of molecular recognition was more pronounced for 4-bromomandelic acid (**A-IV**), where (*R*)-**58** showed significant results, while the methoxy derivative (*R*)-**59** failed to distinguish signals (Figure 28) (Table 3, entry 4).

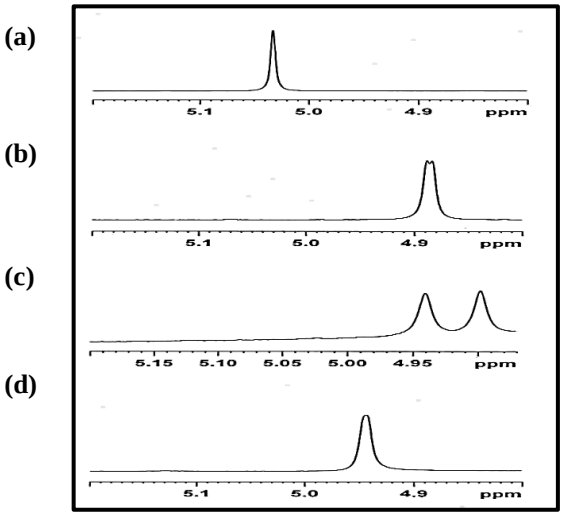

Figure 28 ^{1}H NMR Spectra of: (a) (±) 4-Bromomandelic acid (b) with (*R*)-**54** (c) with (*R*)-**58** (d) with (*R*)-**59**

In the next two chlorine containing derivatives of mandelic acid (**A-V** and **A-VI**) interesting pattern was observed. Where 4-chloromandelic acid (**A-V**) could not be effectively recognized, its isomer 2-chloromandelic acid (**A-VI**) was well differentiated by (*R*)-**58** and (*R*)-**59** (Figure 29) (Table 3, entry 5 & 6).

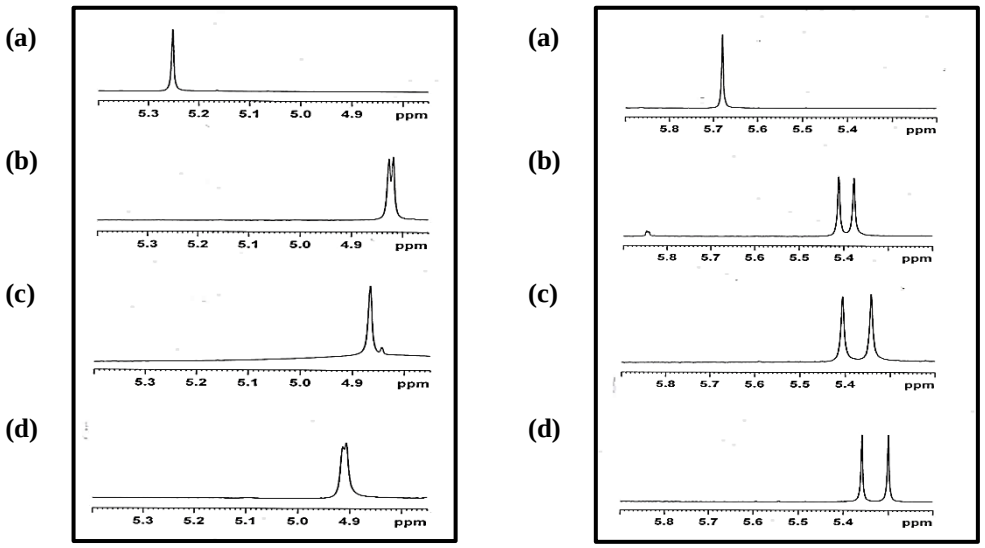

Figure 29 ^{1}H NMR Spectra of: (a) (±) 4-Chloromandelic acid (left), (a) (±) 2-chloromandelic acid (right) with (b) (*R*)-**54**, (c) with (*R*)-**58**, (d) with (*R*)-**59**

Consistent observation was seen for mandelic acids with electron releasing substituents (**A-VII** and **A-VIII**), where also the nitro derivative (*R*)-**58** was more effective (Figure 30) (Table 3, entry 7 & 8).

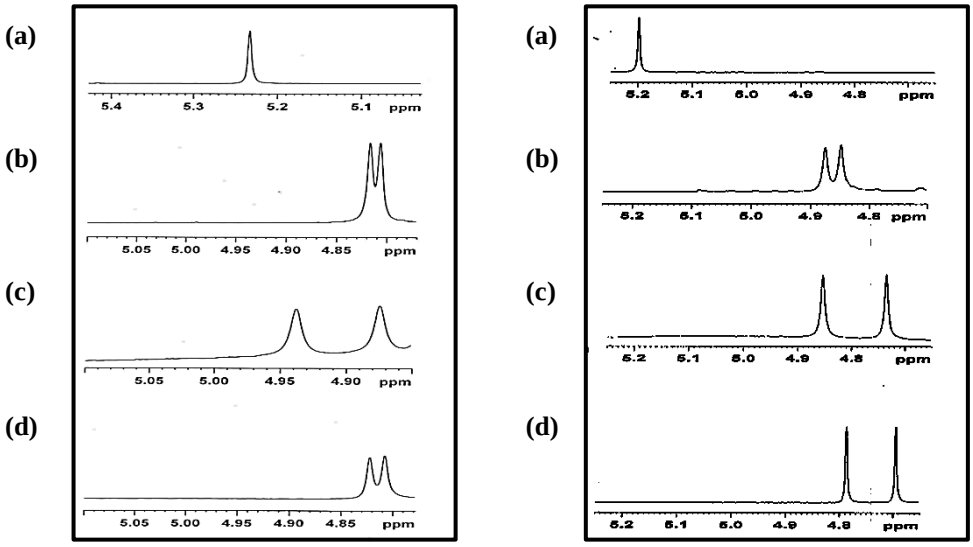

Figure 30 ^{1}H NMR Spectra of (a) (±) 4-Methyl mandelic acid (left) (a) (±)Methylenedioxy mandelic acid (b) with (*R*)-**54** (c) with (*R*)-**58** (d) with (*R*)-**59**

Presence of free hydroxyl group at α-position of mandelic acid could play a significant role in fixing the configuration of its diastereomeric salt with CSA. This was investigated by performing couple of experiments with protected hydroxyl group in α-methoxyphenylacetic acid (**A-IX**) and α-acetoxyphenylacetic acid (**A-X**) (Table 3, entry 9 & 10).

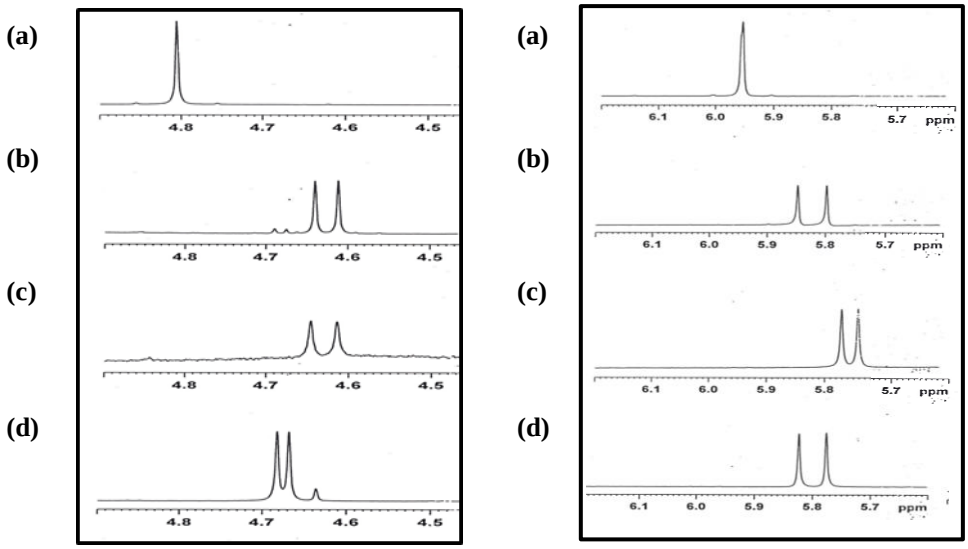

Figure 31 ^{1}H NMR Spectra of (a) (±) *O*-Methoxy mandelic acid (left) (a) (±) *O*-Acetoxy mandelic acid (b) with **(*R*)-54** (c) with **(*R*)-58** (d) with **(*R*)-59**

In comparison to **A-1**, both these derivatives showed inferior recognition establishing the role of hydroxyl unit. This is further established by α-halophenylacetic acids (**A-XI** & **A-XII**, entry 11 & 12).

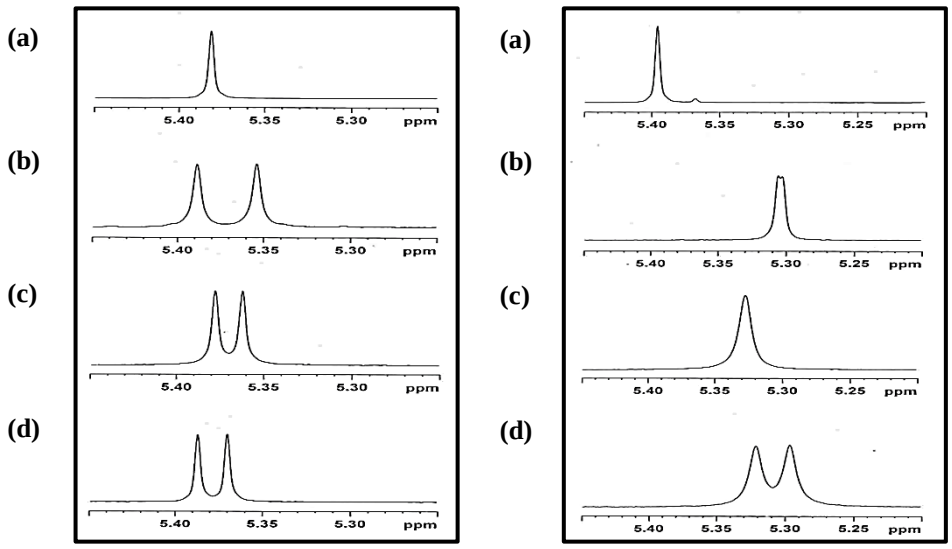

Figure 32 ^{1}H NMR Spectra of: (a) (±) α-Bromophenyl acetic acid (left), (a) (±) α-chlorophenyl acetic acid (right), (b) with (*R*)-**54**, (c) with (*R*)-**58**, (d) with (*R*)-**59**

Table 3 Comparison of the ability of CSA to discriminate $C_{\alpha}H$ signals of chiral acids[a]

No	Substrate	(*R*)-**54**		(*R*)-**58**		(*R*)-**59**	
		Δδ	ΔΔδ	Δδ	ΔΔδ	Δδ	ΔΔδ
1	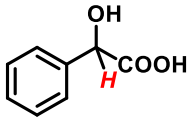 A-I	-0.431	0.123	-0.379	0.146	-0.253	0.037
2	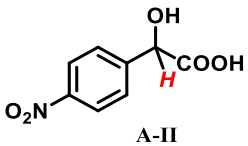 A-II	-0.405	--[b]	-0.343	0.014	-0.425	0.005
3	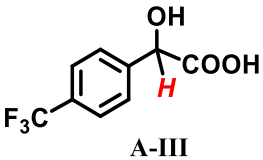 A-III	-0.351	0.077	-0.284	0.022	-0.371	0.041
4	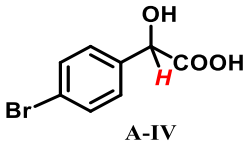 A-IV	-0.346	0.004	-0.312	0.042	-0.288	--[b]
5	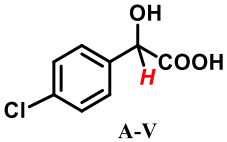 A-V	-0.429	0.008	-0.386	--[b]	-0.342	0.007
6	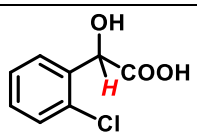 A-VI	-0.285	0.034	-0.305	0.064	-0.350	0.058

7	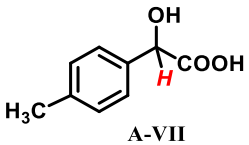 A-VII	-0.421	0.010	-0.327	0.042	-0.418	0.014
8	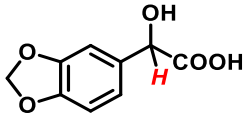 A-VIII	-0.336	0.027	-0.404	0.119	-0.457	0.092
9	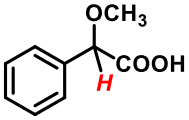 A-IX	-0.179	0.028	-0.164	0.021	-0.130	0.015
10	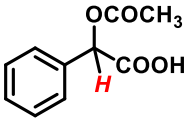 A-X	-0.130	0.050	-0.195	0.029	-0.153	0.040
11	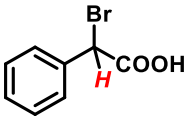 A-XI	-0.010	0.034	-0.011	0.016	-0.003	0.017
12	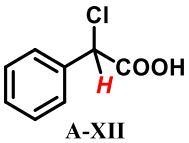 A-XII	-0.092	0.003	-0.068	--[b]	-0.087	0.025

[a] In $CDCl_3$ (20mM), [b] Not resolved

The exploration of ability of molecular recognition was then extended to other type of molecules. Amino acids are important synthetic blocks in medicinal and allied chemistry and determination of their optical purity is critical, particularly for unnatural ones. Recently, there are few reports available where few CSAs are presented for successful discrimination of signals by NMR or UV/fluorescence[66,67] analysis.

For this study we have selected three derivatives of *N*-tosyl amino acids. When ^{1}H NMR was recorded by similar procedure, we could detect discrimination of two type of hydrogens, $C_\alpha H$ and $ArCH_3$, which offers method of dual detection. For valine (**AA-1**) all the three CSAs showed good separation for $C_\alpha H$ signal, where (*R*)-**59** showed maximum resolution (Table 4, entry 1). However, the signals of aromatic methyl group did not resolve completely and base line separation was not achieved (Figure 33).

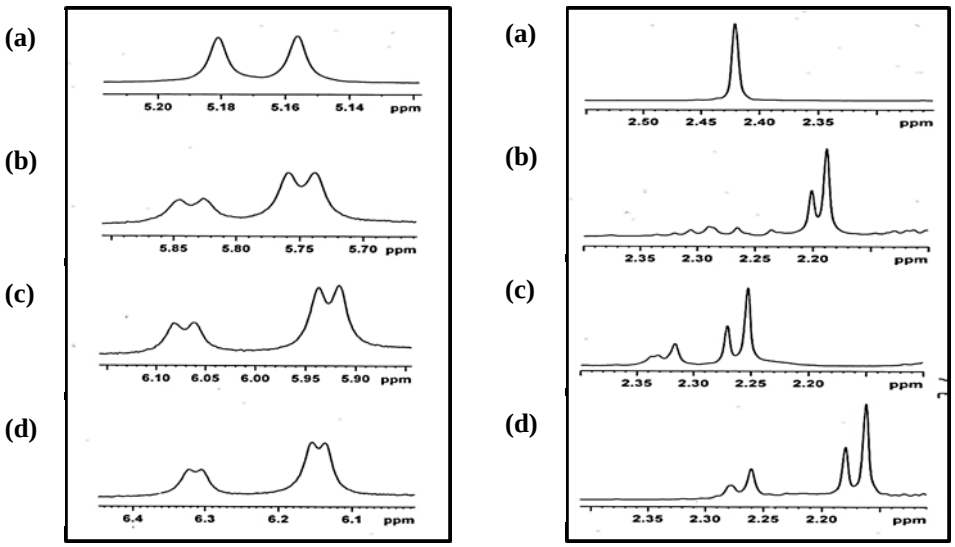

Figure 33 Separation of C$_\alpha$*H* (left) and Ar-C*H*$_3$ (right) proton signal for (2:1::*D*:*L*) mixture of (a) *N*-tosyl valine (b) with (*R*)-**54**; (c) with (*R*)-**58** (d) with (*R*)-**59**

Slightly different observation was seen for alanine (**AA-II**), where the signals of ArC*H*$_3$ and C$_\alpha$*H* did not show much separation, but the C$_\alpha$C*H*$_3$ signal showed moderate resolution (Figure 34) (Table 4, entry 2).

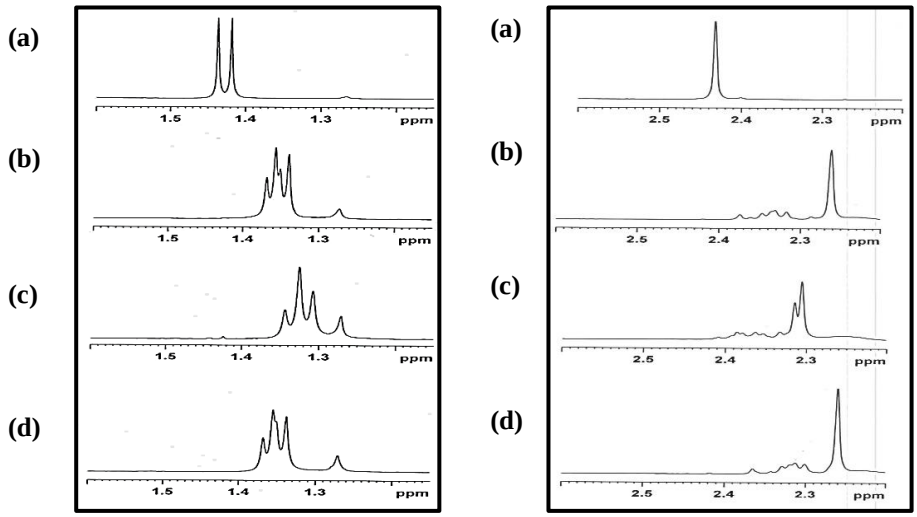

Figure 34 ^{1}H NMR Spectra of C$_\alpha$C*H*$_3$ (left) and Ar-C*H*$_3$ (right) of (a) (±) *N*-tosyl alanine, with (b) (*R*)-**54**, (c) with (*R*)-**58**, (d) with (*R*)-**59**

In the case of phenylglycine (**AA-III**), both ArC*H*$_3$ and C$_\alpha$*H* showed good separation (entry 3) for (*R*)-**54** and (*R*)-**59**, but precipitation was observed in case of (*R*)-**58** (Figure 35).

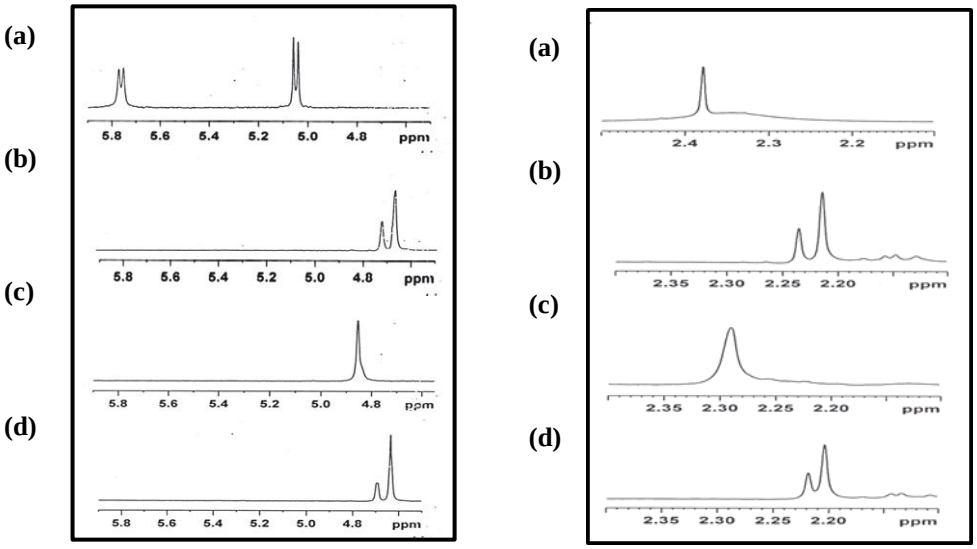

Figure 35 ^{1}H NMR Spectra of -N*H* (left) and Ar-CH_3 (right) proton signal for (2:1::*D*:*L*) mixture (a) (±) *N*-tosyl phenyl glycine, with (b) (*R*)-**54**, (c) with (*R*)-**58**, (d) with (*R*)-**59**

The study was conducted for another acid derivative 2-hydroxy-3-methoxy-3,3-diphenylpropanoic acid (**B-I**), which is an intermediate for few pharmaceuticals.[20] The signals of C$_\alpha$*H* did show good separation in (*R*)-**54**, with superior resolution with (*R*)-**59** (Table 4, entry 4).

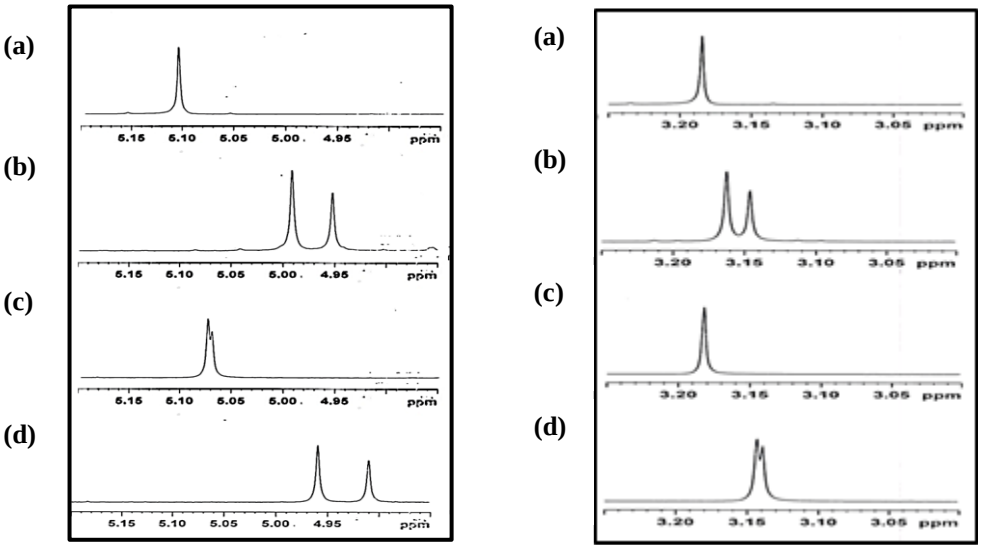

Figure 36 ^{1}H NMR Spectra for Cα*H* (left) and OCH_3 (right) (a) (±) 2-hydroxy-3-methoxy-3,3-diphenylpropanoic acid (b) with (*R*)-**54** (c) with (*R*)-**58** (d) with (*R*)-**59**

Table 4 Discrimination of *N*-Ts amino acids **AA-1** to **AA-III** and **B-I**[a]

Substrate			(*R*)-54		(*R*)-58		(*R*)-59	
			Δδ	ΔΔδ	Δδ	ΔΔδ	Δδ	ΔΔδ
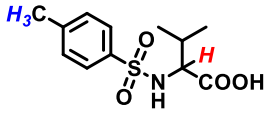	AA-I	α-*H*	+0.623	0.087	+0.832	0.145	+1.062	0.168
		Ar-C*H*$_3$	-0.226	0.012	-0.159	0.018	-0.249	0.017
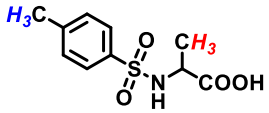	AA-II	α-C*H*$_3$	-0.074	0.012	-0.102	0.018	-0.074	0.013
		Ar-C*H*$_3$	-0.169	--[b]	-0.123	0.008	-0.074	0.013
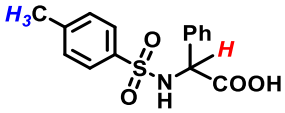	AA-III	α-*H*	-1.063	0.055	--[c]	--[c]	-1.101	0.056
		Ar-C*H*$_3$	-0.154	0.021	--[c]	--[c]	-0.167	0.015
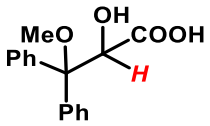	B-I	α-*H*	-0.135	0.039	-0.028	0.003	-0.173	0.050

[a] In $CDCl_3$ (20mM), [b] Not resolved, [c] precipitation observed

4.2.2.3 Determination of Accuracy of Analysis:

The Chiral Solvating Agent will find application only if it can be used for accurate determination of enantiomeric excess of samples of unknown purity. Recording a routine ^{1}H NMR spectra by simply mixing the analyte and appropriate CSA is a relatively simple operation. To test the accuracy of determination of enantiomeric excess by this chiral discrimination, control experiments were conducted with scalemic samples of known purity of mandelic acid and (*R*)-**58**. A linear relationship was established between the observed and actual values of enantiomeric excess, which confirms that the present set of CSAs can be used for practical application (Figure 37).

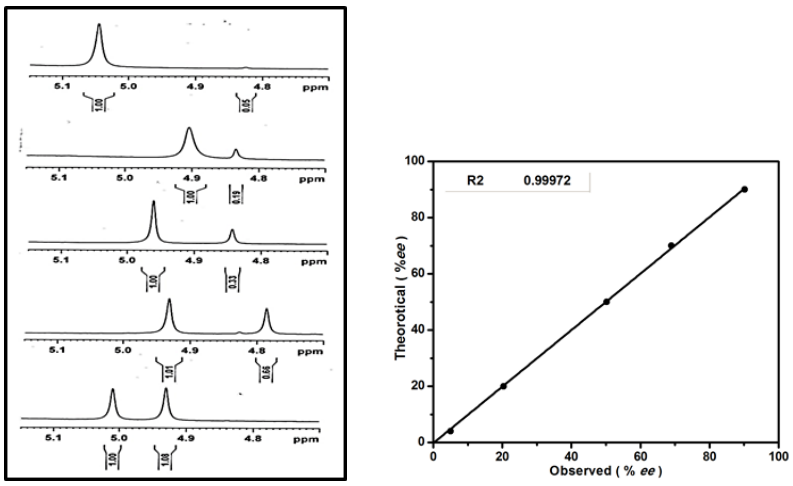

Figure 37 Selected region of ^{1}H NMR spectra of scalemic mixture of mandelic acid in the presence of (*R*)-**58** and its correlation between theoretical and observed %*ee* values (right)

4.2.2.4 Determination of Stoichiometry of the complex using UV-Visible Spectroscopy:

The molecular recognition of isomers of analyte by chiral CSA involve specific interactions and it is important to understand this by conducting further experiments. The stoichiometric ratio of the complex formed was obtained by continuous variation method using host (*R*)-**58** and guest (*R*)-**A-I** utilizing UV-Visible spectroscopy. The total concentration of host and guest in $CHCl_3$ was kept constant ($2.0X10^{-4}$ $molL^{-1}$), while the molar fraction of guest ([G]/([H]+[G])) was varied. This set of experiment was performed using (*R*)-**58** and (*R*)-mandelic acid to analyze the stoichiometry of the complex formed during recognition. A plot of the change in the absorption maximum (at 263 nm) *vs* increasing molar fraction of guest is depicted as Jobs plot in Figure 38. The UV-Vis absorption of the host reached a maximum when the molar fraction of the guest was 0.50, which signifies that host and guest form a 1:1 complex.

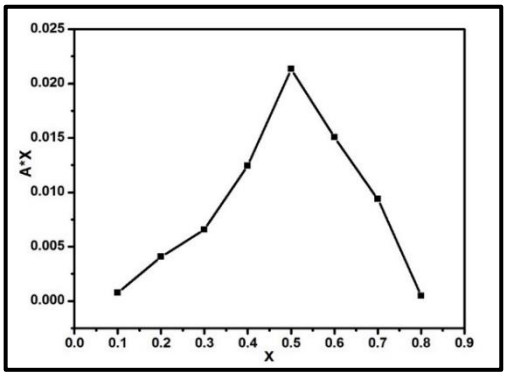

Figure 38 Jobs plot for (*R*)-**58** with (*R*)-MA (at 263 nm) using UV-Vis spectroscopy; Absorption maxima at 0.5 indicates 1:1 complex formation between host and guest; the total concentration of host and guest is 1.0 X 10^{-4} $molL^{-1}$

Using the same method, Jobs plot for receptors (*R*)-**54**, (*R*)-**58** and (*R*)-**59** with (*L*)-*N*-tosyl valine was carried out. The total molar concentration of the solution was maintained (1.0 X 10^{-4} $molL^{-1}$) while the molar fractions of the CSAs under study ((*R*)-**54**, (*R*)-**58** and (*R*)-**59**) as well as (*L*)-*N*-tosyl valine was varied and the change in absorbance was measured. The plot for change in absorbance (at 245 nm) *vs* molar fraction of (*L*)-*N*-tosyl valine presented that all the three CSAs showed a maxima at value 0.5 indicating that 1:1 complexes were formed between (*L*)-*N*-tosyl valine and all the three CSAs under study (Figure 39).

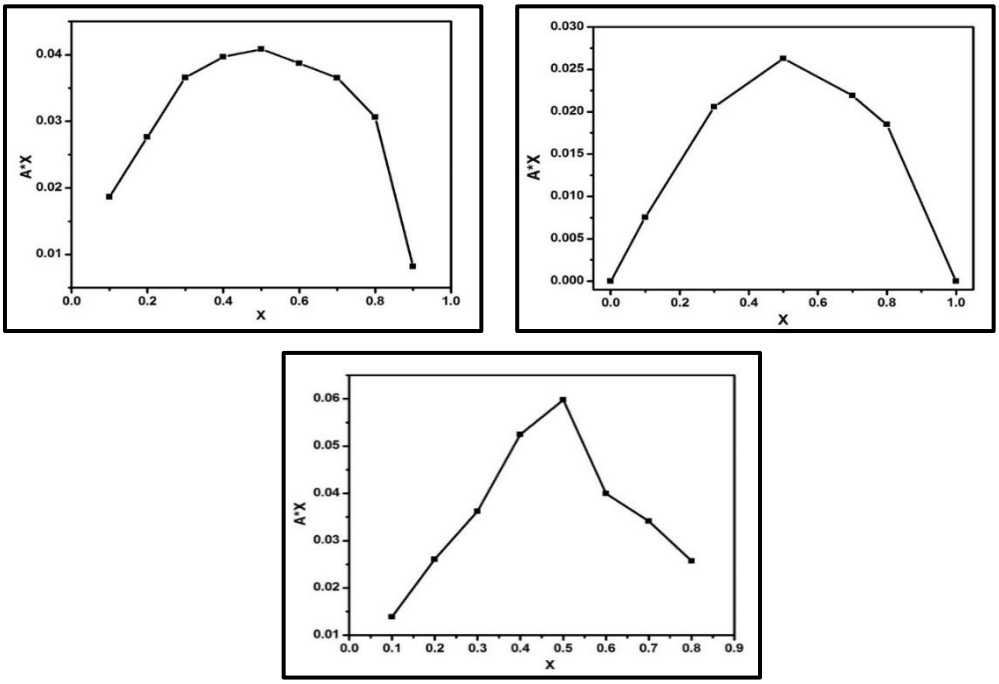

Figure 39 Jobs plot for (a) (*R*)-**54** (b) (*R*)-**58** (c) (*R*)-**59** with *L*-*N*-Tosyl Valine (at 245 nm) using UV-Vis spectroscopy; Absorption maxima at 0.5 indicates 1:1 complex formation between host and guest; the total concentration of host and guest is 1.0 X 10^{-4} $molL^{-1}$

4.2.2.5 Determination of Binding Constants using UV-Vis Spectroscopy:

UV-Visible spectroscopy is one of the best tools to study the host-guest binding due to its high sensitivity and easy operation. The changes in the intensities of absorption bands for chiral host upon complex formation is monitored by performing UV titrations. This can quantitatively determine the extent of complexation and hence the thermodynamics of molecular recognition.

For a fixed concentration of the host, the absorbance of all the hosts enhanced gradually with increase in concentration of each enantiomer of *R*-/*S*-**A-I** or *D*-/*L*-**AA-I**. The variation in the absorption intensity for the two enantiomers, indicated to their different interactions with the CSAs. The association constants (K_R and K_S for **A-I** or K_L and K_D for **AA-I**) and correlation coefficients (R) were determined by using modified Benesi-Hildebrand equation (plot of 1/ΔA versus 1/[G]).[68–70]

$$\frac{1}{A-Ao} = \frac{1}{Ka} * \frac{1}{C} + I$$

The binding constants for complexes formed between both the enantiomers of the guest with the chiral host were calculated from the slope of the plot. The correlation coefficients R (>0.99) for all the linear plots, confirms the formation of 1:1 complex between receptors

and the guest as well as reliability of the data. The CSAs under study are UV active, whereas the test analyte weakly absorbs in this region. For a fixed concentration of CSA **(*R*)-54** ($1X10^{-4}$M), increasing molar ratio of optically pure mandelic acid causes an increase in the absorbance of **(*R*)-54**. The change in the absorption intensity of **(*R*)-54** with both the enantiomers of mandelic acid varies to a different degree and this difference is proportionally related to the enantiomeric recognition of the CSA (Figure 40).

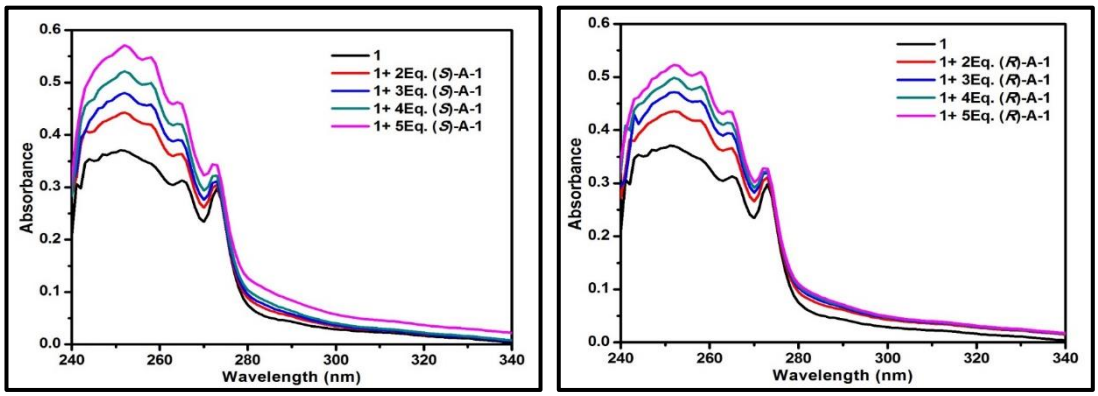

Figure 40 UV-Vis titration curve for (*R*)-**54** ($1X10^{-4}$M) with increasing molar ratio of (a) (*S*)-Mandelic acid $2X10^{-4}$M, $3X10^{-4}$M, $4X10^{-4}$M, $5X10^{-4}$M (b) (*R*)-Mandelic acid $2X10^{-4}$M; $3X10^{-4}$M; $4X10^{-4}$M; $5X10^{-4}$M (λ:265nm)

Bernesi-Hildebrand plot between the change in absorbance of (*R*)-**54** on addition of (*S*)-mandelic acid and (*R*)-mandelic acid respectively, is a linear fit plot giving the slope of which gives the value of K*s* and K_R.

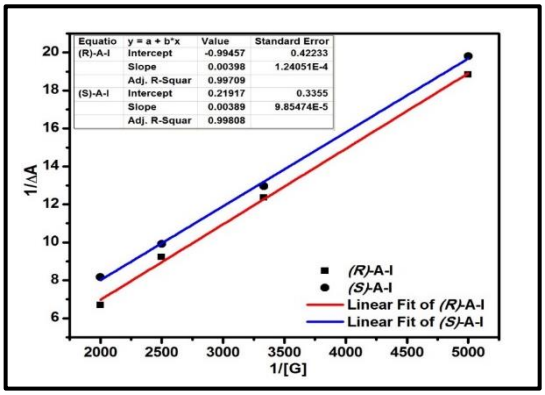

Figure 41 Benesi-Hildebrand plot for (*R*)-**54** with (*R*) and (*S*)-Mandelic acid showing a linear fit, plotted at λ_{abs} 265nm

For all the three CSAs (*R*)-**54**, (*R*)-**58** and (*R*)-**59**, the value of K_R is quite high compared to K_S for **A-I**, concluding that they form stronger complexes with (*R*)-**A-I** as compared to its (*S*)-isomer.

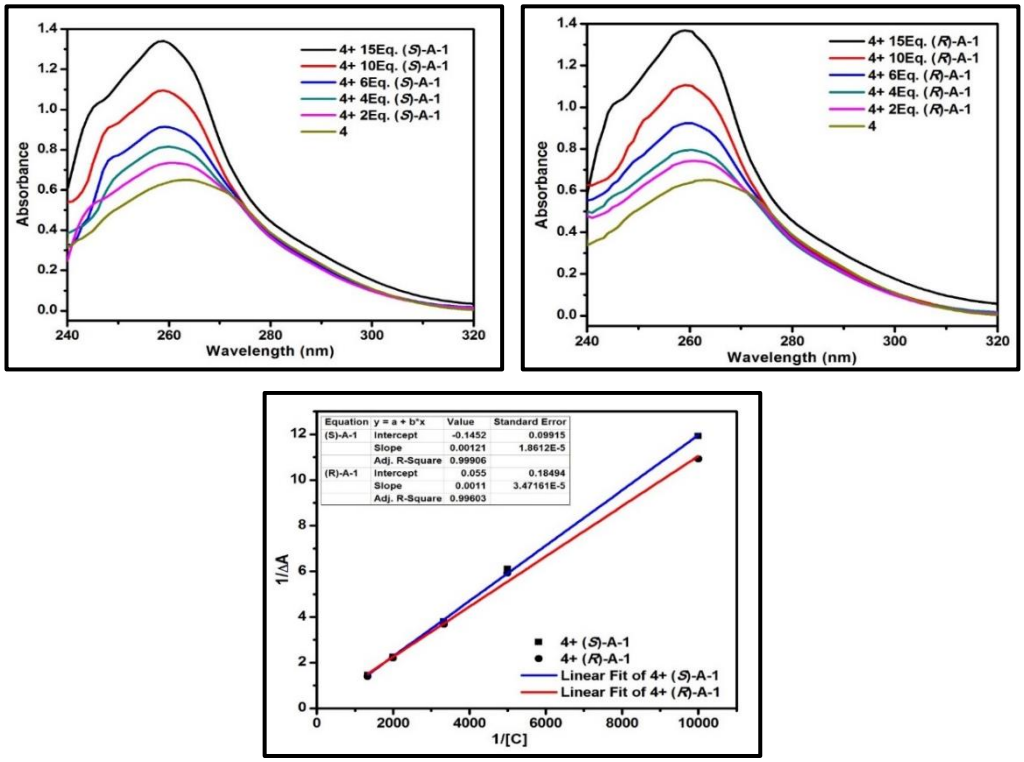

Figure 42 UV-Vis titration curve for (*R*)-**58** (5X10^{-5}M) with increasing molar ratio of: (a) (*S*)-**A-1** (b) (*R*)- **A-1** 1X10^{-4}M; 2X10^{-4}M; 3X10^{-4}M; 5X10^{-4}M; 7.5X10^{-4}M (c) Benesi-Hildebrand plot for (*R*)-**58** with (*R*) and (*S*)-**A-1** showing a linear fit, plotted at λ_{abs} 263nm

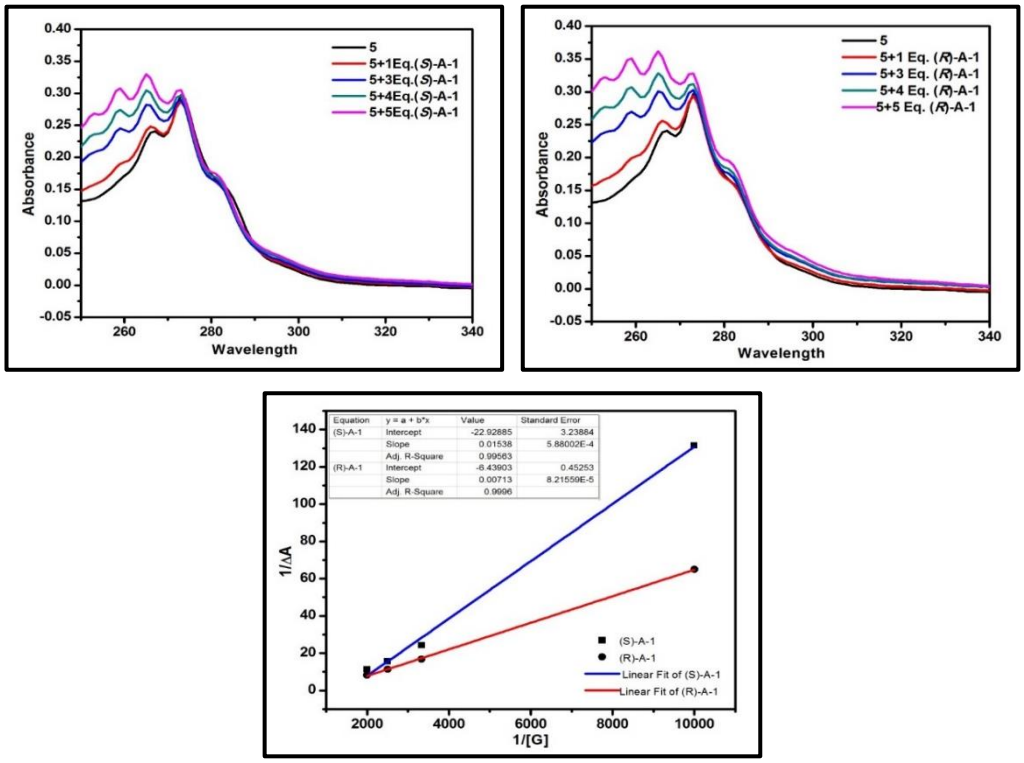

Figure 43 UV-Vis titration curve for (*R*)-**59** (5X10^{-5}M) with increasing molar ratio of: (a) (*S*)-**A-1** (b) (*R*)-**A-1**5X10^{-5}M; 1.5X10^{-4}M; 2X10^{-4}M; 2.5X10^{-4}M (c) Benesi-Hildebrand plot for (*R*)-**59** with (*R*) and (*S*)-**A-1**showing a linear fit, plotted at λ_{abs} 267nm

The binding constant values are the maximum for (*R*)-**58**, confirming the formation of stronger complex of **A-I** with (*R*)-**58** amongst the three CSAs under present study.

Similar study was performed for *N*-tosyl valine (**AA-I**) with all the three receptors (*R*)-**54**, (*R*)-**58** and (*R*)-**59**. All the three receptors showed stronger binding with (*D*)-enantiomer while (*R*)-**59** showed the highest value for K_D indicating its better complexation.

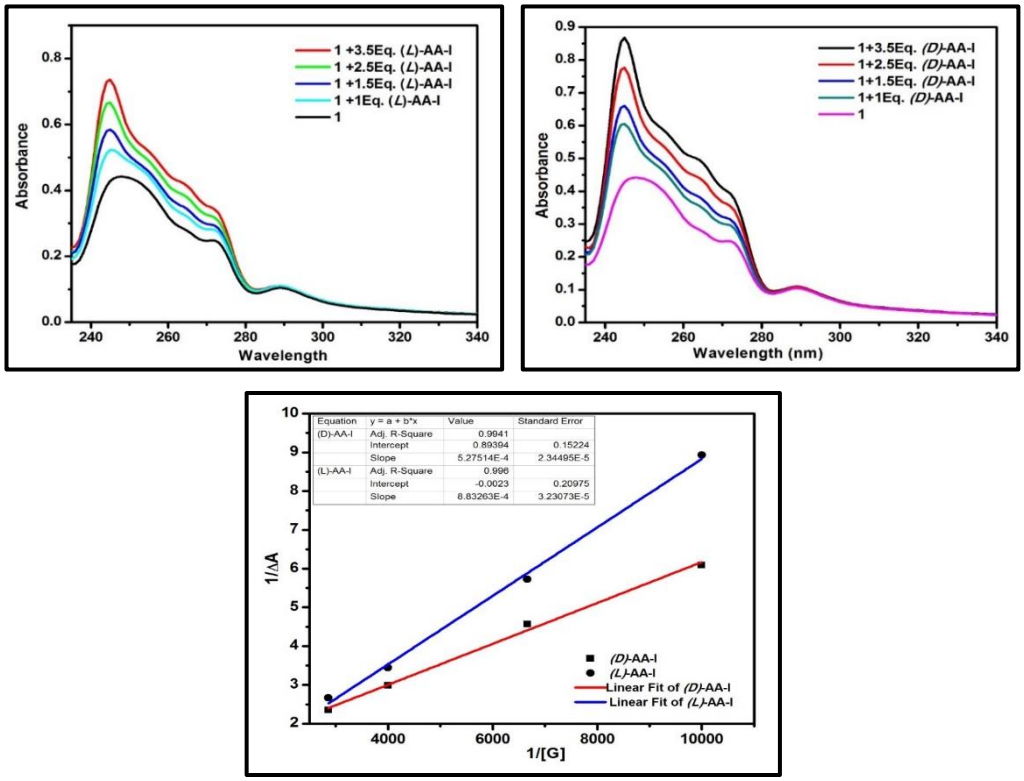

Figure 44 UV-Vis titration curve (*R*)-**54** ($1.2X10^{-4}$M) with increasing: (a) (*L*)-**AA-1** (b) (*D*)-**AA-1** $1.2X10^{-4}$M; $1.8X10^{-4}$M; $3X10^{-4}$M; $4.2X10^{-4}$M (c) Benesi-Hildebrand plot for (*R*)-**54** with (*D*) and (*L*)-**AA-1** showing a linear fit, plotted at λ_{abs} 245nm

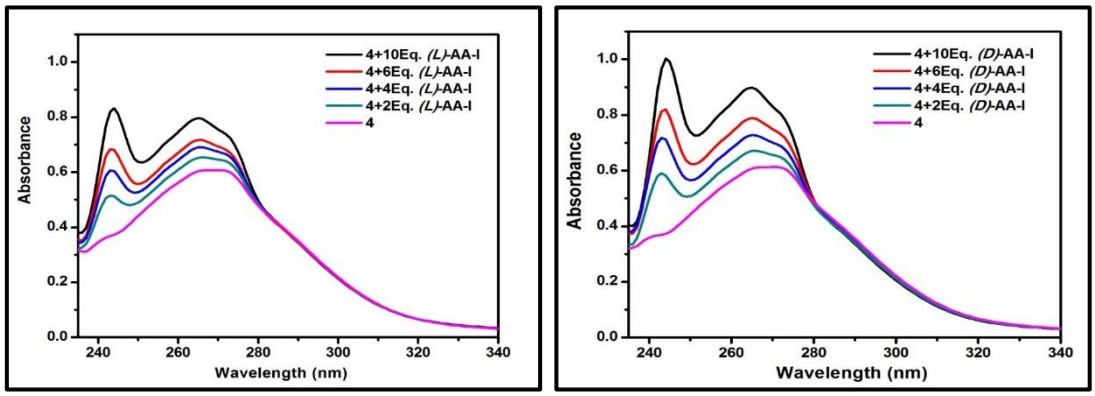

Figure 45 UV-Vis titration curve for (*R*)-**58** at $5X10^{-5}$M concentration with increasing molar ratio of (a) (*L*)-**AA-1** (b) (*D*)- **AA-1** $1X10^{-4}$M; $2X10^{-4}$M; $3X10^{-4}$M; $5X10^{-4}$M (λ:245nm)

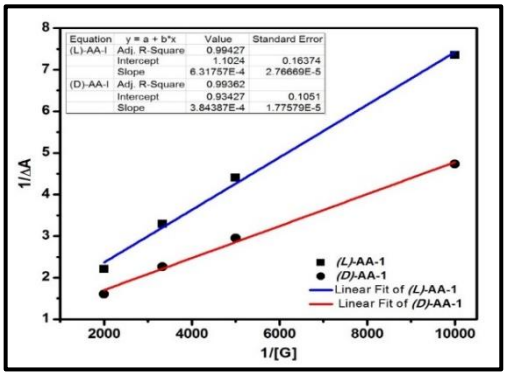

Figure 46 Benesi-Hildebrand plot for (*R*)-**58** with (*D*) and (*L*)-**AA-1** showing a linear fit, plotted at λ_{abs} 245nm

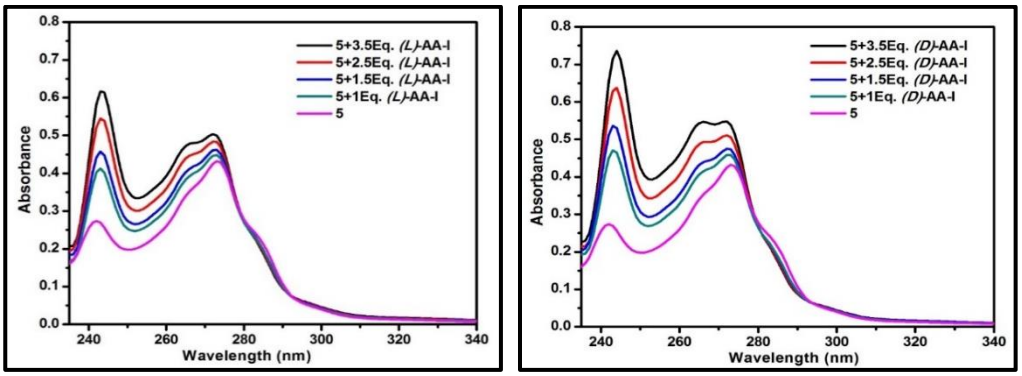

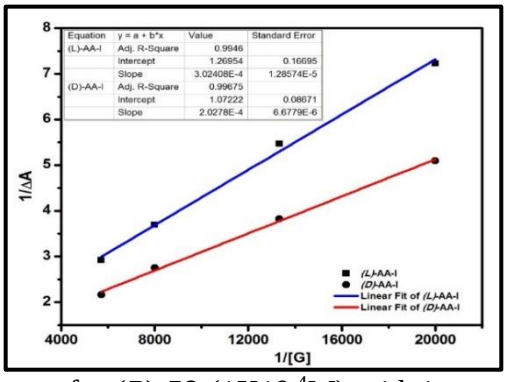

Figure 47 UV-Vis titration curve for (*R*)-**59** (1X10^{-4}M) with increasing: (a) (*L*)-**AA-1** (b) (*D*)-**AA-1** 1X10^{-4}M; 1.5X10^{-4}M; 2.5X10^{-4}M; 3.5X10^{-4}M (c) Benesi-Hildebrand plot of (*R*)-**59** with (*D*) and (*L*)-**AA-1** showing a linear fit, plotted at λ_{abs} 242nm

The binding constants for complexes formed between both the enantiomers of the guest with the chiral host were calculated from the slope of the plot and the associated change in Gibbs free energy was also determined (Table 5 & 6).

Table 5 Association constant K for UV response with CSAs

Substrate	(*R*)-54	(*R*)-58	(*R*)-59
(*R*)-**A-I**	257.0694	909.0909	140.2525
(*S*)-**A-I**	251.2563	826.4463	65.0195
(*D*)-**AA-I**	1895.6843	2601.5448	4931.5428
(*L*)-**AA-I**	1132.1656	1582.8871	3306.7908

Table 6 Gibbs free energy (ΔG)[a] of CSAs with isomers of substrates

Substrate	(*R*)-54	(*R*)-58	(*R*)-59
(*R*)-**A-I**	-13.7558	-16.8868	-12.2539
(*S*)-**A-I**	-13.6991	-16.6506	-10.3483
(*D*)-**AA-I**	-18.7085	-19.4931	-21.0784
(*L*)-**AA-I**	-17.4308	-18.2615	-20.0877

[a]Calculated with ΔG = - RT lnK

The results of binding study were in accordance with the conclusions drawn by NMR experiments (Table 3 and 4) where **(*R*)-58** showed the best recognition towards **A-I** and **(*R*)-59** showed the best results with **AA-I**.

4.2.2.6 Determination of Primary Interaction with Acidic Substrates:

The basic interaction between the CSA and **A-1** should be proton transfer to nucleophilic nitrogen of amine, resulting in its salt formation with carboxylate moiety. This was established by recording FT-IR spectra of mixture of **A-1** and (*R*)-**58**, where the carbonyl stretch (1716 cm^{-1}) disappeared and the new strong peaks for $-COO^-$ appeared (1622 and 1608 cm^{-1}) (Figure 48).

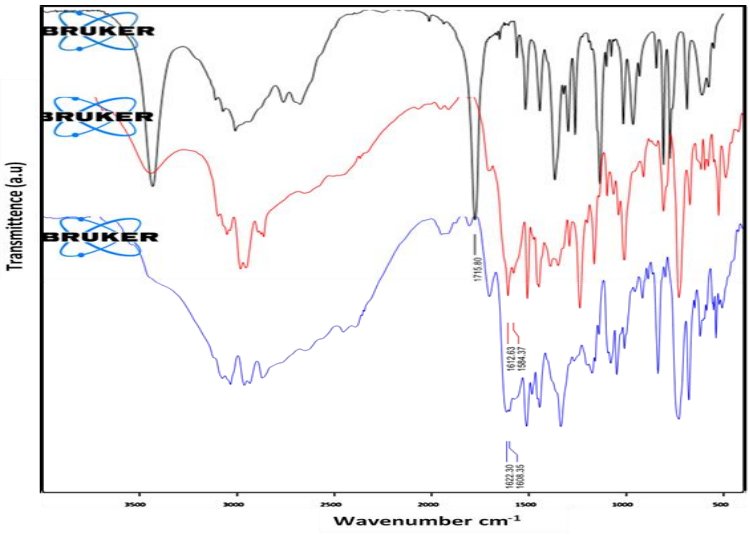

Figure 48 IR Spectra of: (a) (±) Mandelic acid (b) with (*R*)-**58** (c) with (*R*)-**59**

4.2.2.7 Crystallographic Discussion on Diastereomeric Salts:

The salt of (*R*)-**58** and (*S*)-Mandelic acid (**A-I**) showing the atom-numbering scheme are depicted in Figure 49. The thermal ellipsoids are drawn at the 50% probability level, and H atoms are shown as small spheres with arbitrary radii. Compound (*R*)-**58** and (*R*)-Mandelic acid (**A-I**) crystallized in the chiral monoclinic space group $P2_1$. The crystal structure contained one molecule of each (*R*)-**58** and (*R*)-Mandelic acid (**A-I**) in the asymmetric unit.

The C−O bond lengths (~1.243−1.266Å) of acidic group show that proton transfer has occurred from (*R*)-MA to amine moiety of the (*R*)-**58**, revealing the complex to be a salt. In the crystal structure both molecules are stitched to each other through conventional N-H···O hydrogen bond.

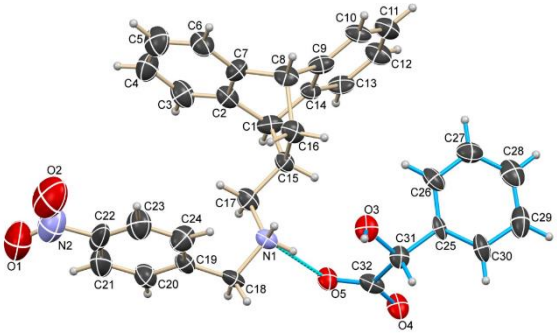

Figure 49 The ORTEP of the salt of (*R*)-58 and (*R*)-MA

The association is extended helically across the crystallographic 2_1 screw axis (*b*-axis) through O-H···O hydrogen bond between hydroxyl OH of (*R*)-MA and carboxyl O of (*R*)-**58** (O3-H3A···O5; H3A···O5=1.947Å, O3···O5=2.670Å and ∠O3-H3A···O5=147°) as well as N-H···O hydrogen bond between other N-H group of (*R*)-**58** and carboxyl O of (*R*)-MA (N1-H1B···O4; H1B···O4=1.902Å, N1···O4=2.779Å, ∠N1-H1B···O4=168°). The adjacent helices along the c-axis are loosely packed through van der Waals forces to generate the 2D packing on the *bc* plane (Figure 50 & 51).

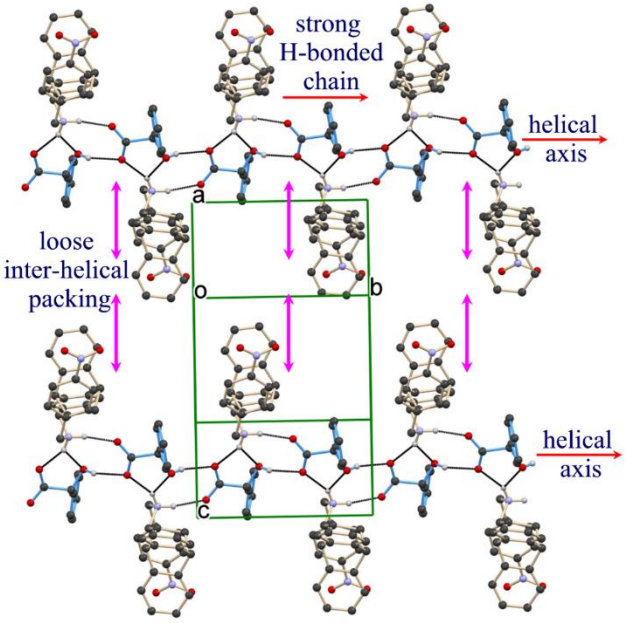

Figure 50 Molecular packing of the salt of (*R*)-58 and (*R*)-MA across the helical axis

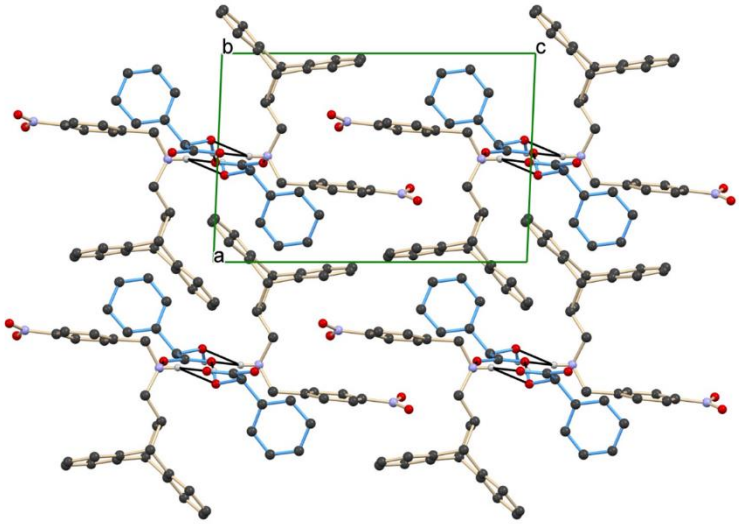

Figure 51 Molecular packing of the salt of (*R*)-58 and (*R*)-MA down the helical axis

The crystals of the other diastereomeric salt pair, (*R*)-**58** and (*S*)-MA belongs to orthorhombic chiral space group $P2_12_12_1$. The crystal structure contains three molecules of each (*R*)-**58** and (*S*)-MA along with a molecule of toluene as a solvent of crystallization in the asymmetric unit. All the three molecules of (*R*)-**58** are labelled with trailers A, B and C and three molecules of (*S*)-MA are labelled with trailers D, E and F. The C-O bond lengths of carboxylic acid groups (~1.248−1.263Å) show that proton transfer has occurred from (*S*)-MA to amine moiety of the (*S*)-**58**, revealing the complex to be a salt (Figure 52).

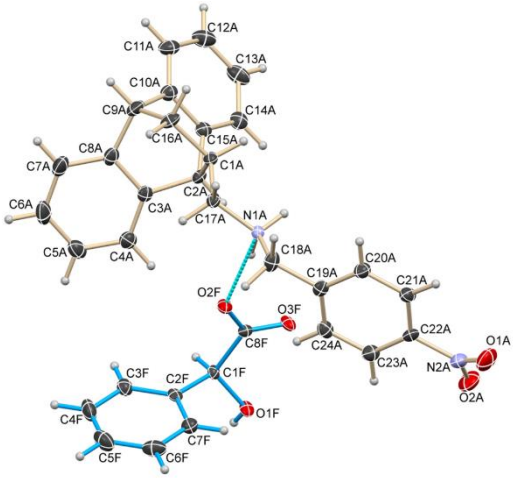

Figure 52 The ORTEP of the alt of (*R*)-58 and (*S*)-MA (A-I)

In the crystal structure molecule A (green) of (*R*)-**58** generates a helical assembly along the *a*-axis with molecule F of (*S*)-MA (cyan) through N-H···O hydrogen bonding interactions namely, N1A-H1A1···O2F (H1A1···O2F=1.854Å, N1A···O2F=2.736Å and ∠N1A-H1A1···O2F=162.6°), N1A-H1A2···O3F (H1A2···O3F=1.853Å, N1A···O3F=2.754Å and

∠N1A-H1A2···O3F=169.8°). On the other hand both molecules B (blue) and C (red) of (*R*)-**58** associate with molecules D and E of (*S*)-MA to generate the composite helical assemblies across the crystallographic 2_1-screw axis (a-axis) through another sets of conventional N-H···O hydrogen bonds. The hydrogen bonds namely N1B-H1B1···O2E (H1B1···O2E=1.877Å, N1B···O2E=2.735Å, ∠N1B-H1B1···O2E=156.5°), N1B-H1B2···O3D (H1B2···O3D=1.781Å, N1B···O3D=2.677Å and ∠N1B-H1B2···O3D= 167.5°), N1C-H1C1···O2D (H1C1···O2D=1.837Å, N1C···O2D=2.722Å, ∠N1C-H1C1···O2D=163.7°) and N1C-H1C2···O3E (H1C2···O3E=1.901Å, N1C···O3E=2.802Å, ∠N1C-H1C2···O3E=170.5°) are very string and close to linearity. In the helical assembly the (*S*)-MA molecules are also associated with each other through O-H···O hydrogen bonds. The molecule F of (*S*)-MA form helical assembly through O1F-H1FO···O3F (H1FO···O3F =1.822Å, O1F···O3F=2.660Å, ∠O1F-H1FO···O3F=176.4°) hydrogen bond along the helical assemblies of molecule A of (*R*)-**58**. Both molecules D and E of (S)-MA generate the helical assembly across the helices of molecules B and C of (*R*)-**58** through O-H···O hydrogen bonding interactions involving O-H and carboxyl oxygen of (*S*)-MA, (H1DO···O2E=1.863Å, O1D···O2E=2.675Å, ∠O1D-H1DO···O2E=162.2°; H1EO···O2D =1.904Å, O1E···O2D=2.686Å, ∠O1E-H1EO···O2D=154.5°).

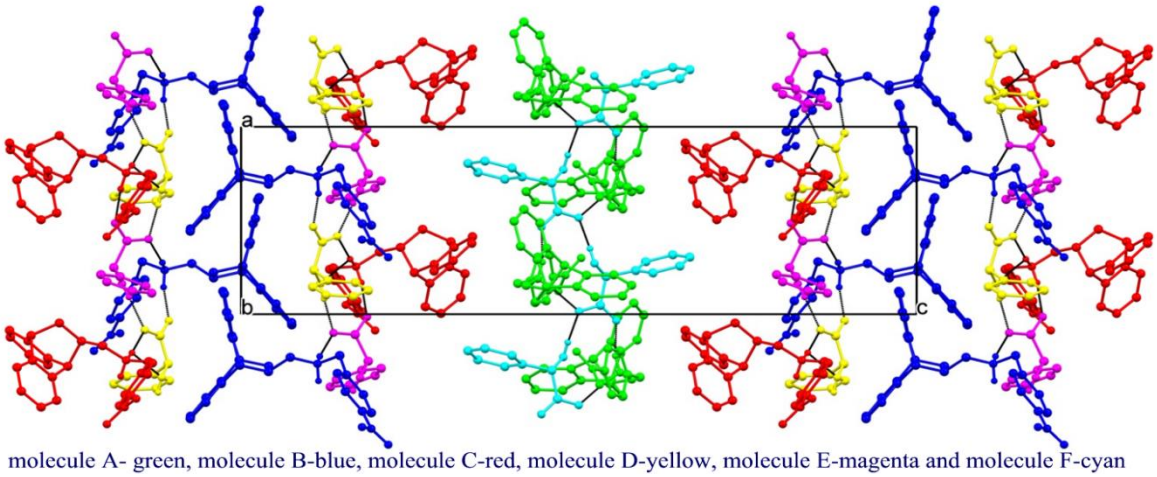

molecule A- green, molecule B-blue, molecule C-red, molecule D-yellow, molecule E-magenta and molecule F-cyan

Figure 53 Helical assemblies of the molecules of (*R*)-58 and (*S*)-MA across the crystallographic 21-screw axis (a-axis)

Hence, the helical assemblies of molecule A of (*R*)-**58** and molecule F of (*S*)-MA and the composite helix of molecules B and C of (*R*)-**58** and molecules D and E of (*S*)-MA are loosely associated to each other through van der Waals interactions along the c-axis (Figure 53).

A close examination of crystal structure of (*R*)-**58** with MA shows that one molecule of MA undergoes double hydrogen bonding with the C16-*H* as well as with C21A-*H*. Assuming that the corresponding crystal structure of (*R*)-**54** with MA undergoes the similar interactions, one can conclude that the better recognition of (*R*)-**58** towards discrimination of MA is attributed to the more acidic nature of the C21A-*H*. This hydrogen atom will be more electron deficient due to the presence of electron withdrawing $–NO_2$ group at the *meta* position leading to stronger complexation with MA. Lack of any substituent on the benzyl moiety of (*R*)-**54**, renders the –H attached to C21A atom to be relatively electron rich causing a weaker interaction with the O atom of –COO group of MA leading to weaker complexation. Hence, the presence of $–NO_2$ group at the *para* position in (*R*)-**58** facilitates a stronger interaction with MA leading to better recognition of MA as compared to (*R*)-**54**. This hypothesis corroborates with the values of resolution of NMR signals in CSA experiments.

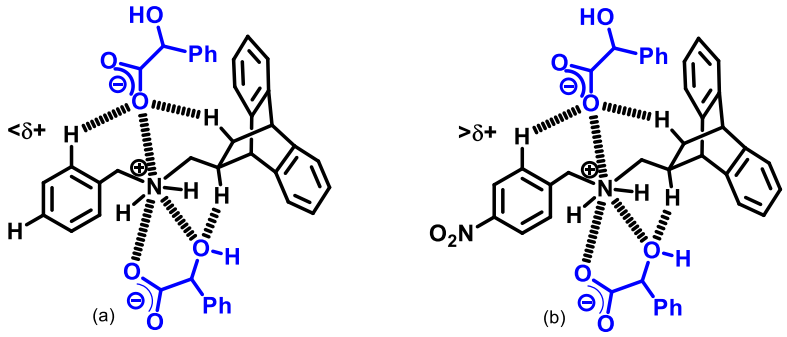

Figure 54 Proposed model to show electronic effect on roof shape CSA for molecular recognition. In (a), the benzyl amine (*R*)-54 has relatively weaker Ar-H···HO interaction as compared to one for (*R*)-58; as in (b).

4.2.3 Effect of distance of chiral center from amine group on chiral recognition:

Another parameter that greatly affects the chiral discrimination ability of a host, is the distance of the chiral center from the group undergoing binding interactions. Correlating the resolving power of CSA with the distance between the primary binding site (in our case –NH group) and the chiral center could enable us to understand the distance-geometry relationship and its effect on molecular recognition. In a few reports, it has been mentioned that an inverse relationship exists between the flexibility of the primary binding site and chiral resolution or the conformational rigidity dominates the binding interactions.[71]

The derivatives of chiral secondary roof shape amines synthesized by us in the earlier sections possess chiral center associated with the roof shape moiety to be one carbon away from the secondary amine group. The primary site of interaction is one sp^3 carbon away from the chiral center, providing some amount of molecular flexibility to the molecule. In order to make the amines conformationally more rigid, we focused our synthesis towards a chiral roof shape secondary amine where the amino group is directly attached to the chiral center of the roof shape moiety and compare their CSA activity. We expect that the effect of molecular recognition in these ligands will be more pronounced due to the conformational rigidity of the amino group and its close proximity to the chiral center.

4.2.3.1 Synthesis of the ligands:

Since carboxylic acids cannot only be converted into a large number of derivatives like amides, anhydrides, esters, carbamates *etc*. but their importance in the fields of biopolymers, food industry, medicinal and pharmaceuticals also makes them important synthetic targets. We utilized the roof shape ester **(50)** synthesized in the earlier section, to access roof shape acid **(60)** in almost quantitative yield by subjecting it to hydrolysis in basic condition using KOH in methanol (Scheme 14). The ^{1}H NMR spectra for **60** showed disappearance of the signals for ethyl group protons, which was also confirmed by ^{13}C NMR spectra showing a peak at **δ** 179.7 corresponding to the C=O carbon atom. The IR spectra clearly showed the disappeareance of band from 1727 cm^{-1} for **50** for C=O stretching frequency for ester group and appearance of a sharp band 1707 cm^{-1} for **60** corresponding to the C=O stretching frequency for acid group.

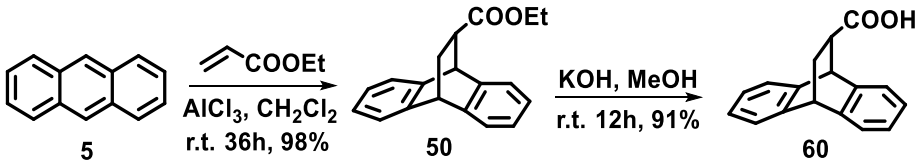

Scheme 14 Synthesis of roof shape racemic acid (60)

We planned to synthesize amide derivative **(61)** which can be obtained from condensation of the acid **(60)** with primary amine. It is necessary to activate the carboxylic acid by the use of coupling reagents prior to the reaction with amine. The most common approach used for the synthesis of amide is the use of thionyl chloride or phosphorous pentachloride for the activation of acid to acid chloride followed by the attack by amine. However, these reagents are known to be harsh and possess corrosive nature making them reagents of less

choice. The coupling reagent we utilized was cyanuric chloride which is environmentally benign and hence green. Utilizing this strategy, acid **(60)** was subjected to amide formation in the presence of cyanuric chloride as the coupling reagent and triethyl amine as base in acetone. This reaction smoothly proceeded at room temperature furnishing our desired product in good yield. The formation of **61** was confirmed by its ^{1}H NMR spectra which showed two broad singlets at **δ** 5.45 and 5.05 due to the two amide protons and a peak at **δ** 176 in ^{13}C NMR for the carbon of amide group. Having synthesized **61**, it was then subjected to Hofmann rearrangement which is an efficient method to convert amides into carbamates *via* C-C to C-N bond rearrangement. This reaction is important in synthetic organic chemistry as it provides a mode to access a class of products which is difficult to synthesize using other routes. We used dibromamine-T (which is readily prepared from Chloramine-T and Br_2) in presence of DBU in methanol giving the corresponding methyl carbamate **(62)** in moderate yield (Scheme 15).

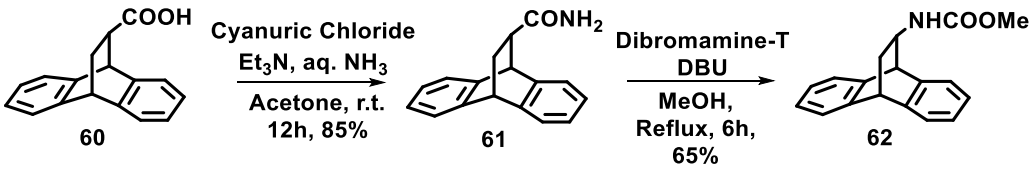

Scheme 15 Synthesis of roof shape carbamate derivative (62) as masked amine

The ^{1}H NMR for **62** showed the presence of a sharp singlet for three protons at **δ** 3.65 due the –C*H*$_3$ protons and a broad singlet at **δ** 3.74 for the –N*H* proton of the carbamate unit. The characteristic signals of a doublet and triplet having a coupling constant of 2.0 and 1.6 Hz at **δ** 4.4 and 4.29 respectively confirm the structure of the molecule. ^{13}C NMR spectra shows a signal at **δ** 156.34 which corresponds to the carbamate carbon atom. The IR spectra shows a sharp band at 3312 cm^{-1} due to N-H stretching and another sharp band at 1690 cm^{-1} due to the C=O stretching frequency of the carbamate unit. The HRMS spectra for this compound showed a molecular ion peak at 302.1121 which is in agreement with the exact mass of the molecule.

In order to access the roof shape amine where the amino group is directly attached to the roof shape moiety, the racemic **62** was subjected to deprotection using tetrabutyl ammonium fluoride in refluxing THF (Scheme 16).[72] The formation of the desired product **(63)** was confirmed by the simplification of the ^{1}H NMR spectra. The disappearance of the signal corresponding to –C=O group in the ^{13}C NMR as well as IR spectra are clear indication of

the conversion. This roof shape amine can be utilized for the synthesis of various secondary amines using the strategies stated earlier.

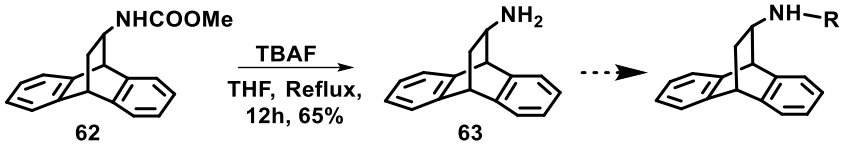

Scheme 16 Deprotection of carbamate (62) to amine (63) for accessing roof shape secondary amines

4.2.3.2 Resolution and Determination of Absolute Configuration:

The Diels-Alder reaction between anthracene and ethyl acrylate gives **50** as a racemic mixture which is confirmed by chiral HPLC showing two well resolved peaks on CHIRALPAK IC using 5% mixture of isopropanol in hexane with flow rate 1mL/min at UV 254nm (Figure 55).

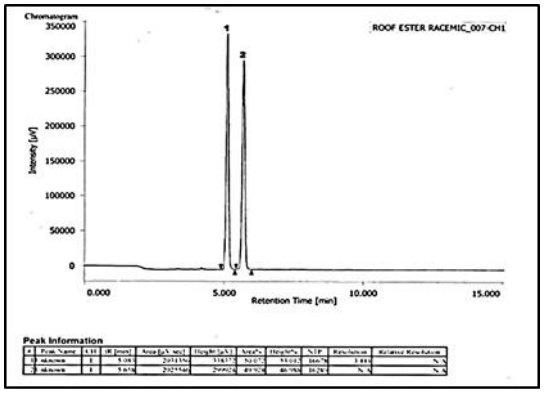

Figure 55 HPLC chromatogram for racemic 50

In order to resolve this molecule, we synthesized roof shape acid which could be effectively subjected to resolution using various means like co-crystallization with chiral bases or diastereomer formation. The synthesized acid **(60)** was subjected to crystallization with various chiral bases. Commercially available quinine, brucine and cinchonidine were utilized in a 1:1 ratio for diastereomeric salt formation in a variety of solvents. The crystals formed were carefully separated and the roof shape acid **(60)** was regenerated by mild acidification of the aqueous layer containing the salt. The roof shape acid **(60)** was extracted in the organic layer, concentrated and subjected to chiral HPLC. As we were unable to develop conditions for the accurate analysis of this roof shape acid, we esterified it to its ethyl ester derivative which was successfully analyzed using chiral HPLC. However, we failed to obtain *ee* >50% for the acid in spite of repeated efforts (Figure 56).

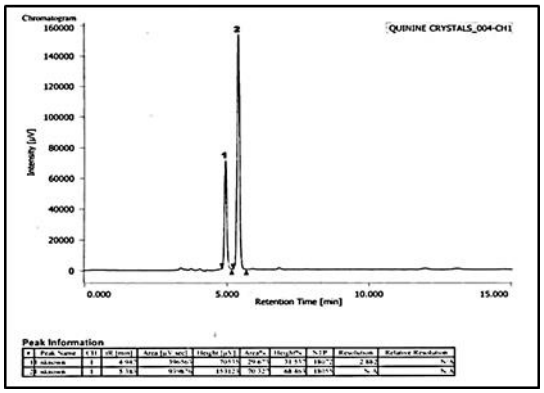

Figure 56 HPLC chromatogram for compound 50 showing 50%*ee* obtained by co-crystallization of acid (60) with brucine

Hence, we modified our strategy to the formation of diastereomers with optically pure α-methyl benzyl amine. The racemic acid **(60)** was subjected to amide formation with (*S*)-α-methyl benzyl amine using cyanuric chloride and triethyl amine in acetone (Scheme 17). The two diastereomers hence obtained were subjected to crystallization in various organic solvents. Best result was obtained in chloroform-hexane (30%) where one diastereomer ***(R,S)*-64** crystallized out from the racemate whereas the other diastereomer ***(S,S)*-64** remained in the mother liquor.

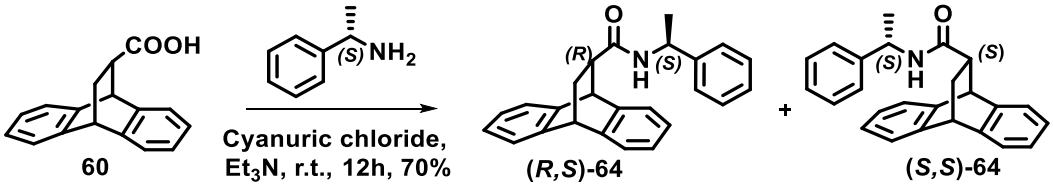

Scheme 17 Resolution of (60) by formation of diastereomeric amide

The diastereomeric purity (*de*) of the compounds was established by ^{1}H NMR spectra and was found to be >98% *de*. For racemic sample of **64**, characteristic two doublets were observed in the aliphatic region at **δ** 1.36-1.35 (d, *J*=6.8Hz, 3H) and 1.29-1.28 (d, *J*=6.8Hz, 3H) corresponding to the methyl group in both the diastereomers. The ^{1}H NMR of the crystallized diastereomer showed a sharp doublet at **δ** 1.35 corresponding to the –C*H*$_3$ protons of the chiral amine unit which appears at **δ** 1.28 for the diastereomer that remains in the mother liquor. The α-proton of the chiral amine moiety appears as a quartet at **δ** 5.0 and the presence of characteristic signals of doublet and triplet for the bridge head protons of the roof shape moiety can be seen at **δ** 4.5 and 4.3 respectively confirming the formation of the desired chiral amide.

The absolute configuration of the chiral center of roof shape moiety was determined by carrying out single crystal XRD for the diastereomer that crystallized out. The absolute configuration of the roof shape moiety was found to be *R* with respect to the known chiral center of the amine which was *S* (Figure 57). Hence we concluded that out of both the diastereomers present in the racemate, **(*R,S*)-64** crystallized out in the form of colourless needles and **(*S,S*)-64** remained in the mother liquor.

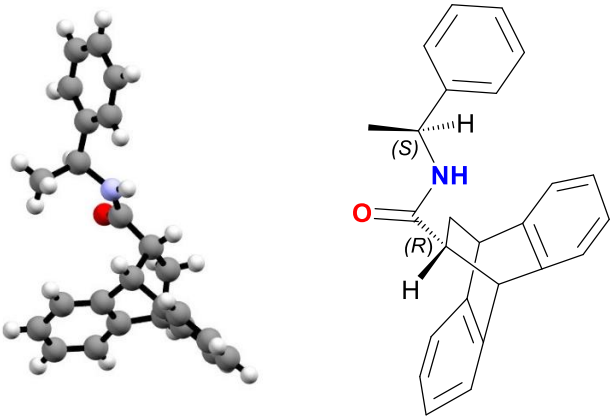

Figure 57 ORTEP diagram of the crystallized compound establishing the configuration at the roof shape chiral center to be (*R*)

Having separated the amides in their optically pure form, the cleaving of the chiral auxiliary to obtain roof shape primary amide in its enantiomerically pure form was necessary. The synthesized chiral amide ***(R,S)*-64** was successfully hydrolyzed using *p*-toluenesulfonic acid in refluxing toluene to obtain enantiomerically pure ***R*-61**. The optically pure primary amide ***R*-61** was then subjected to Hofmann rearrangement using conditions developed before to furnish **62** (Scheme 18).

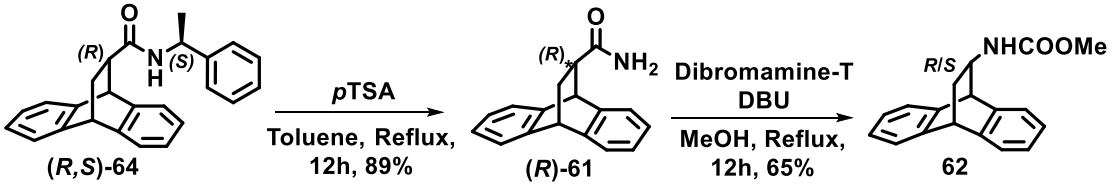

Scheme 18 Synthesis towards optically active carbamate 62

Chiral HPLC for racemic **61** showed two well resolved peaks at t_R 7.1 and 8.2 mins with almost equal peak areas. The enantiomeric purity of ***R*-61** was determined to be 96% with the first major peak appearing at t_R 7.1 followed by a minor peak at t_R 8.3 mins having area under the peak to be 98% and 2% respectively (Figure 58). Hence, we can assign the first peak that appears in the HPLC chromatogram for racemic **61** to correspond to *R*-enantiomer and the peak that appears later corresponds to the *S*-enantiomer.

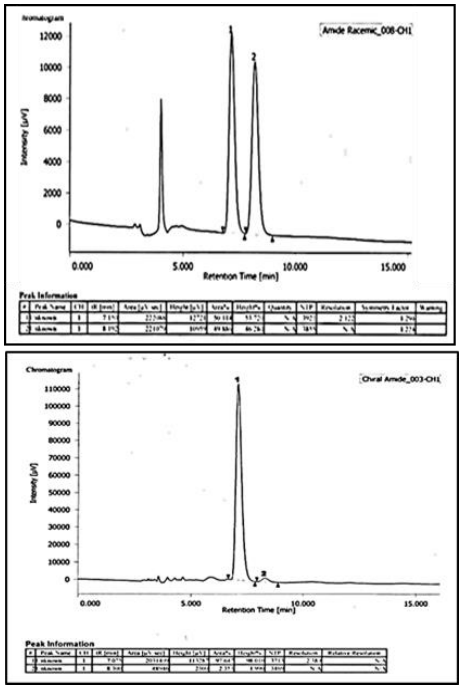

Figure 58 HPLC chromatogram for 61 showing (a) racemic (b) 96%*ee*

The carbamate **62** was also analyzed using chiral HPLC to determine its enantiomeric purity (Figure 59).

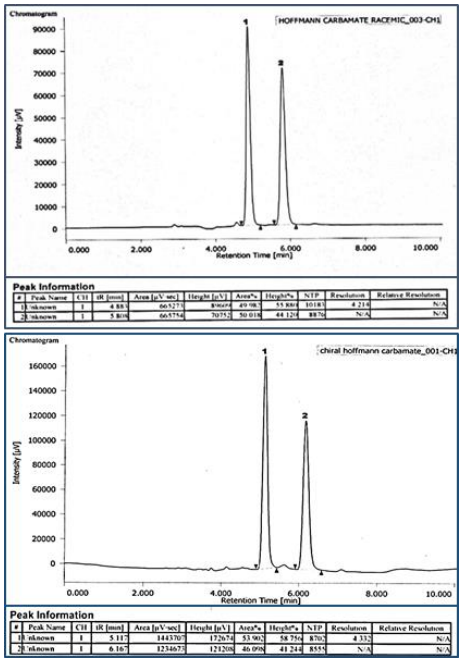

Figure 59 HPLC chromatogram for 62 showing (a) racemic (b) from (*R*)-61

Chiral HPLC for racemic **62** on Chiralcel OD-H using 20% IPA-hexane as the mobile phase, showed two well resolved peaks at t_R 5.1 and 6.2 mins with almost equal peak areas. However, the enantiomeric purity of ***R*-61** which was determined to be 96% *ee* diminished

completely during the course of reaction and **62** underwent complete racemization. Hence, even though the conversion from **61** to **62** occurred in good yield, it lead to complete racemization of the product. Hence, we were unsuccessful in obtaining enantiomerically pure **62** from ***R*-61**. The modification or change in the reaction conditions involving the use of NBS-DBU,[73,74] NaOH-Br_2, ArI-Oxone[75] and NBS-NaOMe[76] did not lead us to obtain the desired **62** in enantiomerically pure form. All the methods mentioned, gave moderate yields with complete racemization during the course of reaction. Having failed in carrying out resolution in the early stages of the synthesis, we moved towards the resolution of roof shape amine, hence, carrying out resolution in the later stages of synthesis.

We employed the use of various chiral acids like (*R*)-mandelic acid, (*S*)-camphor sulfonic acid, *L*-tartaric acid and *L*-dibenzoyl tartaric acid for the 1:1 diastereomeric salt formation in a variety of solvent systems. However, we were unable to obtain resolution of roof shape amine **63** and hence we resort to diastereomer formation utilizing a chiral auxiliary. (*R*)-Menthyl chloroformate was the reagent of choice due to its commercial availability and easy cleavage at a later stage of resolution. Diastereomeric carbamate mixture was obtained by the reaction of racemic **63** with (*R*)-menthyl chloroformate in the presence of triethyl amine as base in dichloromethane (Scheme 19).

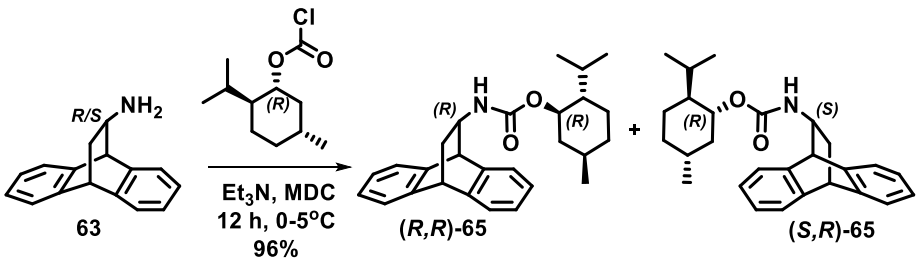

Scheme 19 Resolution of amine 63 by forming diastereomeric menthyl carbamate

The diastereomeric carbamate mixture was purified by column chromatography on silica gel and subjected to crystallization. Slow evaporation of a solution of the mixture from hexane lead to the formation of plate like crystals. These crystals were carefully separated and were analyzed using SCXRD to confirm the structure and to determine the absolute configuration of the chiral center associated with the roof shape moiety (Figure 60). It was seen that with respect to the fixed stereochemistry of the menthyl unit which is (*R*), the absolute configuration obtained for the chiral center associated with the roof shape moiety is also (*R*). Hence the diastereomer (*R,R*)-**65** crystallized out and (*S,R*)-**65** remained in the mother liquor.

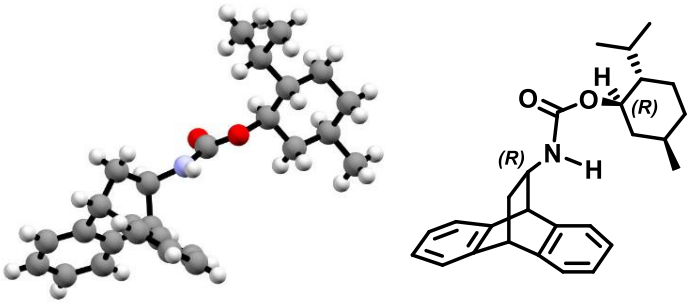

Figure 60 ORTEP diagram of the crystallized diastereomer showing the stereochemistry at the chiral center of roof shape moiety to be (*R*)

The crystals were carefully separated and the mother liquor was concentrated to obtain white solid. Both the samples were subjected to chiral HPLC on Chiralcel OD-H using a solvent mixture of 5% IPA-hexane as mobile phase and a flowrate of 1mL/min.

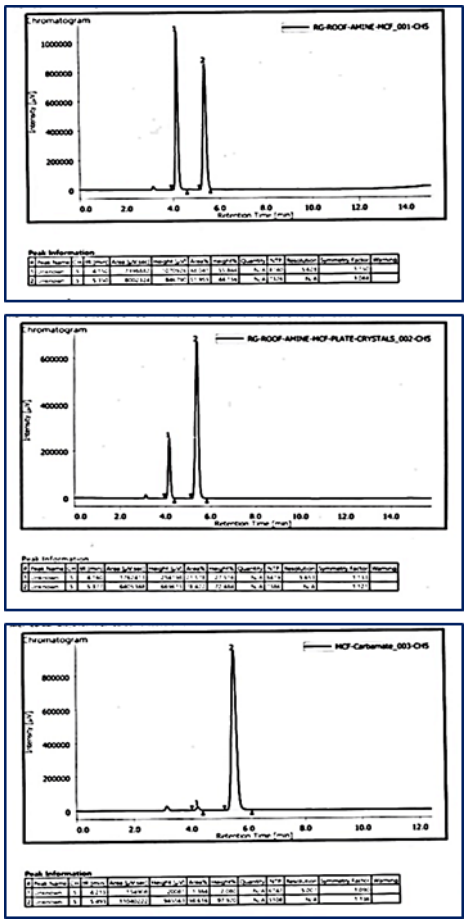

Figure 61 HPLC chromatogram of diastereomeric carbamate 65 (a) racemic (b) 57% *de* (c) 97% *de*

Racemic sample showed two sharp well resolved peaks at t_R 4.15 and 5.35 possessing equal area under the curve. The both the crystals and mother liquor were found to be enriched to about 57% and 47% *de* respectively. The crystals were then subjected to a second cycle of

crystallization in the same solvent and HPLC was recorded for the crystals attained thereafter. These crystals were found to be 97% diastereomerically pure (Figure 61). Hence, effective separation of the diastereomers on the basis of the difference in their solubility in hexane was practically achieved. This could further be correlated with configuration obtained from SCXRD of the crystallized diastereomer, concluding that the peak at t_R 4.15 corresponds to (*S*,*R*)-**65** whereas that at t_R 5.35 is due to (*R*,*R*)-**65**.

The deprotection of chiral carbamate (*R*,*R*)-**65** to obtain optically pure amine (*R*)-**63** is underway. Once we obtain the roof shape amine in its enantiomerically pure form, we will subject it to secondary amine **(66)** formation by using reductive amination of its imine with benzaldehyde (Scheme 20). We expect this chiral roof shape secondary amine to show better activity for the molecular recognition of racemic acids due to its increased rigidity and closeness to the chiral center.

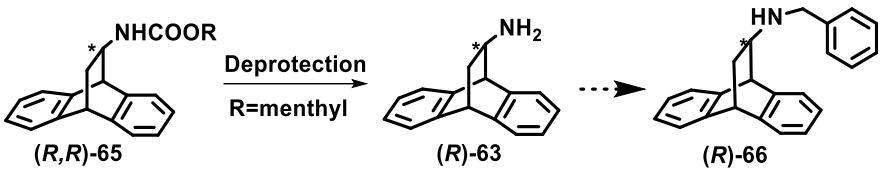

Scheme 20 Synthetic route towards optically pure 66

4.3 Conclusion:

In summary, we have prepared optically pure roof shape secondary amines, study of their applications for discrimination of signals of chiral acidic compounds by NMR spectroscopy. In the first section we have evaluation the match and mismatch effect of an additional chiral center on the molecular recognition. The diastereomers hence synthesized, showed a degree of selectivity in molecular recognition. One of the diastereomers **(*R*,*R*)-55** was found to be more effective for recognition of mandelic acid and its derivatives, whereas its diastereomer **(*R*,*S*)-55** could discriminate between enantiomers of weakly acidic BINOL derivatives. We have also investigated the two pairs of diastereomeric salts by single crystal X-ray diffraction analysis to establish the conformation of the hydrogen attached to the chiral carbon of mandelic acid. In one pair we observed shielding effect due to its position above the aromatic ring of the bicyclic roof shape moiety, while in other the hydrogen is oriented away resulting in downfield shift in NMR analysis.

In the next section we have explored the effect of electron withdrawing and releasing group on the benzyl moiety of roof shape amine and compared their ability to discriminate enantiomers of chiral substrates using NMR and UV spectroscopic techniques. It was found that the electron withdrawing substituent **(*R*)-58** increased the recognition towards mandelic acid derivatives, whereas the introduction of electron releasing group **(*R*)-59** was successfully utilized for the chiral discrimination of *N*-tosyl amino acid derivatives. Investigations of the binding properties by UV spectral analysis and single crystal X-ray diffraction of the diastereomeric salts have helped us to understand the supramolecular forces which govern this process of chiral molecular recognition. The practical utility of these CSAs has been established by study of scalemic mixture and for the analysis of sample with unknown optical purity.

The last section involves the synthesis of chiral roof shape secondary amine where the amino group is directly attached to the chiral center of the roof shape moiety and compare their CSA activity. We expect that the effect of molecular recognition in these ligands will be more pronounced due to the conformational rigidity of the amino group and its close proximity to the chiral center.

4.4 Experimental Data:

***N*-benzyl-1-((12*R*)-9,10-dihydro-9,10-ethanoanthracen-12-yl)methanamine** [*(R)*-**54**]:

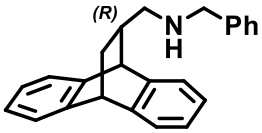

A mixture of **53** (0.3g, 7.69mmol), cesium carbonate (0.54g, 15.3mmol) and benzylamine (0.16g, 15.3mmol) was taken in a dry round bottom flask and heated under nitrogen atmosphere (120 ^{o}C, 12 h). After completion of the reaction, cold water was added to the reaction mixture and was extracted with ethyl acetate (3X25mL). The organic layer was collected, dried over anhydrous Na_2SO_4 and concentrated under reduced pressure to obtain the crude product. The product was purified by column chromatography over silica gel using light petroleum ether and ethyl acetate as eluent to get the product *(R)*-**54** as colourless oil (0.13g, 55%). **[α]$_D$**: +14.6 (*c*=1 in $CHCl_3$).

^{1}H NMR (400 MHz, $CDCl_3$): δ 7.36-7.32 (m, 3H), 7.31-7.29 (m, 3H), 7.28-7.23 (m, 3H), 7.15-7.09 (m, 4H), 4.38-4.37 (d, *J*=2.0Hz, 1H), 4.28-4.27 (t, *J*=2.4Hz, 1H), 3.81-3.78 (d, *J*=13.2Hz, 1H), 3.74-3.70 (d, *J*=13.2Hz, 1H), 2.36-2.33 (bs, 1H), 2.33-2.29 (dd, *J*=11.2Hz, 5.6Hz, 1H), 2.22-2.17 (dd, *J*=11.2Hz, 5.6Hz, 1H), 2.16-2.11 (m, 1H), 2.04-1.98 (m, 1H), 1.18-1.14 (ddd, *J*=12.0Hz, 4.4Hz, 2.4Hz, 1H).

^{13}C NMR (100 MHz, $CDCl_3$): δ 144.1, 143.8, 143.7, 140.5, 39.9, 128.4(2C), 128.2(2C), 127.1, 125.8, 125.6(2C), 125.5, 125.3, 123.5, 123.4, 123.0, 54.0, 53.8, 46.7, 44.1, 38.6, 33.1.

IR (Neat): ν 3064.9, 3022.4, 2939.1, 2862.8, 2815.3, 1603.4, 1583.8, 1455.2, 1199.9, 1114.2, 747.4, 698.7, 555.7 cm.$^{-1}$

Mass (DIP-EI): *m/z*(%) 236.3(9), 325.2(51), 324.2(31), 177.9(100), 119.9(94), 90.8(82).

HRMS (TOF ES+): *m/z* calculated for $C_{24}H_{24}N$ $[M+H]^+$ is 326.1903, found 326.1898.

***(R)*-*N*-(((12*R*)-9,10-dihydro-9,10-ethanoanthracen-12-yl)methyl)-1-phenylethan-1-amine** [*(R,R)*-**55**]:

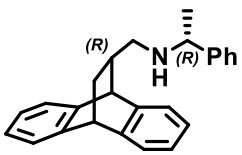

Synthetic procedure was similar to the one described above, using *(R)*-α-Phenylethylamine instead of benzyl amine. The product *(R,R)*-**55** was obtained as white solid on purification using column chromatography on silica gel (0.23 g, 87%), M.P. 103 ^{o}C. **[α]$_D$**: +49.1 (*c*=1 in $CHCl_3$)

^{1}H NMR (400 MHz, $CDCl_3$): δ 7.37-7.31 (m, 5H), 7.28-7.25 (m, 2H), 7.22-7.20 (m, 1H), 7.17-7.14 (m, 1H), 7.13-7.09 (m, 2H), 7.08-7.02 (m, 2H), 4.37-4.36 (d, *J*=2.0Hz, 1H), 4.24-4.23 (t, *J*=2.4Hz, 1H), 3.71-3.66 (q, *J*=6.4Hz, 1H), 2.24-2.19 (dd, *J*=11.2Hz, 5.6Hz, 1H),

2.08-2.01 (bs, 1H), 1.98-1.92 (m, 2H), 1.38-1.36 (d, *J*=6.4Hz, 3H), 1.10-1.06 (ddd, *J*=11.7Hz, 4.0Hz, 2.4Hz, 1H).

^{13}C NMR (100 MHz, $CDCl_3$): δ 145.8, 144.3, 143.8, 140.5, 128.4(2C), 126.8, 126.6(2C), 125.7, 125.6, 125.5, 125.4, 125.3, 123.5, 123.4, 122.9, 58.4, 52.7, 46.6, 44.2, 39.1, 33.1, 24.7

IR (KBr): ν 3065.4, 3017.9, 2957.8, 2891.3, 2819.8, 1598.7, 1489.4, 1465.1, 1172.9, 1129.7, 755.7, 704.7, 590.6, 555.9 $cm.^{-1}$

Mass (DIP-EI): *m/z*(%) 339.3(28), 338.4(21), 323.6(37), 177.9(100), 134.2(39), 104.9(82).

HRMS (ESI): *m/z* calculated for $C_{25}H_{26}N$ $[M+H]^+$ is 340.2060, found 340.2055.

(*S*)-N-(((12*R*)-9,10-dihydro-9,10-ethanoanthracen-12-yl)methyl)-1-phenylethan-1-amine [(*R,S*)-**55**]:

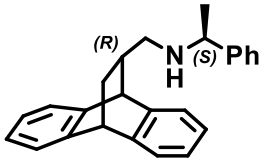

Synthetic procedure is similar to the one described above, using *(S)*-α-Phenylethylamine instead of benzyl amine. The product *(R,S)*-**55** is obtained as pale yellow liquid on purification using column chromatography on silica gel (0.22 g, 85%). **$[\alpha]_D$**: -17.5 (*c*=1 in $CHCl_3$)

^{1}H NMR (400 MHz, $CDCl_3$): δ 7.32-7.24 (m, 9H), 7.12-7.09 (m, 4H), 4.37-4.36 (d, *J*=1.6Hz, 1H), 4.24-4.23 (t, *J*=2.4Hz, 1H), 3.69-3.64 (q, *J*=6.8Hz, 1H), 2.17-2.16 (m, 1H), 2.05-2.03 (m, 2H), 2.02-1.94 (m, 1H), 1.38-1.36 (d, *J*=6.8Hz, 3H), 1.09-1.06 (ddd, *J*=12.0Hz, 4.0Hz, 2.6Hz, 1H)

^{13}C NMR (100 MHz, $CDCl_3$): δ 145.6, 144.1, 143.82, 143.80, 140.6, 128.4(2C), 126.9, 126.6(2C), 125.8, 125.6(2C), 125.5, 124.2, 123.5, 123.3, 123.0, 58.3, 52.5, 46.6, 44.2, 38.7, 33.1, 24.1

IR (Neat): υ 3065.4, 3022.1, 2936.9, 2863.5, 1602.2, 1461.0, 1123.6, 851.1, 725.2, 704.2, 595.64, 501.4 $cm.^{-1}$

Mass (DIP-EI): *m/z*(%) 339.3(8), 178.1(25), 97.1(35), 69.2(60), 68.6(100).

HRMS (TOF ES+): *m/z* calculated for $C_{25}H_{26}N$ $[M+H]^+$ is 340.2060, found 340.2060.

(*R*)-11-(azidomethyl)-9,10-dihydro-9,10-ethanoanthracene [(*R*)-**56**]:

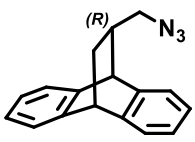

To a mixture of *(R)*-tosyl [(*R*)-**53**] (0.4g, 1.33mmol) and sodium azide (0.87g, 13.2mmol) was added in dry DMF (5 mL) in a dry round bottom flask and heated to 80°C for 18 hours. The reaction mixture was cooled

after the completion of the reaction (TLC), poured onto water and allowed to stir for 15mins at room temperature. The solution was then extracted using ethyl acetate (3X50mL), dried over anhydrous sodium sulfate and concentrated under reduced pressure. The residue was subjected to column chromatography on silica gel to obtain (*R*)-11-(azidomethyl)-9,10-dihydro-9,10-ethanoanthracene **(*R*)-56** as a colourless viscous liquid (0.34g, Yield 98%) **$[\alpha]_D$**: +10.44 (*c*=1.0, $CHCl_3$)

^{1}H NMR ($CDCl_3$, 400MHz) δ 7.34-7.28 (m, 4H); 7.19-7.14 (m, 4H); 4.37 (s, 1H); 4.31 (s, 1H); 3.06-3.02 (dd, *J*=12.0Hz, 6.4Hz, 1H); 2.77-2.72 (m, 1H); 2.24-2.21 (m, 1H); 2.07-2.00 (m, 1H); 1.16-1.12 (m, 1H).

^{13}C NMR ($CDCl_3$, 100MHz) δ 143.6; 143.4; 143.3; 139.7; 126.3; 125.9; 125.8; 125.5 (2C); 123.7; 123.5; 123.3; 55.7; 46.2; 43.9; 38.4; 32.4.

IR (KBr): *v* 3066, 3017, 2946, 2926, 2863, 2085, 1457, 1352, 1279, 1202, 1159, 1113, 903, 870, 752, 551 cm.$^{-1}$

(*R*)-(9,10-dihydro-9,10-ethanoanthracen-11-yl)methanamine [(*R*)-**57**]:

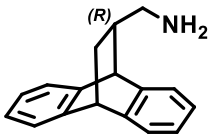

A mixture of azide (*R*)-**56** (0.365g, 1.4mmol) and Pd/C (0.027g, 10%w/w) in methanol (50 mL) was taken in a clean and dry 100mL round bottom flask. The reaction mixture was stirred at 0-5^{o}C under H_2 atmosphere (6 h). The crude reaction mixture was then filtered over a compactly filled celite bed which is kept moist with methanol. The filterate was then concentrated and directly subjected to column chromatography on alumina to obtain (*R*)-(9,10-dihydro-9,10-ethanoanthracen-11-yl)methanamine **(*R*)-57** as a colourless solid (0.29 g, Yield 90%, M.P. 190^{o}C).

^{1}H NMR ($CDCl_3$, 400MHz) δ 7.35-7.26 (m, 4H); 7.16-7.08 (m, 4H); 4.97 (bs, 2H); 4.35-4.34 (d, *J*=2.0Hz, 1H); 4.29-4.28 (t, *J*=2.4Hz, 1H); 2.41 (m, 2H); 2.16-2.12 (m, 1H); 2.06-2.01 (m, 1H); 1.21-1.17 (m, 1H).

^{13}C NMR ($CDCl_3$, 100MHz) δ 143.7; 143.5; 143.4; 139.9; 126.2; 125.9; 125.8; 125.7; 125.3; 123.6; 123.5; 123.2; 46.2; 43.9; 32.8.

IR (KBr): *v* 2947, 2918, 2861, 2683, 2606, 2096, 1637, 1541, 1459, 1406, 1336, 1150, 1119, 1042, 1011, 755, 649, 622, 554, 466 cm.$^{-1}$

HRMS: Calculated for $C_{17}H_{18}N$ (M + 1) = 236.1439. Found 236.1437.

(*R*)-1-(9,10-dihydro-9,10-ethanoanthracen-11-yl)-*N*-(4-nitrobenzyl)methanamine [(*R*)-**58**]:

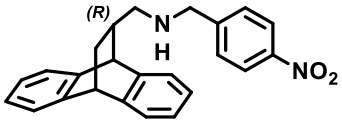

In a round bottom flask, (*R*)-**57** (0.1g, 0.43mmol) and *p*-nitro benzaldehyde (0.064g, 0.43mmol) were dissolved in dry methanol (5 mL) at room temperature under nitrogen atmosphere (6 h). After the completion of the reaction which is marked by the disappearance of (*R*)-**57** on TLC, sodium borohydride (0.024g, 0.64mmol) is added portion wise allowing the reaction mixture to vigorous stir at room temperature for another 4h. The crude mixture is concentrated under reduced pressure to remove methanol and purified by column chromatography on silica gel to obtain (*R*)-1-(9,10-dihydro-9,10-ethanoanthracen-11-yl)-*N*-(4-nitrobenzyl)methanamine **(*R*)-58** as a brown solid (0.13 g; Yield 80%, M.P. 146^{o}C) **$[\alpha]_D$:** +18.5 (*c*=1.0, $CHCl_3$).

^{1}H NMR ($CDCl_3$, 400MHz): δ 8.21-8.18 (d, *J*=8.8 Hz, 2H); 7.51-7.49 (d, *J*=8.8 Hz, 2H); 7.31-7.22 (m, 4H); 7.14-7.08 (m, 4H); 4.37-4.36 (d, *J*=2.0 Hz, 1H); 4.28-4.27 (t, *J*=2.4 Hz, 1H); 3.87-3.82 (d, *J*=14.4 Hz, 1H); 3.82-3.78 (d, *J*=14.4 Hz, 1H); 2.30-2.25 (dd, *J*=11.2 Hz, 6.0 Hz, 1H); 2.18-2.14 (dd, *J*=11.2 Hz, 8.4 Hz, 1H); 2.12-2.06 (m, 1H); 2.03-1.97 (m, 1H); 1.18-1.13 (m, 1H).

^{13}C NMR ($CDCl_3$, 100MHz): δ 148.4, 146.9, 143.9, 143.8, 143.7, 140.5, 128.6 (2C), 125.9, 125.7, 125.6, 125.5, 125.2, 123.6 (2C), 123.5, 123.4, 123.1, 54.3, 53.2, 46.7, 44.1, 38.8, 32.9.

IR (KBr): *v* 3335, 3066, 2948, 2903, 2788, 1597, 1510, 1461, 1338, 1225, 1203, 1172, 1105, 842, 758, 639, 624, 560, 460 cm^{-1}.

HRMS: Calculated for $C_{24}H_{23}O_2N_2$ (M + 1) = 371.1754. Found 371.1750.

(*R*)-1-(9,10-dihydro-9,10-ethanoanthracen-11-yl)-*N*-(4-methoxybenzyl)methanamine [(*R*)-**59**]:

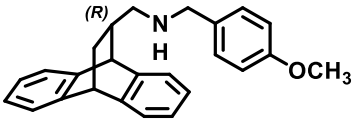

In a round bottom flask, (*R*)-**57** (0.1g, 0.43mmol) and *p*-methoxy benzaldehyde (0.058g, 0.43mmol) were dissolved in dry methanol (5 mL) at room temperature under nitrogen atmosphere for 6h. After the completion of the reaction which is marked by the disappearance of (*R*)-amine on TLC, sodium borohydride (0.024g, 0.64mmol) is added portion wise allowing the reaction mixture to vigorous stir at room temperature for another 4h. The crude mixture is concentrated under reduced pressure to remove methanol and

purified by column chromatography on silica gel to obtain (*R*)-1-(9,10-dihydro-9,10-ethanoanthracen-11-yl)-N-(4-methoxybenzyl) methanamine **(*R*)-59** as a colourless liquid (0.113g; Yield 75%) **$[\alpha]_D$**: +15.1 (*c*=1.0, $CHCl_3$).

^{1}H NMR ($CDCl_3$, 400MHz): δ 7.29-7.22 (m, 6H); 7.12-7.09 (m, 4H); 6.89-6.87 (dd, *J*=6.4 Hz, 2.0 Hz, 2H); 4.35-4.34 (d, *J*=2.0 Hz, 1H); 4.27-4.26 (t, *J*=2.4 Hz, 1H); 3.83 (s, 3H); 3.72-3.68 (d, *J*=13.2 Hz, 1H); 3.65-3.62 (d, *J*=12.8 Hz, 1H); 2.29-2.25 (dd, *J*=10.8 Hz, 6.0 Hz, 1H); 2.18-2.13 (dd, *J*=10.8 Hz, 6.0 Hz, 1H); 2.07 (bs, 1H); 2.02-1.98 (m, 1H); 1.17-1.12 (m, 1H); 0.92-0.90 (m, 1H).

^{13}C NMR ($CDCl_3$, 100MHz): δ 158.6, 144.1, 143.8, 143.7, 140.6, 132.6, 129.3 (2C), 125.8, 125.6 (2C), 125.4, 125.2, 123.4, 123.3, 123.0, 113.8 (2C), 55.3, 54.1, 53.3, 46.7, 44.2, 38.7, 33.1.

IR (Neat): *v*

HRMS: calculated for $C_{25}H_{26}NO$ (M + 1) = 256.2009. Found 236.1862.

9,10-dihydro-9,10-ethanoanthracene-11-carboxylic acid (60):

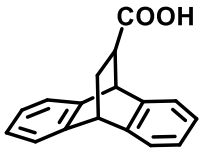

In a round bottom flask, ethyl-9,10-dihydro-9,10-ethanoanthracene-11-carboxylate **(50)** (5g, 17.9mmol) was dissolved in methanol (100mL) to which potassium hydroxide (2.22g, 39.5mmol) was added portion wise. The reaction mixture was stoppered and allowed to stir at room temperature for 12 hours. After the completion of reaction (monitored by TLC marking the disappearance of starting material), it was concentrated under vacuum to remove methanol. Cold water was added to the residue and excess of potassium hydroxide was neutralized by dropwise addition of conc. HCl till litmus turned red. The aqueous layer was transferred to a separating funnel and extracted using ethyl acetate (3X100mL). The combined organic layer was collected, dried over anhydrous sodium sulfate and concentrated. The residue was then subjected to crystallization using 10% ethyl acetate in petroleum ether to afford 9,10-dihydro-9,10-ethanoanthracene-11-carboxylic acid **(60)** as white crystalline solid (4.1g, Yield 91%, M.P. 192^{o}C)

^{1}H NMR (400MHz, $CDCl_3$): δ 7.37- 7.28 (m, 4H), 7.19-7.11 (m, 4H), 4.73-4.72 (d , *J*=2.4Hz, 1H), 4.39-4.38 (t, *J*=2.8Hz, 1H), 2.96-2.92 (ddd, *J*=10.4Hz, 4.8Hz, 2.4Hz, 1H), 2.19-2.14 (ddd, *J*=10.4Hz, 4.8Hz, 2.8Hz, 1H), 2.09-2.02 (ddd, *J*=10.4Hz, 4.8Hz, 2.8Hz, 1H).

^{13}C NMR (100MHz, $CDCl_3$): δ 179.7, 143.8, 143.7, 142.4, 139.8, 126.3, 126.2, 125.8, 125.1, 123.7, 123.6**,** 123.2, 46.6, 44.1, 43.8, 30.6.

Mass (EI) *m/z*: 250 (M, 19%), 178(86%), 177(100%), 176(26%), 88(12%).

IR (KBr): ν 3071, 3020, 2948, 1707, 1461, 1408, 1317, 1230, 920, 755, 629, 529, 519cm^{-1}

9,10-dihydro-9,10-ethanoanthracene-11-carboxamide (61):

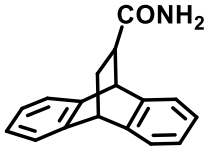

In a round bottom flask, **60** (0.5 g, 2mmol) was dissolved in 20 mL acetone and allowed to stir for 15 min. To this solution triethyl amine (0.278 mL, 2.0mmol) and cyanuric chloride (0.368 g, 1.0mmol) were added and stirred at room temperature for 3h. Later to this reaction mixture, liquor ammonia (0.043 mL, 2.0mmol) was added and allowed to stir for 12 more hours (monitored by TLC). After completion of the reaction, acetone was evaporated and reaction mixture was poured into cold water. The reaction mixture was extracted using ethyl acetate (3X 25mL). The combined organic layer was evaporated to obtain crude product which was purified by column chromatography on silica gel to give pinkish solid **(**0.41g, Yield 85%, M.P. >230^{o}C) **[α]$_D$**: +69^o, *c*=1.0 in $CHCl_3$ (For *R*-**61**).

^{1}H NMR (400 MHz, $CDCl_3$) : δ 7.34-7.28 (m, 4H), 7.17-7.13 (m, 4H), 5.34 (bs, 1H), 5.06 (bs, 1H), 4.56-4.55 (d, *J*=2.4Hz, 1H), 4.41-4.39 (t, *J*=2.8Hz, 1H), 2.83-2.79 (ddd, *J*=10.6Hz, 4.8Hz, 2.4Hz, 1H), 2.17-2.11 (ddd, *J*=10.6Hz, 4.8Hz, 2.8Hz, 1H), 1.96-1.91 (ddd, *J*=10.6Hz, 4.8Hz, 2.8Hz, 1H).

^{13}C NMR (100MHz, $CDCl_3$): δ 176.4, 143.8, 143.1, 142.7, 139.6, 126.5, 126.2, 125.9, 125.4, 123.7, 123.4, 123.3, 47.4, 45.6, 43.8, 32.1.

Mass (EI) *m/z*: 250 (M+1, 19%), 204 (56%), 178 (100%), 172 (78%), 165 (21%).

IR (KBr): ν 3480, 3303, 3169, 3067, 3017, 2962, 2936, 1666, 1605, 1461, 1405, 1306, 1277, 1147, 761, 557, 493 cm^{-1}

(12*R*)-*N*-(*S*)-1-phenylethyl)-9,10-dihydro-9,10-ethanoanthracene-12-carboxamide (64):

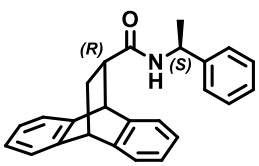

The synthetic procedure is same as stated for 9,10-dihydro-9,10-ethanoanthracene-11-carboxamide, by replacing the addition of liquor ammonia with 1.0 equivalent of (*S*)-α-methyl benzyl amine. (0.5g, Yield: 70%, M.P: >200^{o}C) **[α]$_D$**: -15.5^o, *c*=1.0 in $CHCl_3$ (for **(*R,S*)-64**)

^{1}H NMR (400 MHz, $CDCl_3$) : δ 7.34-7.27 (m, 6H), 7.19-7.16 (m, 1H), 7.14-7.11 (m, 5H), 7.06-7.02 (m, 1H), 5.25-5.23 (d, *J*=7.2Hz, 1H), 5.02-4.95 (dq, *J*=7.2Hz, 6.8Hz, 1H), 4.51-

4.50 (d, *J*=2.0Hz, 1H), 4.39-4.38 (t, *J*=2.8Hz, 1H), 2.81-2.76 (ddd, *J*=10.4Hz, 4.8Hz, 2.4Hz, 1H), 2.16-2.09 (ddd, *J*=10.4Hz, 4.8Hz, 2.8Hz, 1H), 1.95-1.90 (ddd, *J*=10.4Hz, 4.8Hz, 2.8Hz, 1H), 1.36-1.35 (d, *J*=6.8Hz, 3H).

^{13}C NMR (100MHz, $CDCl_3$): δ 172.6, 143.8, 143.2, 142.9, 142.8, 139.7, 128.6 (2C), 127.3, 126.4, 126.2, 126.1 (2C), 126.0, 125.9, 125.3, 123.6, 123.4, 123.3, 48.7, 47.5, 45.7, 43.8, 32.3, 21.5.

Synthesis of Methyl-(9,10-dihydro-9,10-ethanoanthracen-11-yl)carbamate (62):

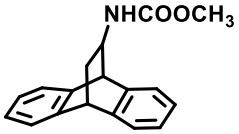

To a round bottom flask containing compound **61** (0.22g, 0.88mmol) and freshly prepared sodium methoxide (0.21g of sodium metal in 5mL MeOH, 8.8mmol) in 20 mL methanol, NBS (0.32 g, 1.77mmol) was added portion wise and allow it to reflux for 12h. After the completion of reaction, methanol was evaporated and reaction mixture was poured onto cold water. The aqueous layer was extracted with ethyl acetate (3X50mL) and organic layer was collected. The organic layer was dried over anhy. Na_2SO_4 and evaporated under reduced pressure to obtain crude product which was purified by column chromatography on silica gel to obtain Methyl-(9,10-dihydro-9,10-ethanoanthracen-11-yl)carbamate **(62)** as a colourless solid (0.07g, Yield 65%, M.P. 132°C)

^{1}H NMR (400MHz, $CDCl_3$): δ 7.36-7.26 (m, 4H), 7.21-7.12 (m, 4H), 4.41-4.40 (d , *J*=2.0Hz, 1H), 4.30-4.29 (t, *J*=2.8Hz, 1H), 4.28 (bs, 1H), 4.21-4.17 (m, 1H), 2.44-2.38 (m, 1H), 1.31-1.27 (m, 1H).

^{13}C NMR (100MHz, $CDCl_3$): δ 156.3, 143.8, 143.0, 141.1, 139.1, 126.6, 126.3, 126.1, 125.9 (2C), 124.7, 123.5**,** 123.4, 52.1, 49.7, 49.6, 43.8, 37.1

Mass (EI) *m/z*: 293 (M^+, 43%), 286 (49%), 250 (78%), 192 (100%), 178 (47%), 158 (49%), 154 (53%), 125 (75%), 111 (93%).

IR (KBr): ν 3312, 3052, 2943, 2876, 1690, 1539, 1461, 1312, 1268, 1159, 1058, 757, 563, 538 cm^{-1}

Synthesis of 9,10-dihydro-9,10-ethanoanthracen-11-amine (63):

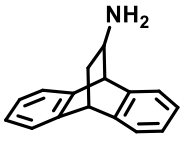

A mixture of methyl-(9,10-dihydro-9,10-ethanoanthracen-11-yl)carbamate **(62)** (0.15g, 0.36mmol) and tetrabutyl ammonium fluoride trihydrate (0.45g, 1.4mmol) was dissolved in 10mL of AR grade THF. The reaction mixture was heated to a temperature of 70°C under nitrogen atmosphere for 18h. The

reaction mixture was concentrated after the completion of the reaction (TLC) and poured onto cold water. The aqueous layer was extracted using ethyl acetate (3X50mL) and the combined organic layer was dried over anhy. Na_2SO_4. The residue obtained upon concentration of the organic layer was subjected to purification by column chromatography to obtain 9,10-dihydro-9,10-ethanoanthracen-11-amine **(63)** as pale brown solid (0.1g, Yield 84%)

^{1}H NMR (400MHz, $CDCl_3$): δ 7.37-7.26 (m, 4H), 7.21-7.10 (m, 4H), 4.27-4.26 (t, *J*=2.4Hz, 1H), 4.14-4.13 (d, *J*=2.8Hz, 1H), 3.35-3.31 (m, 1H), 2.35-2.28 (m, 1H), 1.19-1.14 (m, 1H).

^{13}C NMR (100MHz, $CDCl_3$): δ 143.8, 142.9, 142.5, 139.2, 126.5, 126.3, 125.9, 125.7 (2C), 124.1, 123.4**,** 123.3, 54.0, 50.9, 44.3, 38.7

IR (KBr): ν 3343, 2955, 2874, 1544, 1462, 1420, 1382, 1167, 1018, 932, 752, 661, 554 cm^{-1}

Synthesis of (1*R*,2*S*,5*R*)-2-isopropyl-5-methylcyclohexyl (9,10-dihydro-9,10-ethanoanthracen-12-yl)carbamate (*R*)-65:

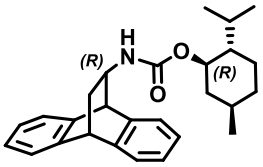

To a solution of **(±)-63** (0.10 g, 0.45 mmol) and triethylamine (0.1 mL, 0.68 mmol) in dichloromethane was added (1*R*,2*S*,5*R*)-(-)-menthyl chloroformate (0.15 mL, 0.68 mmol) drop wise at 0^{o}C under N_2 atmosphere. After completion of the reaction (TLC), the reaction mixture was poured in ice cold water. The aqueous layer was extracted with dichloromethane (2X50 mL), the extracts were combined and the organic layer was dried over Na_2SO_4 and evaporated to obtain a crude solid. The crude product was purified by column chromatography over silica gel using petroleum ether/ethyl acetate as eluent (5%) furnishing a colourless solid (0.17 g, 96%).

^{1}H NMR (400MHz, $CDCl_3$): δ 7.34-7.22 (m, 4H); 7.17-7.09 (m, 4H); 4.58-4.51 (dt, *J*=12.0Hz, 4.0Hz, 1H); 4.43 (s, 1H); 4.27-4.26 (t, *J*=4.0Hz, 1H); 4.10 (m, 1H); 4.08 (bs, 1H); 2.40-2.36 (m, 1H); 2.00-1.60 (m, 2H); 1.55-1.46 (m, 2H); 1.46 (m, 1H); 1.24-1.21 (m, 2H); 1.07-1.03 (m, 1H); 0.92-0.90 (d, *J*=8.0Hz, 3H); 0.88-0.80 (m, 6H); 0.72-0.71 (m, 1H)

IR (KBr): ν 3430, 2955, 2865, 1714, 1500, 1462, 1293, 1253, 1213, 1181, 1093, 1036, 988, 764, 577, 558 cm^{-1}

4.5 Spectral Data:

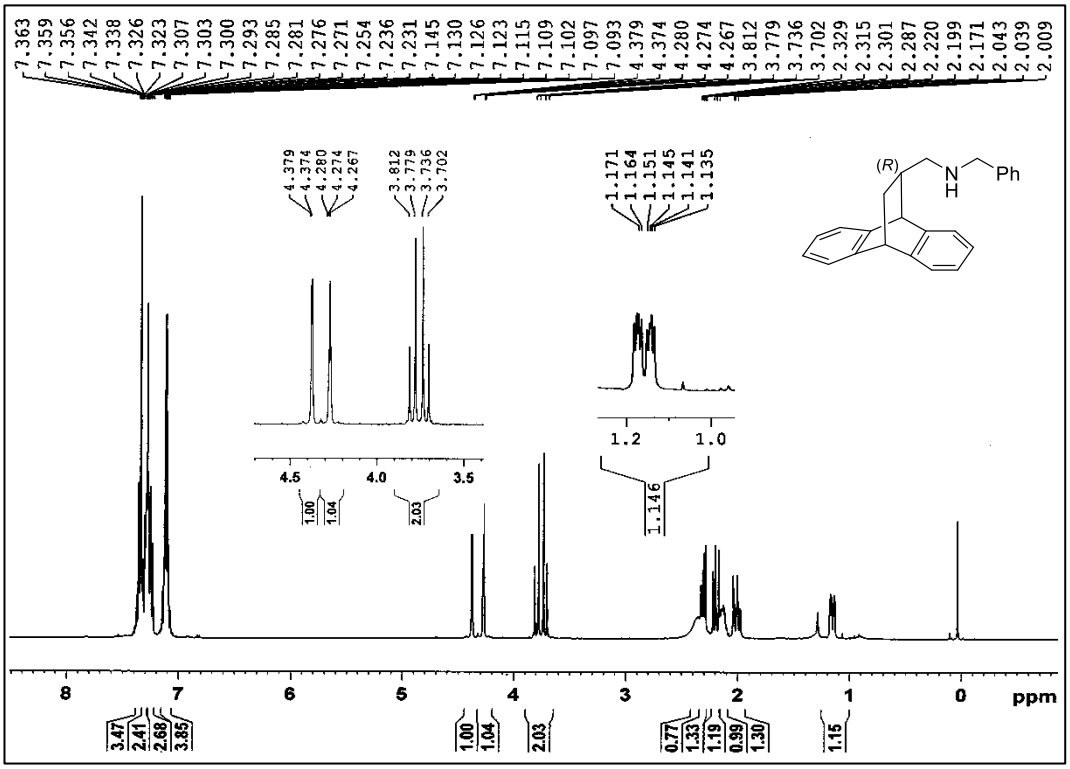

^{1}H NMR Spectra of compound *(R)*-**54** ($CDCl_3$, 400MHz)

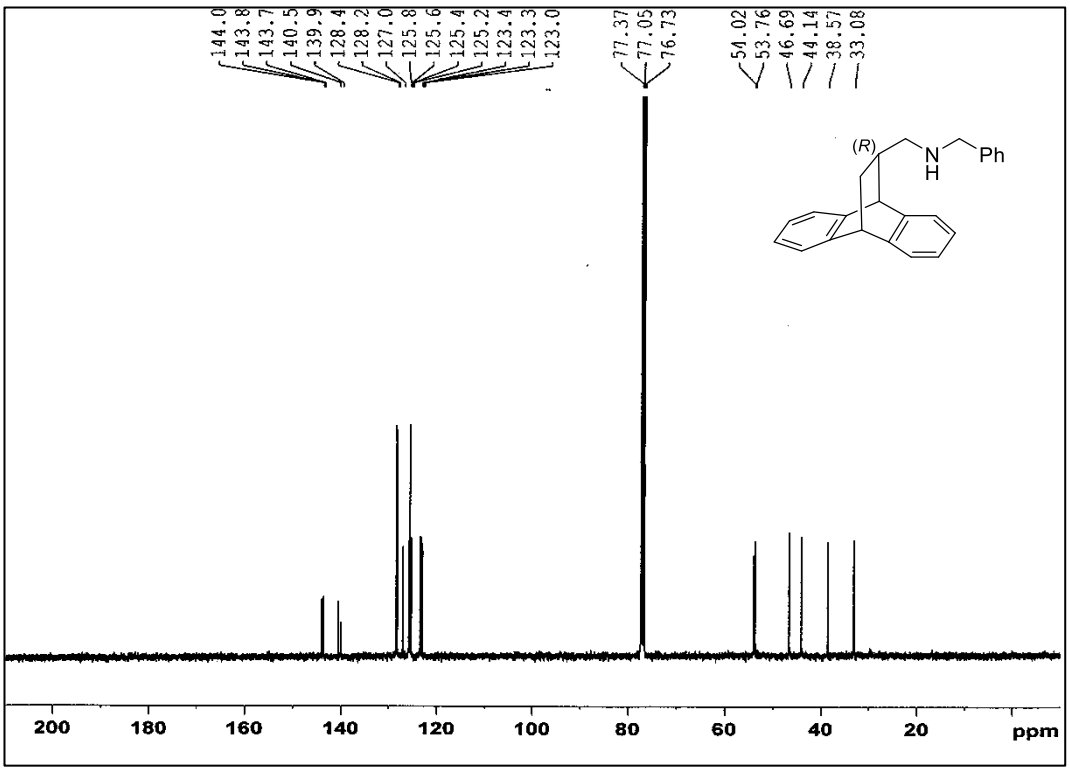

^{13}C NMR Spectra of compound *(R)*-**54** ($CDCl_3$, 100MHz)

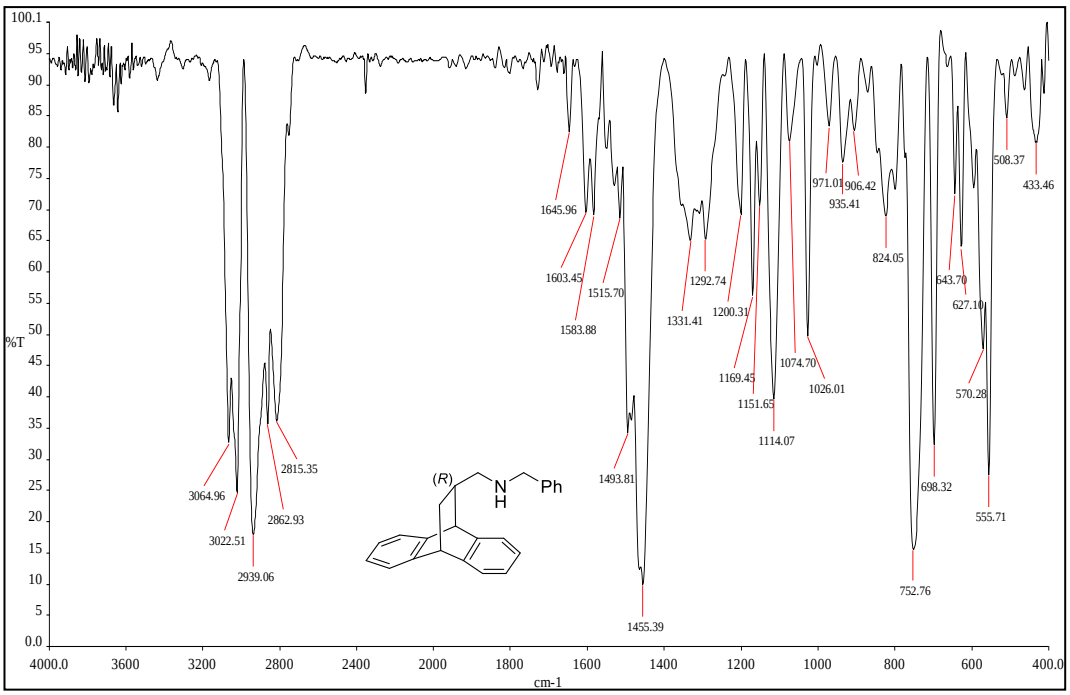

IR Spectra of compound *(R)*-**54**

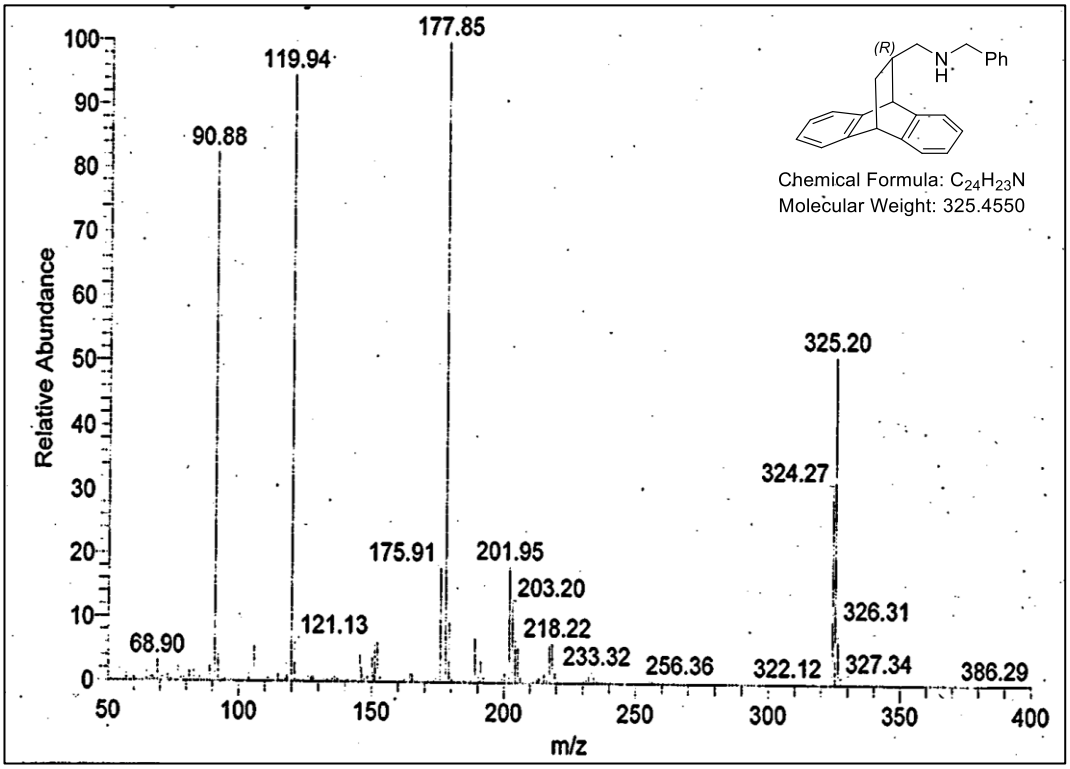

Mass Spectra of compound *(R)*-**54**

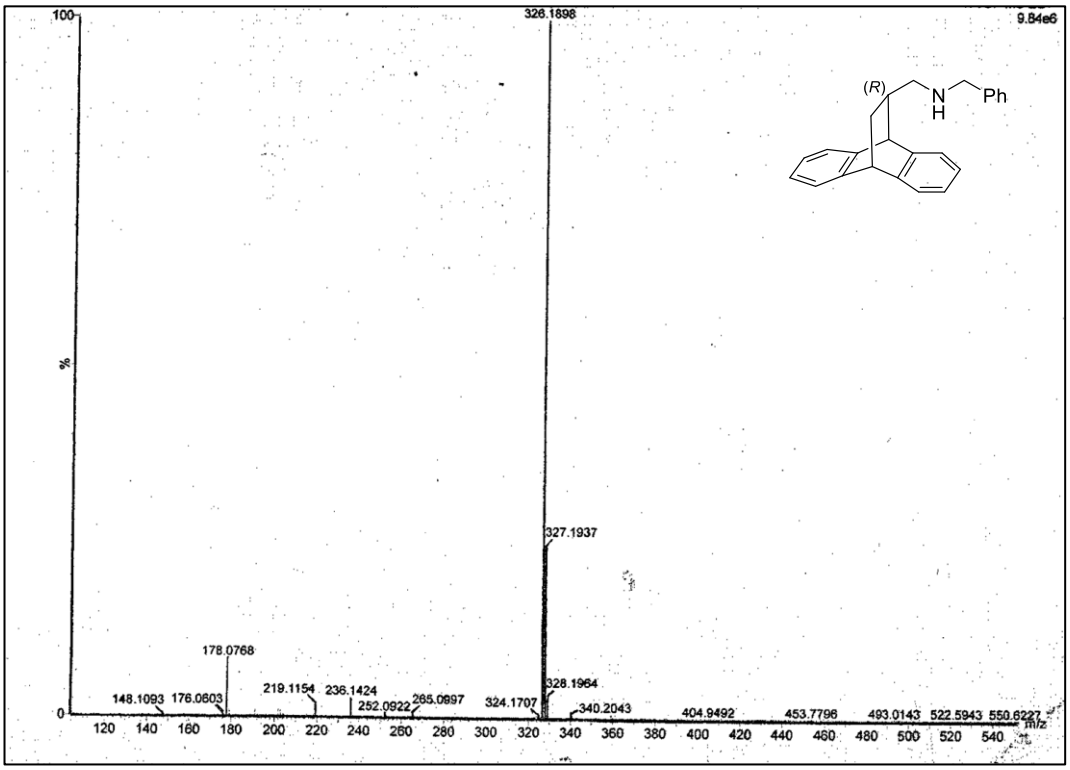

HRMS Spectra of compound *(R)*-**54**

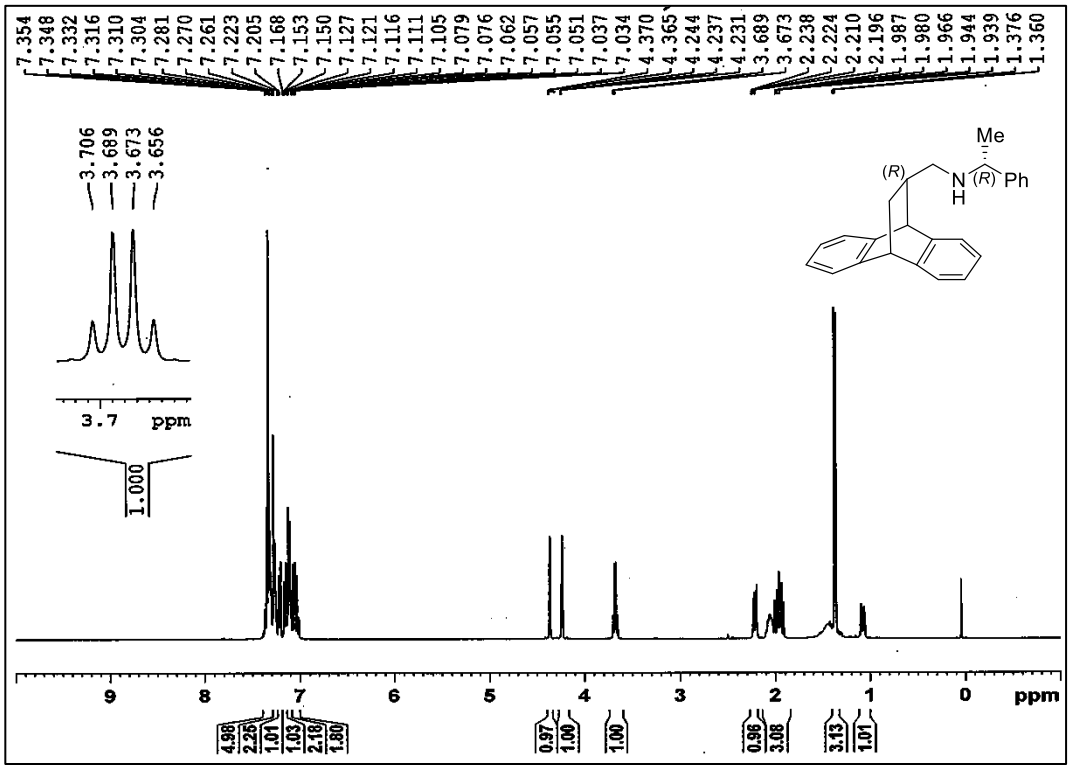

^{1}H NMR Spectra of compound *(R,R)*-**55** ($CDCl_3$, 400MHz)

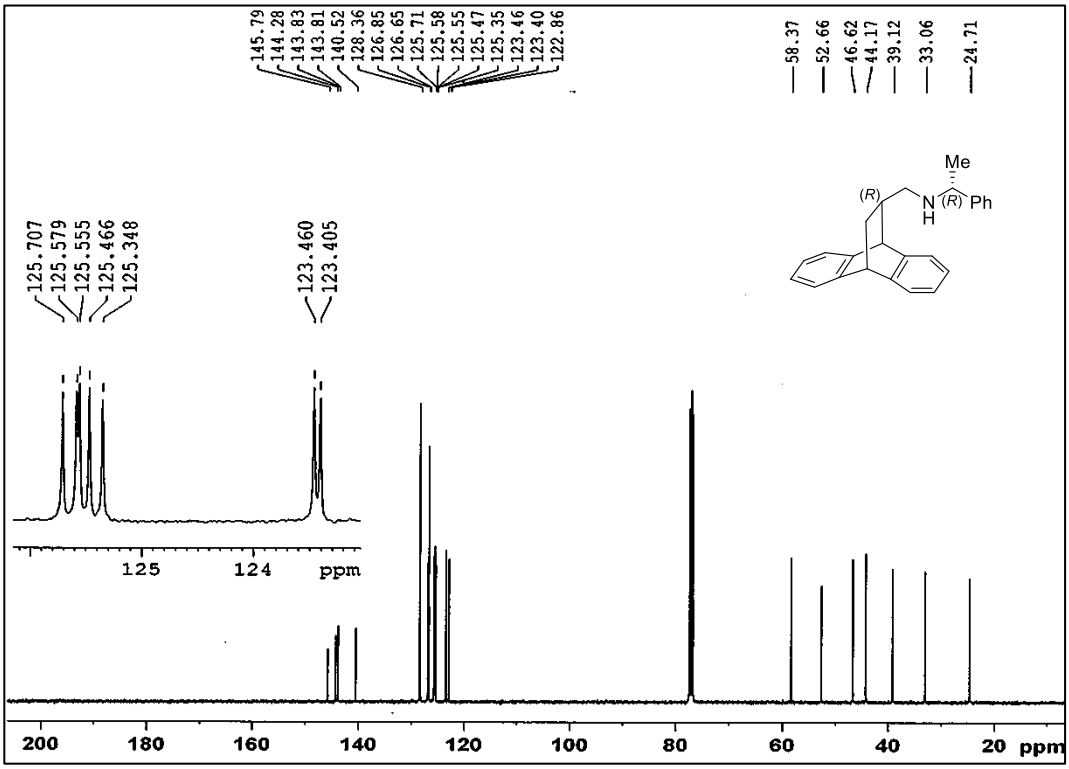

^{13}C NMR Spectra of compound *(R,R)*-**55** ($CDCl_3$, 100MHz)

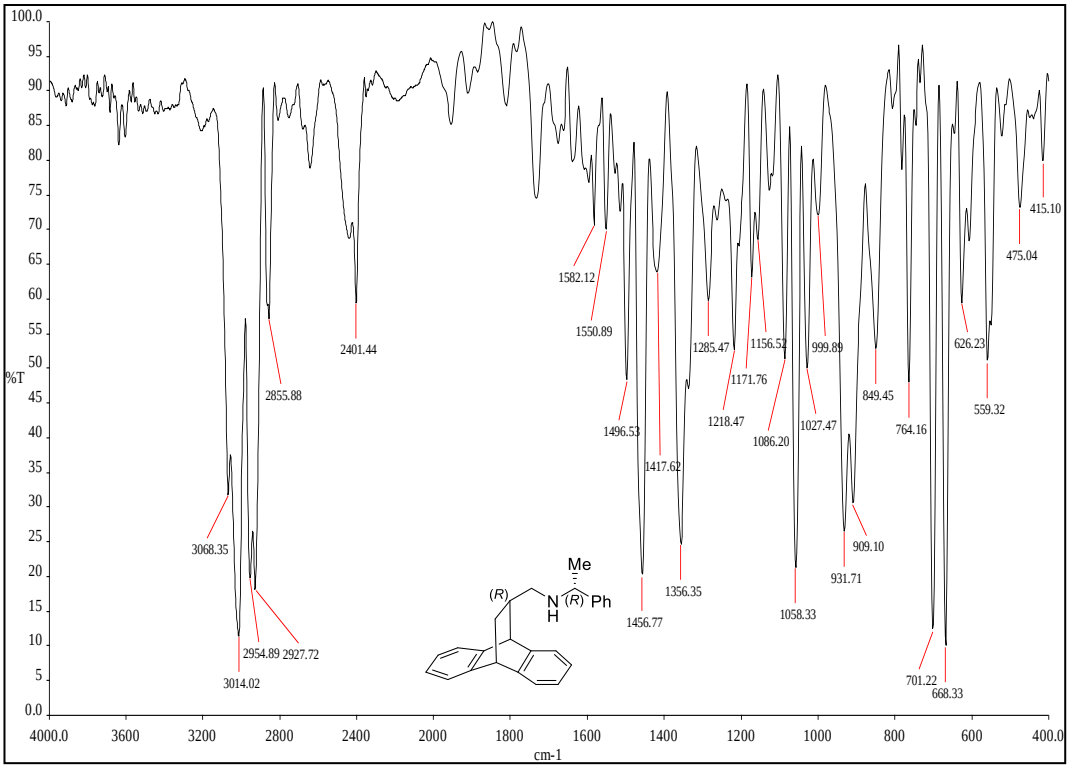

IR Spectra of compound *(R,R)*-**55**

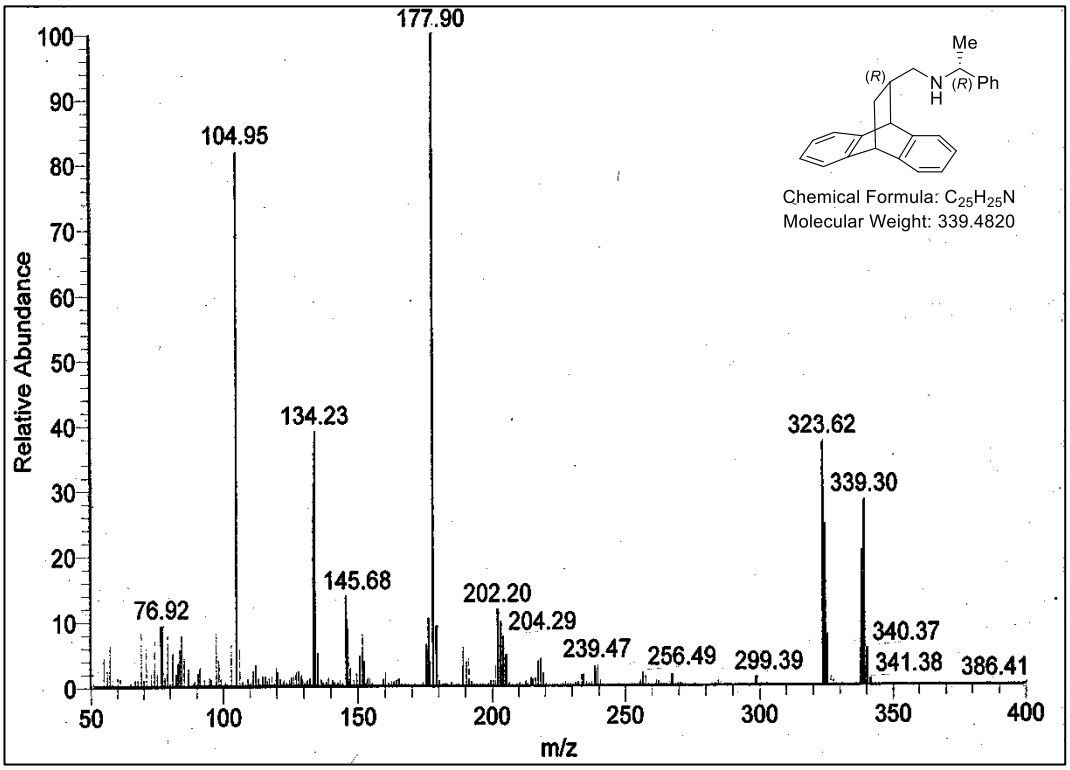

Mass Spectra of compound *(R,R)*-**55**

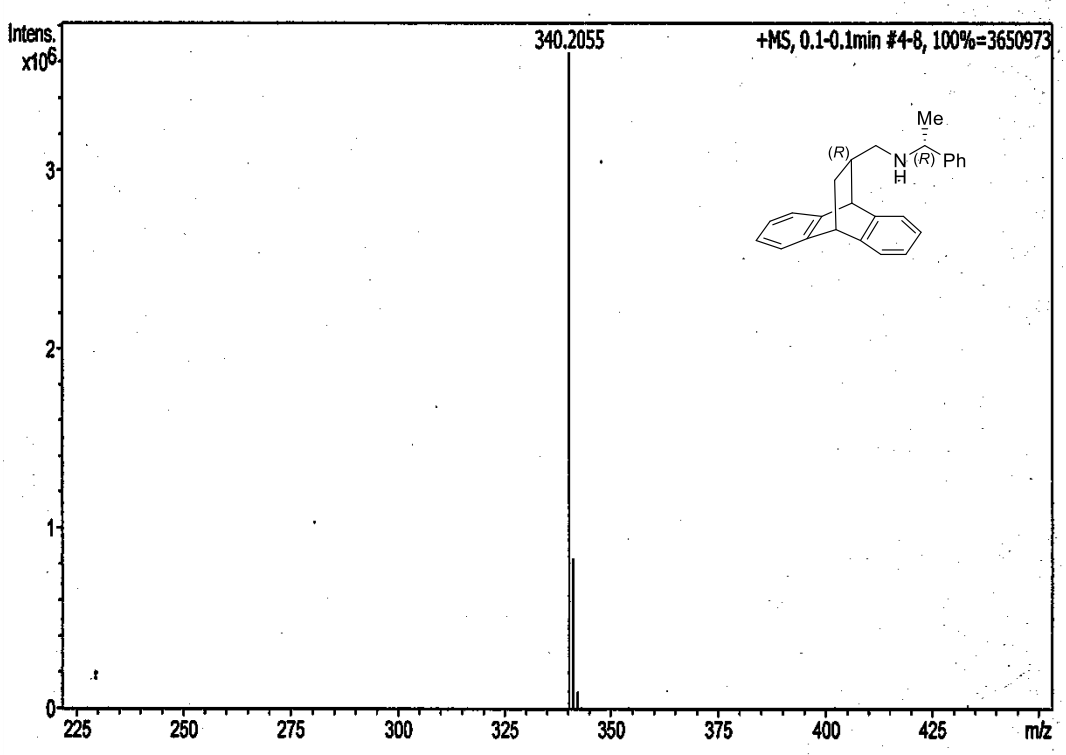

HRMS Spectra of compound *(R,R)*-**55**

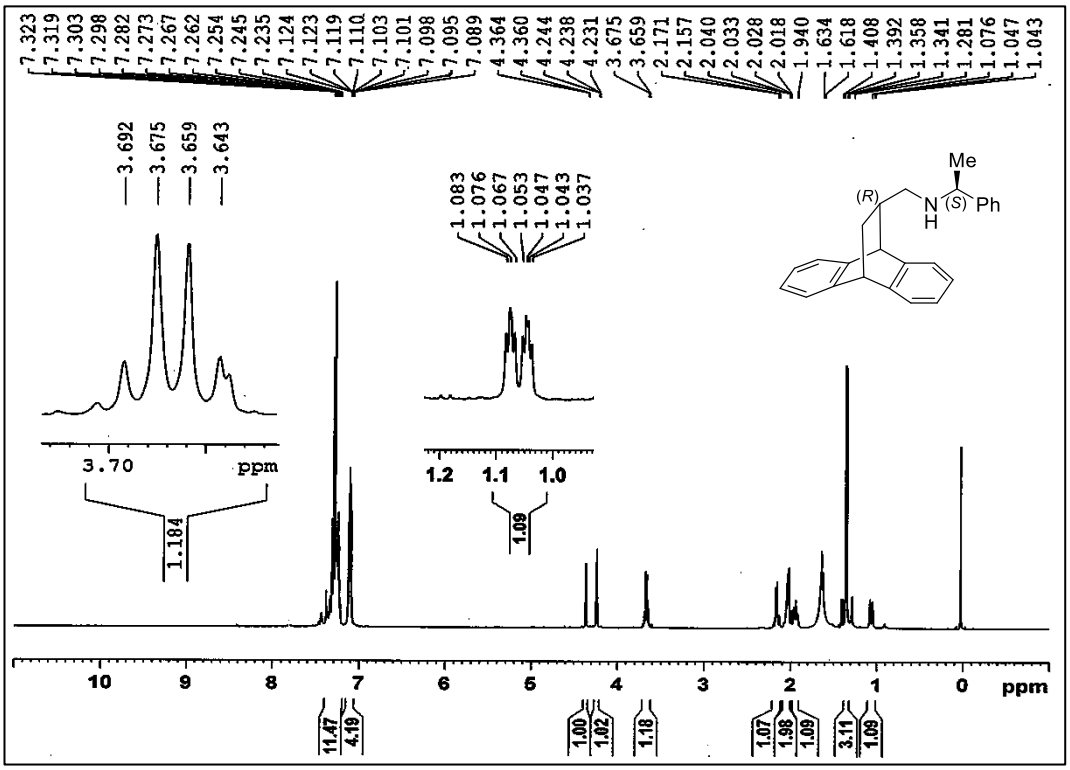

^{1}H NMR Spectra of compound *(R,S)*-**55** ($CDCl_3$, 400MHz)

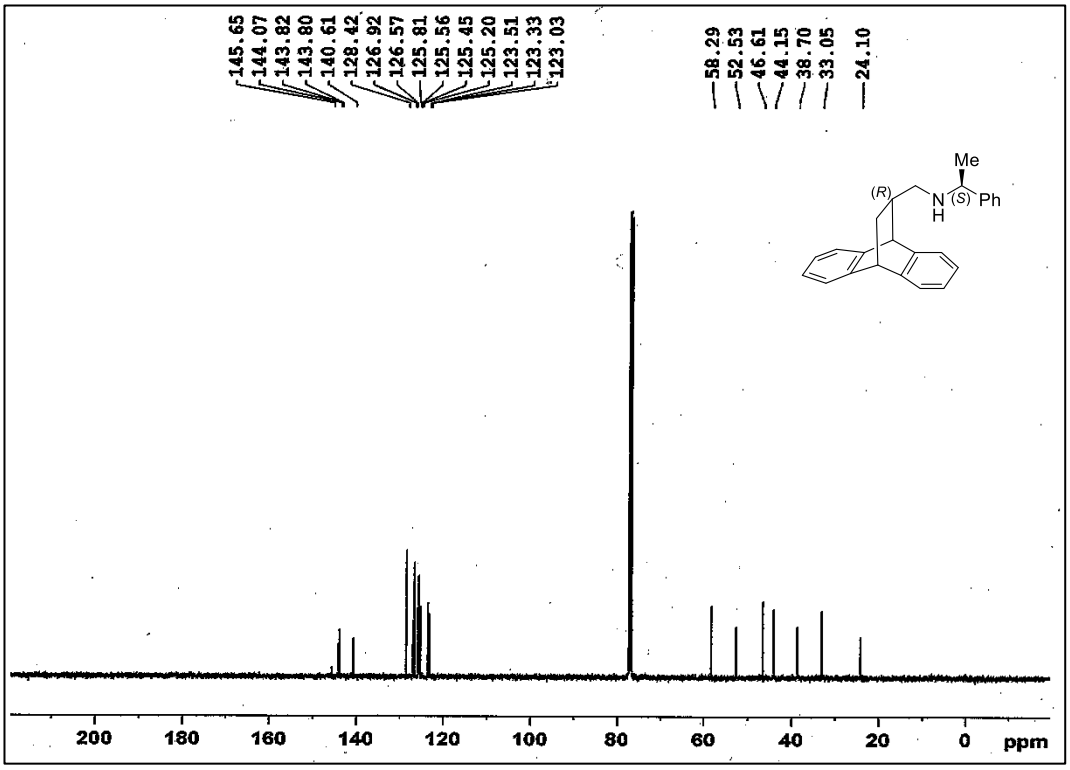

^{13}C NMR Spectra of compound *(R,S)*-**55** ($CDCl_3$, 100MHz)

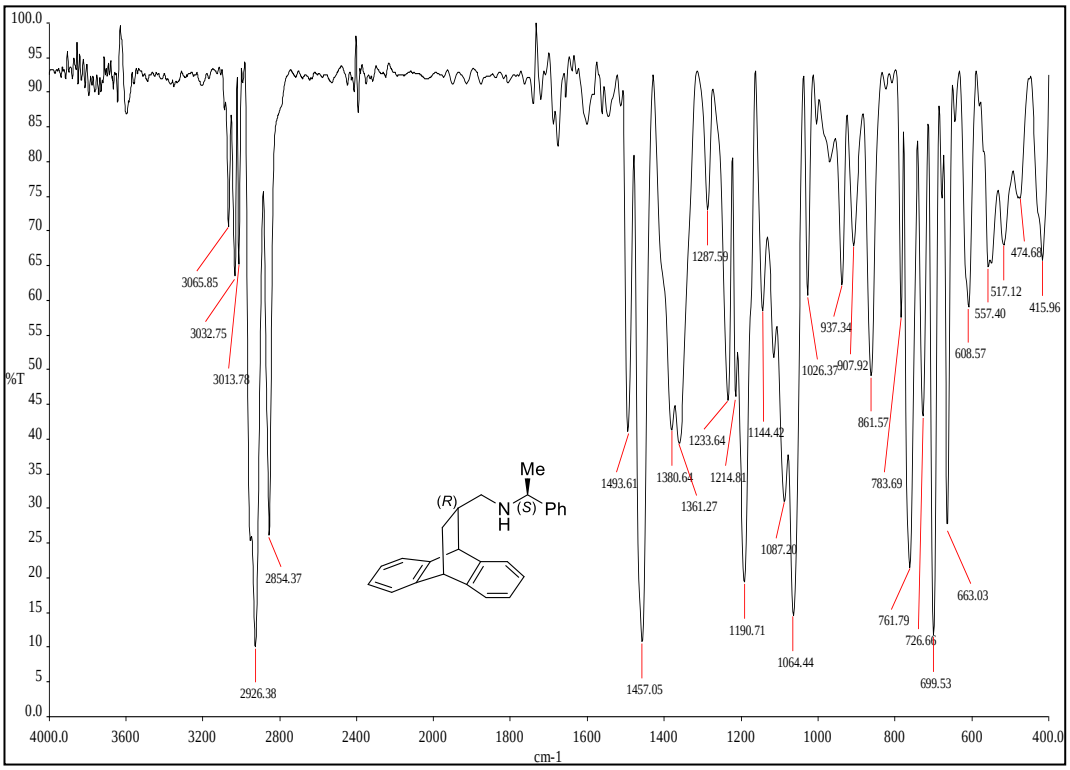

IR Spectra of compound *(R,S)*-**55**

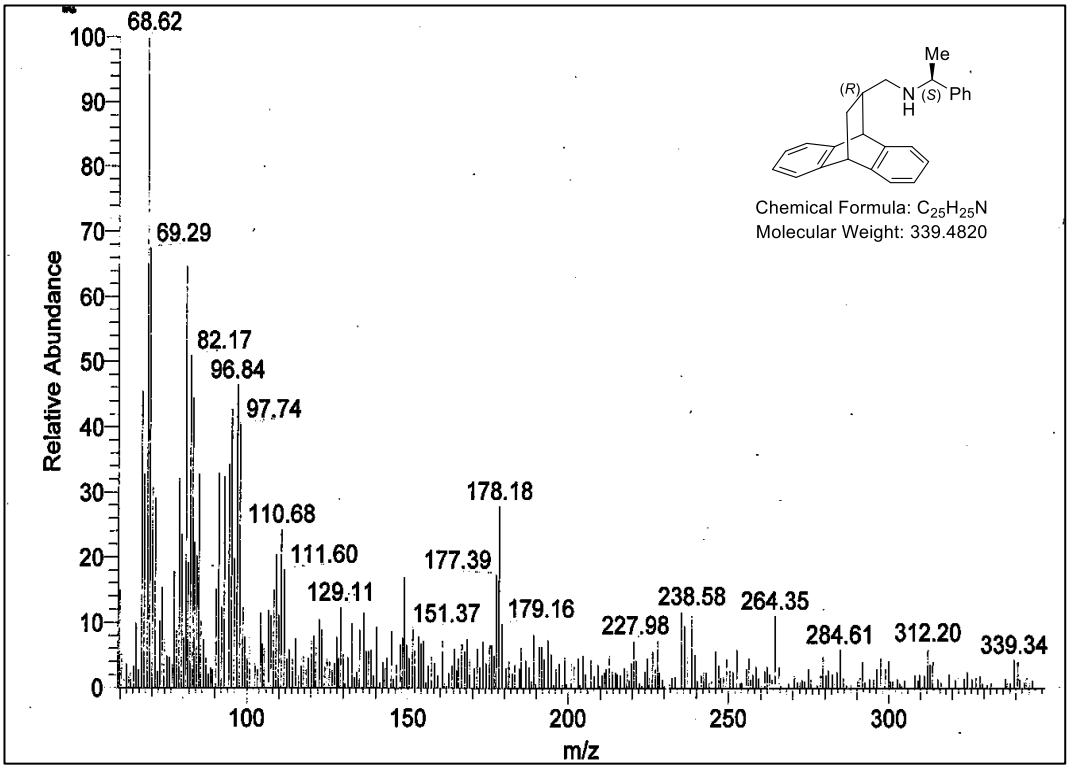

Mass Spectra of compound *(R,S)*-**55**

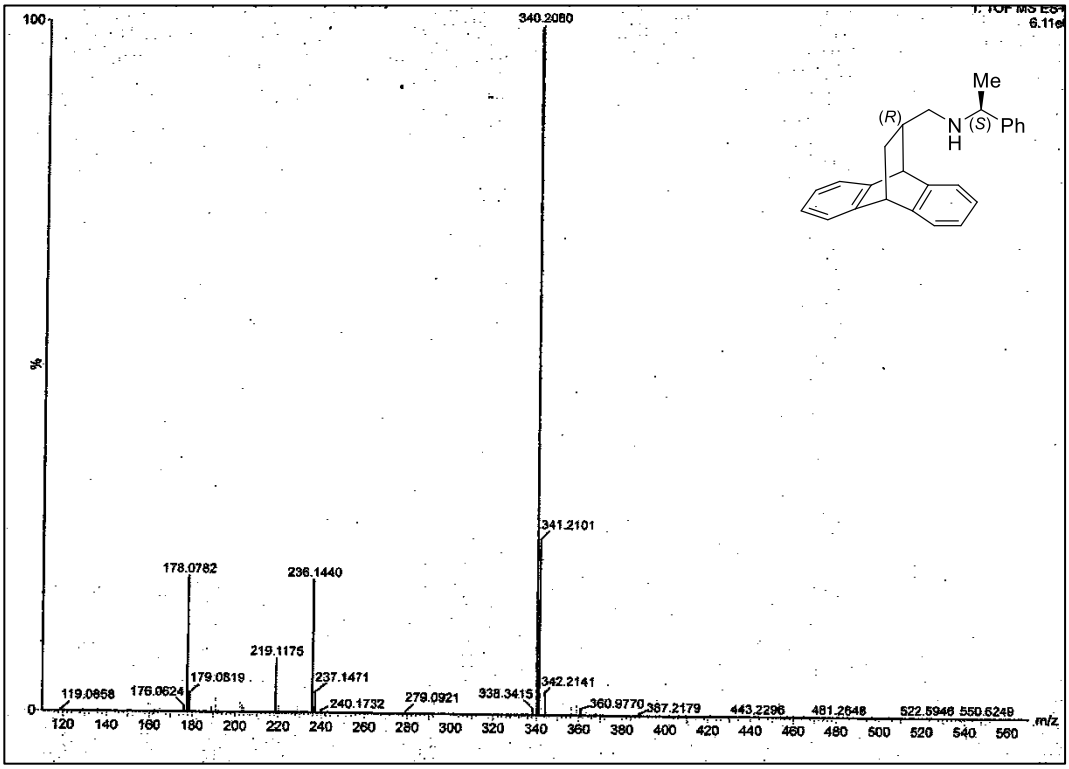

HRMS Spectra of compound *(R,S)*-**55**

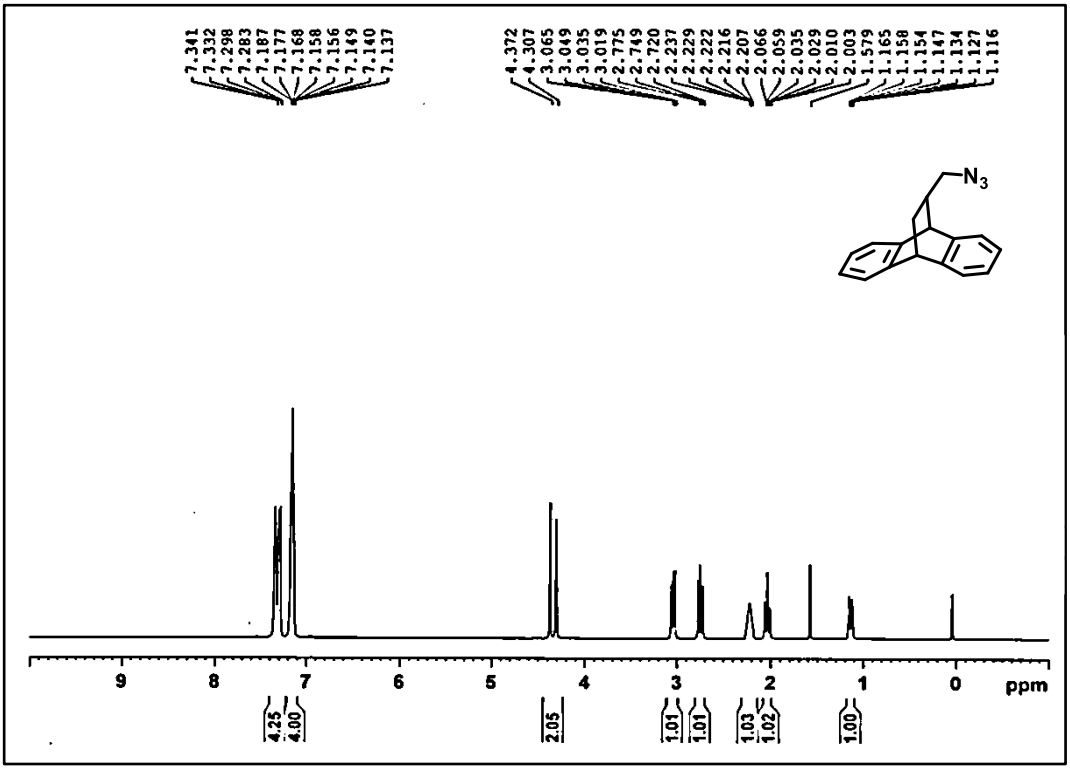

^{1}H NMR Spectra of compound **56** ($CDCl_3$, 400MHz)

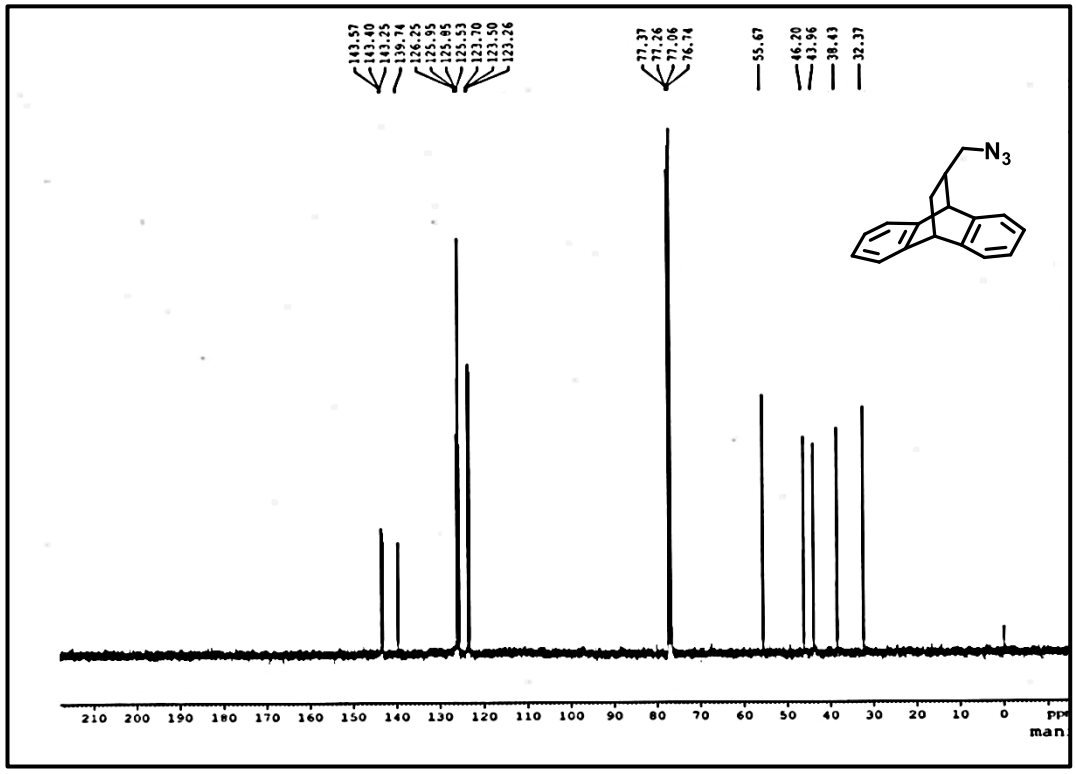

^{13}C NMR Spectra of compound **56** ($CDCl_3$, 100MHz)

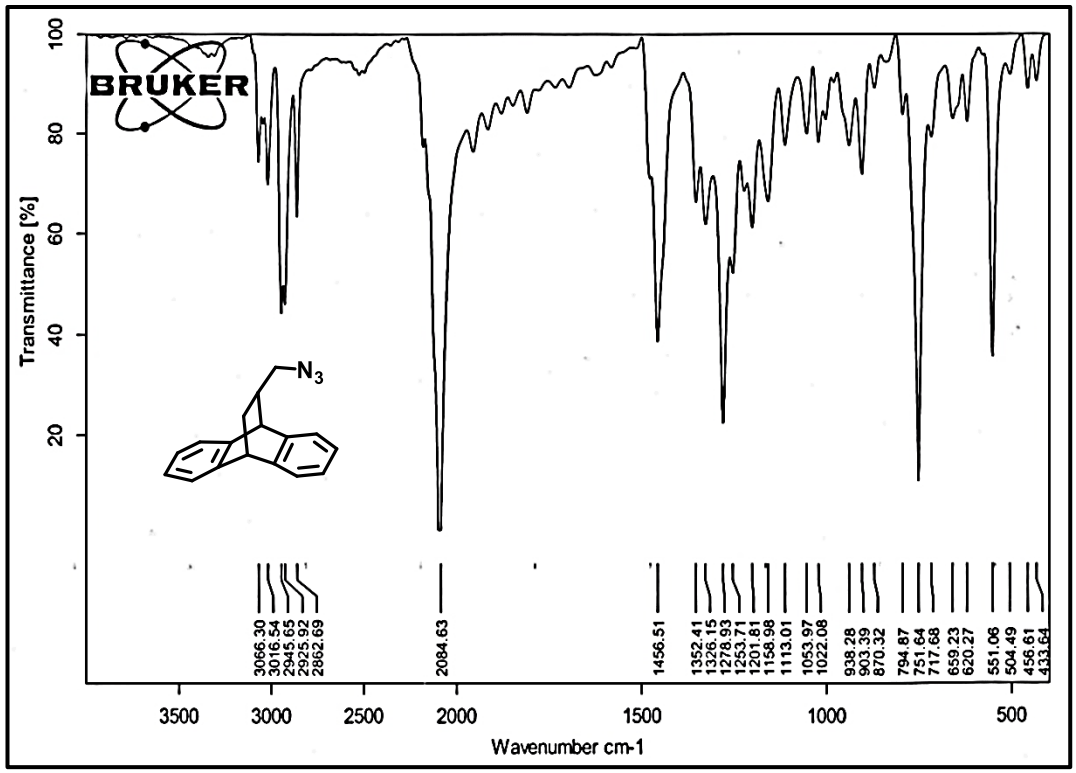

IR Spectra of compound **56**

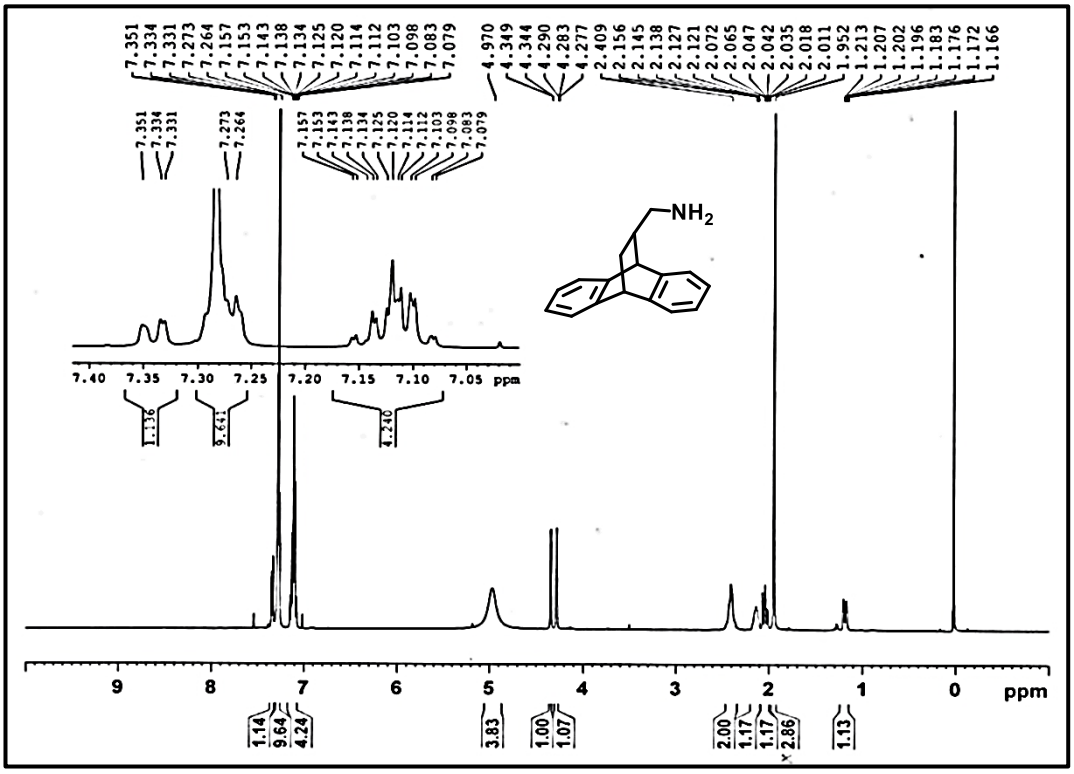

^{1}H NMR Spectra of compound **57** ($CDCl_3$, 400MHz)

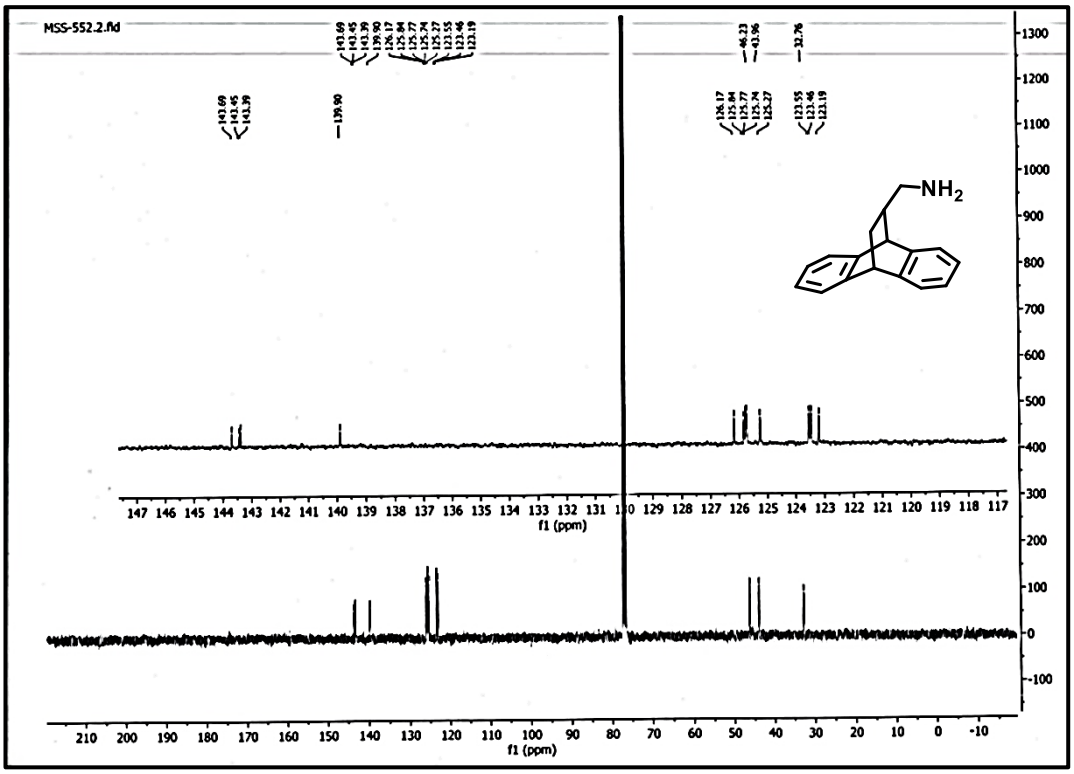

^{13}C NMR Spectra of compound **57** ($CDCl_3$, 100MHz)

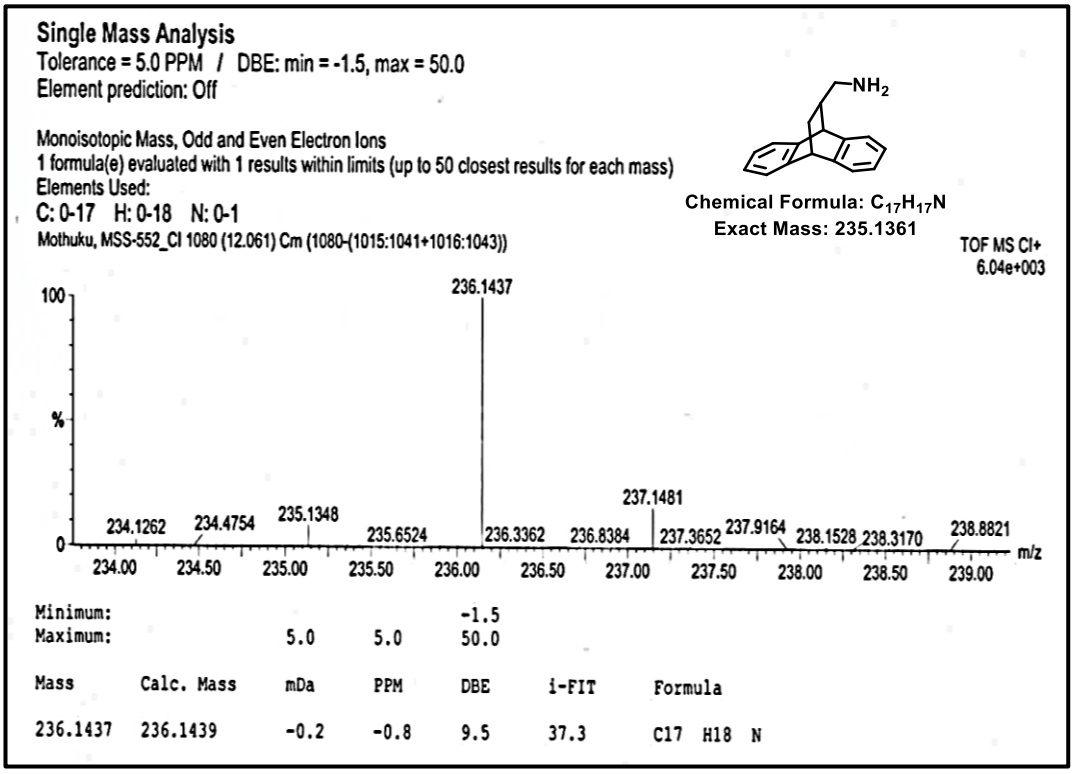

HRMS Spectra of compound **57**

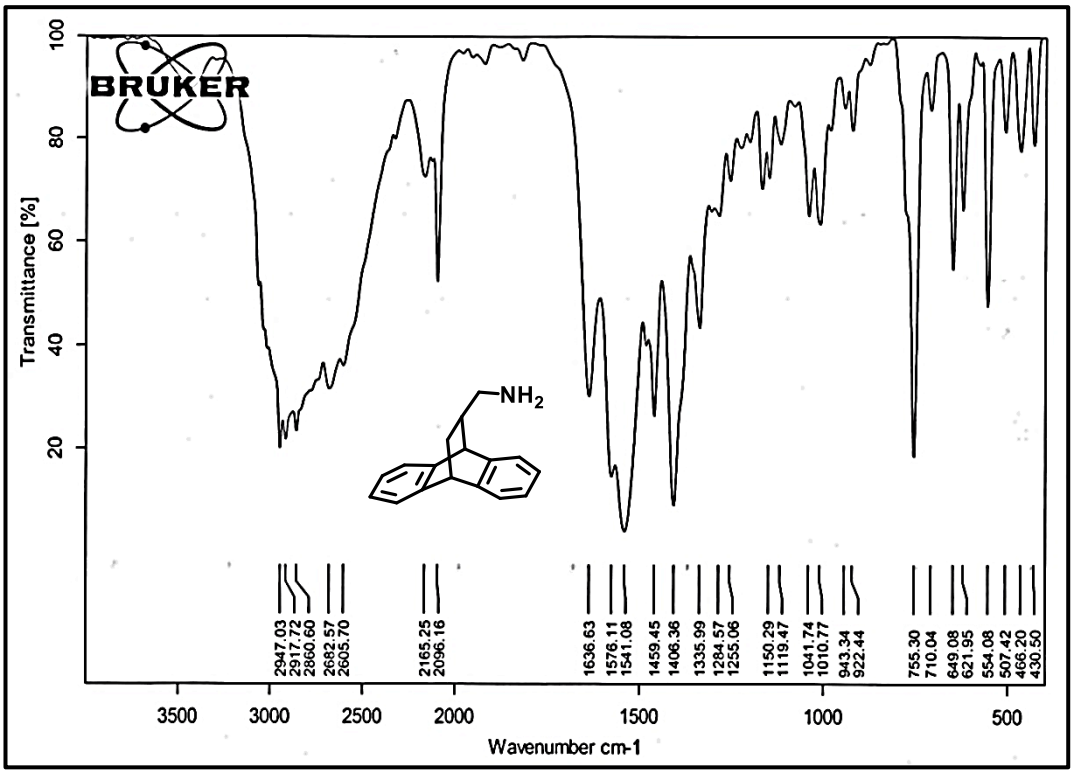

IR Spectra of compound **57**

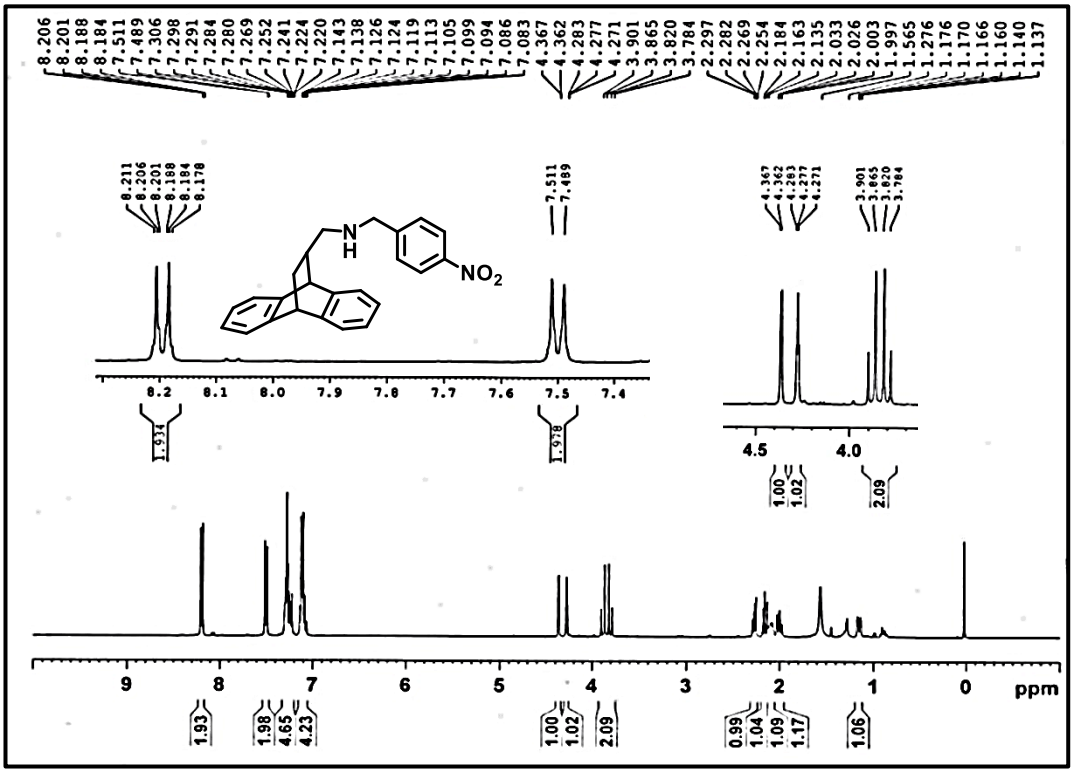

^{1}H NMR Spectra of compound (*R*)-**58** ($CDCl_3$, 400MHz)

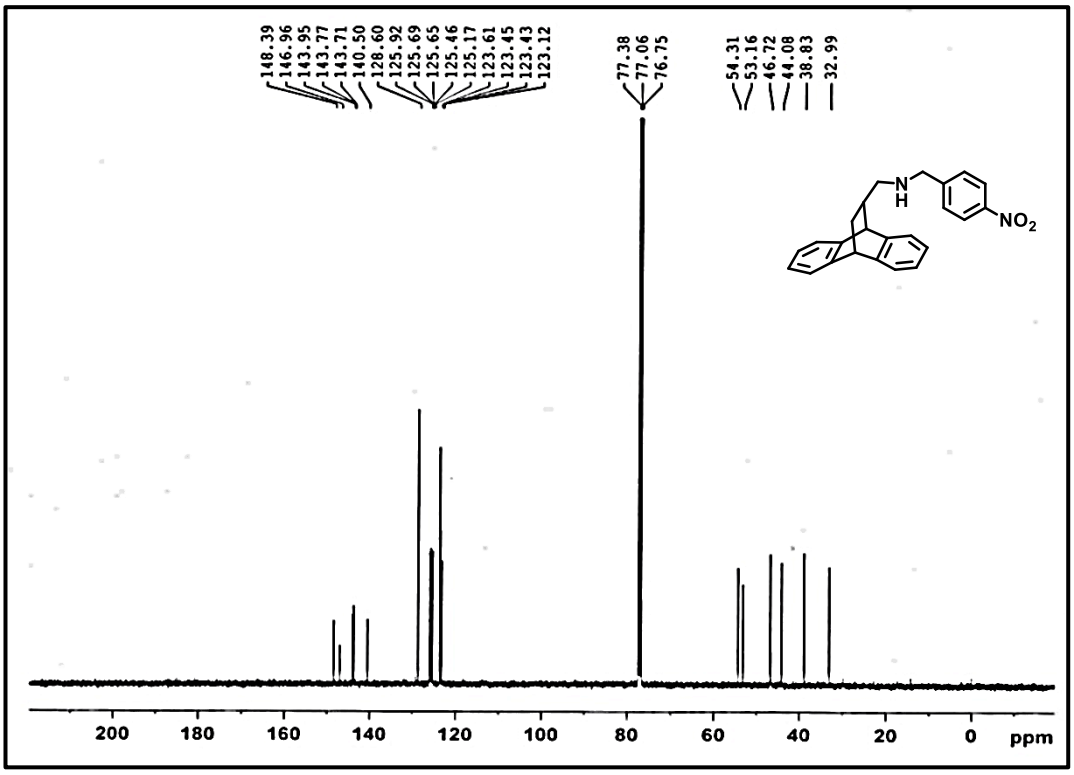

^{13}C NMR Spectra of compound (*R*)-**58** ($CDCl_3$, 100MHz)

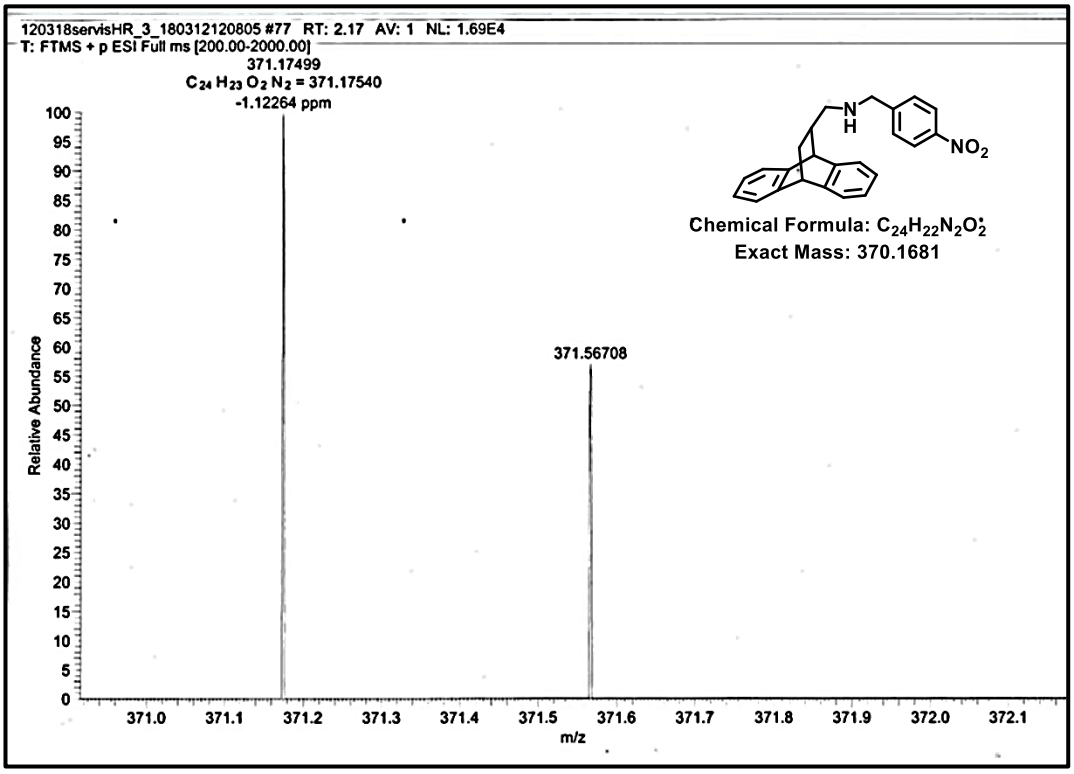

HRMS Spectra of compound (*R*)-**58**

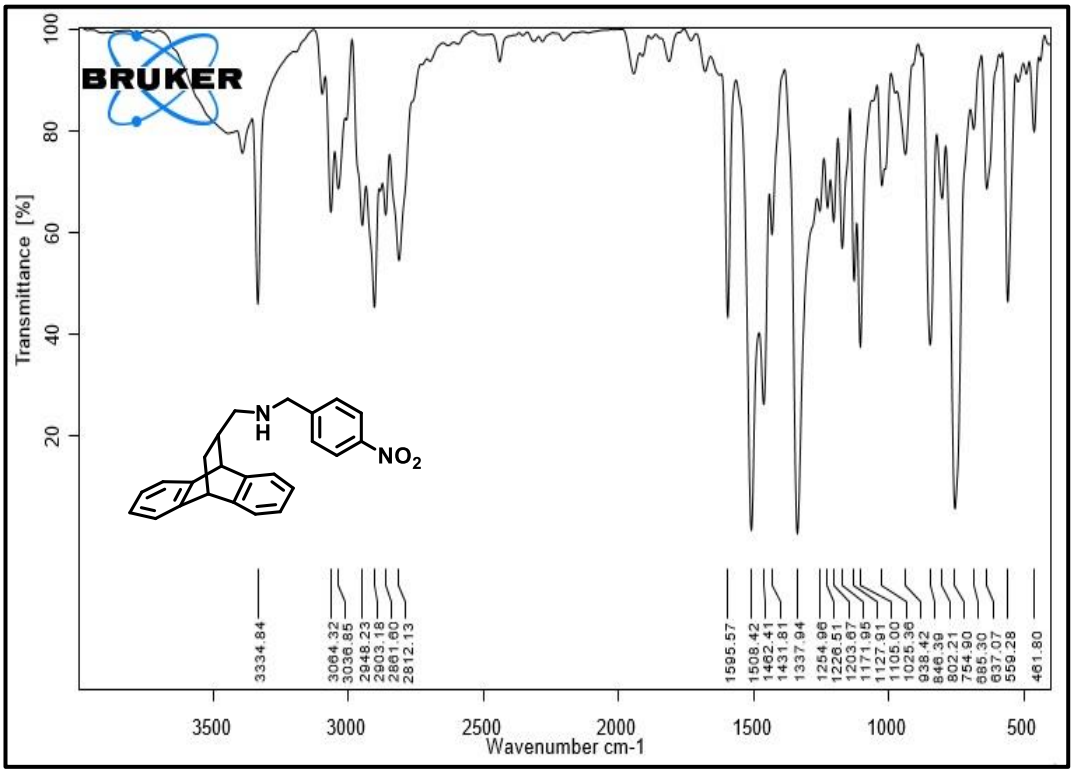

IR Spectra of compound (*R*)-**58**

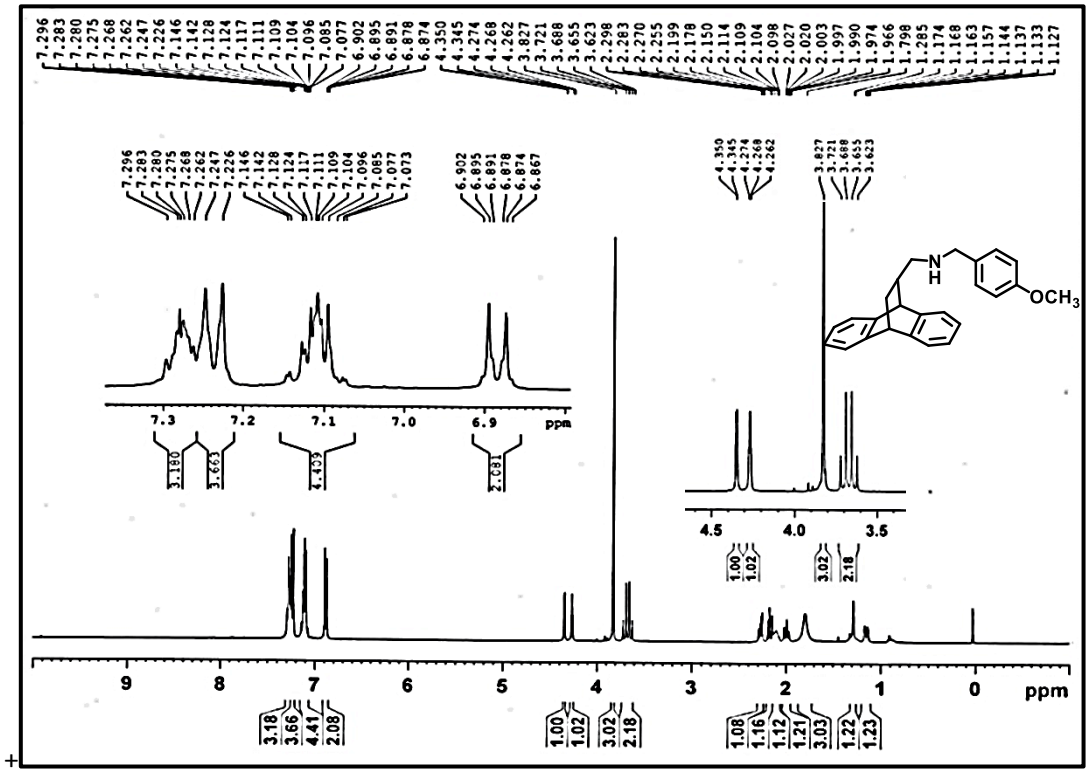

^{1}H NMR Spectra of compound (*R*)-**59** ($CDCl_3$, 400MHz)

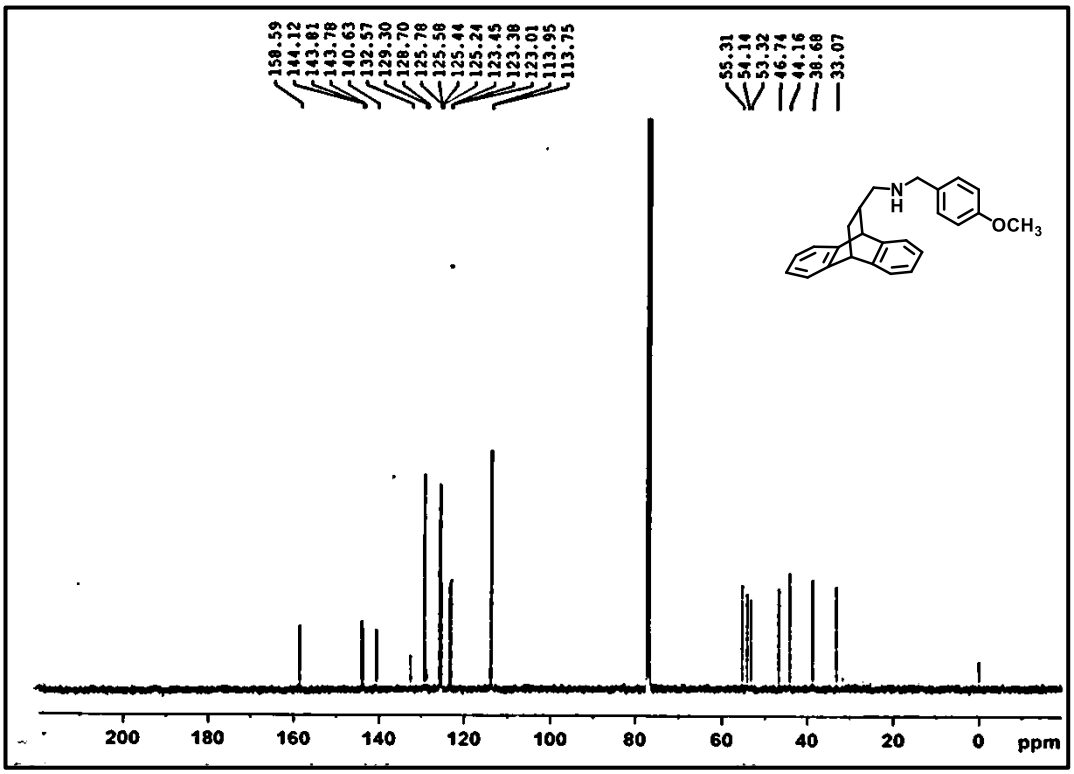

^{13}C NMR Spectra of compound (*R*)-**59** ($CDCl_3$, 100MHz)

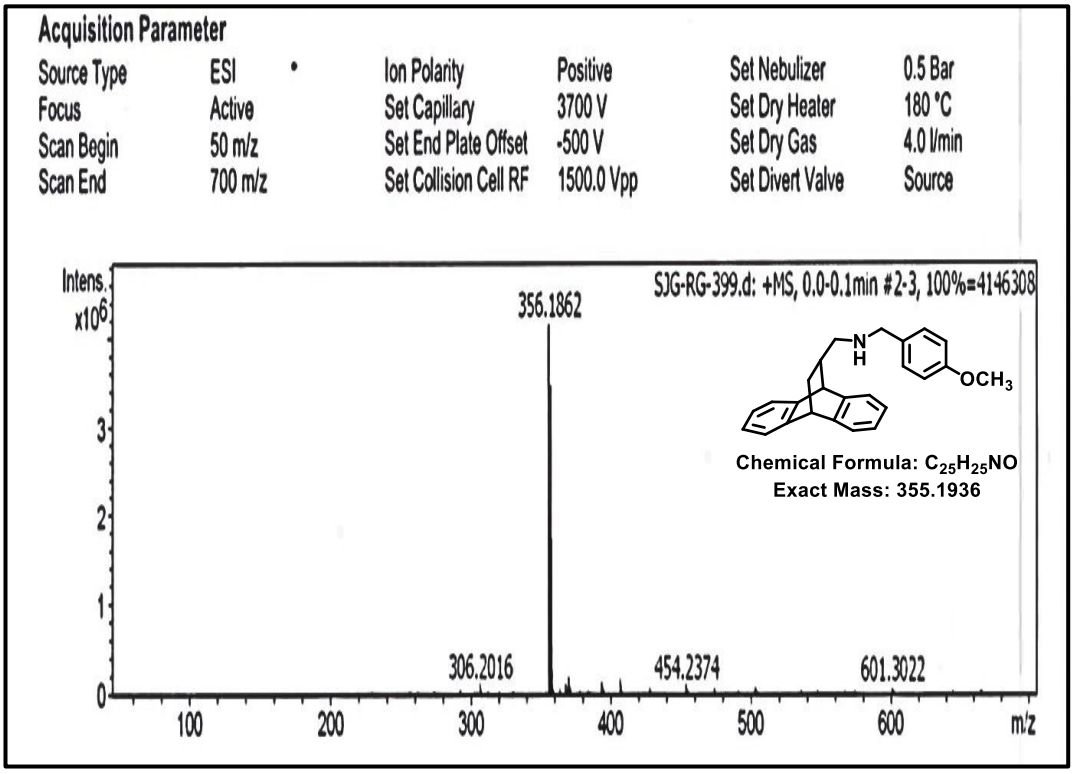

HRMS Spectra of compound (*R*)-**59**

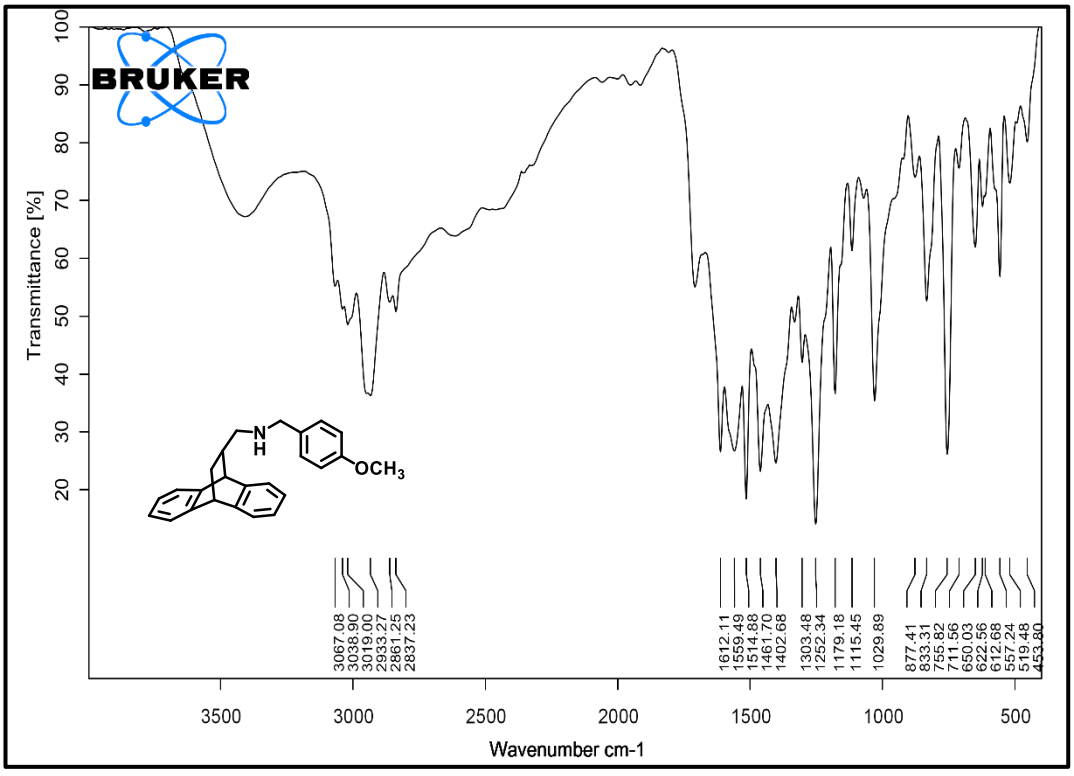

IR Spectra of compound (*R*)-**59**

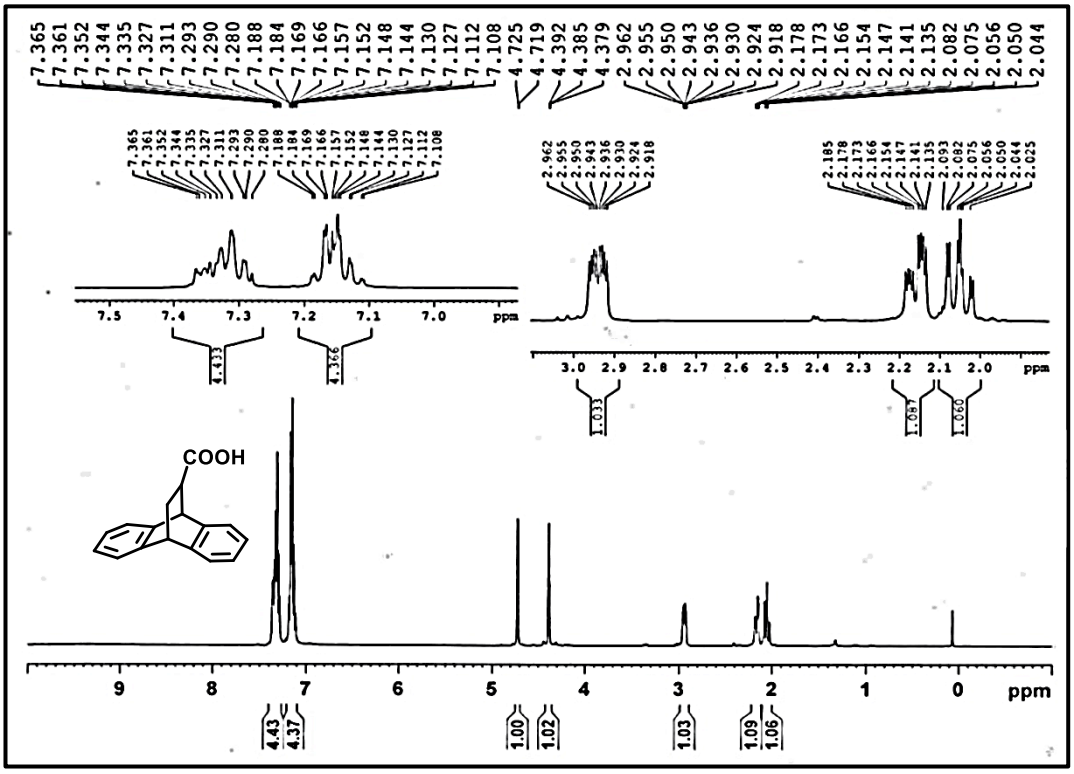

^{1}H NMR Spectra of compound **60** ($CDCl_3$, 400MHz)

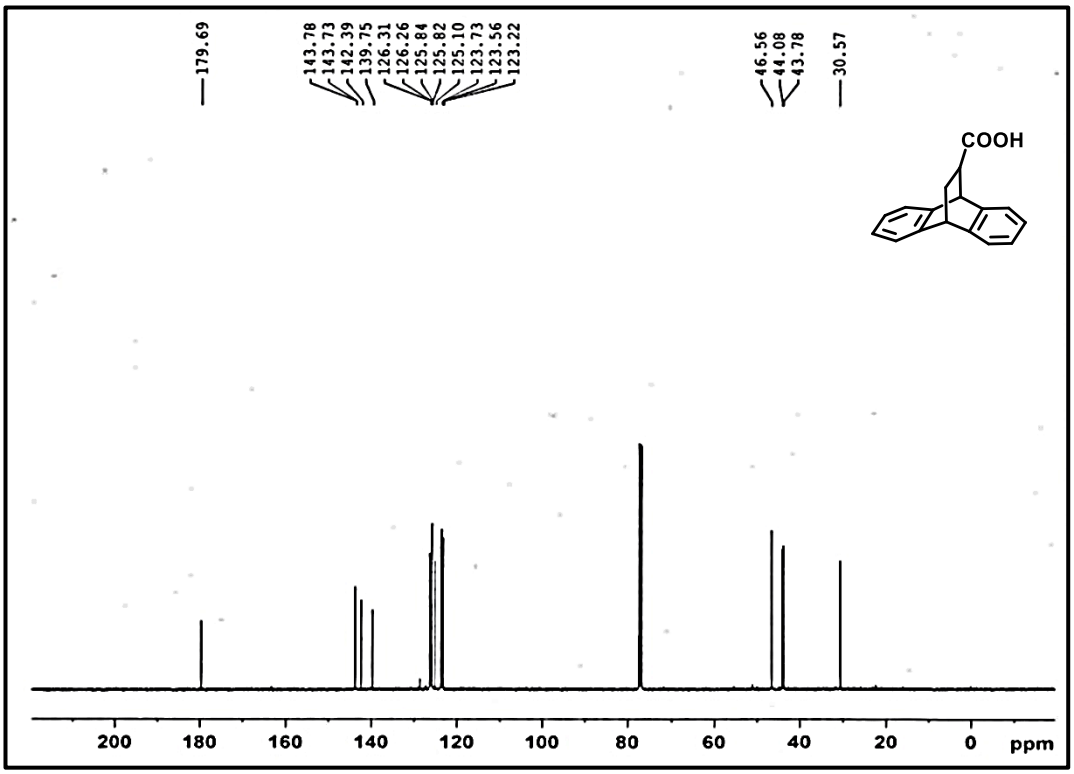

^{13}C NMR Spectra of compound **60** ($CDCl_3$, 100MHz)

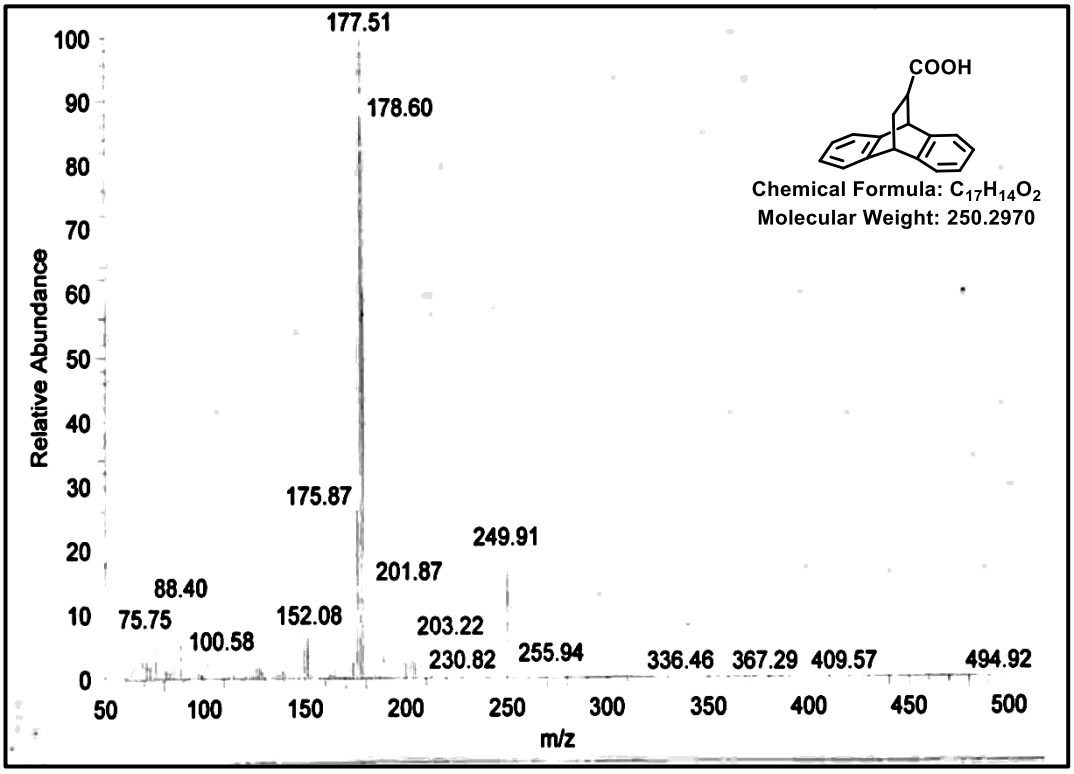

Mass spectra of compound **60**

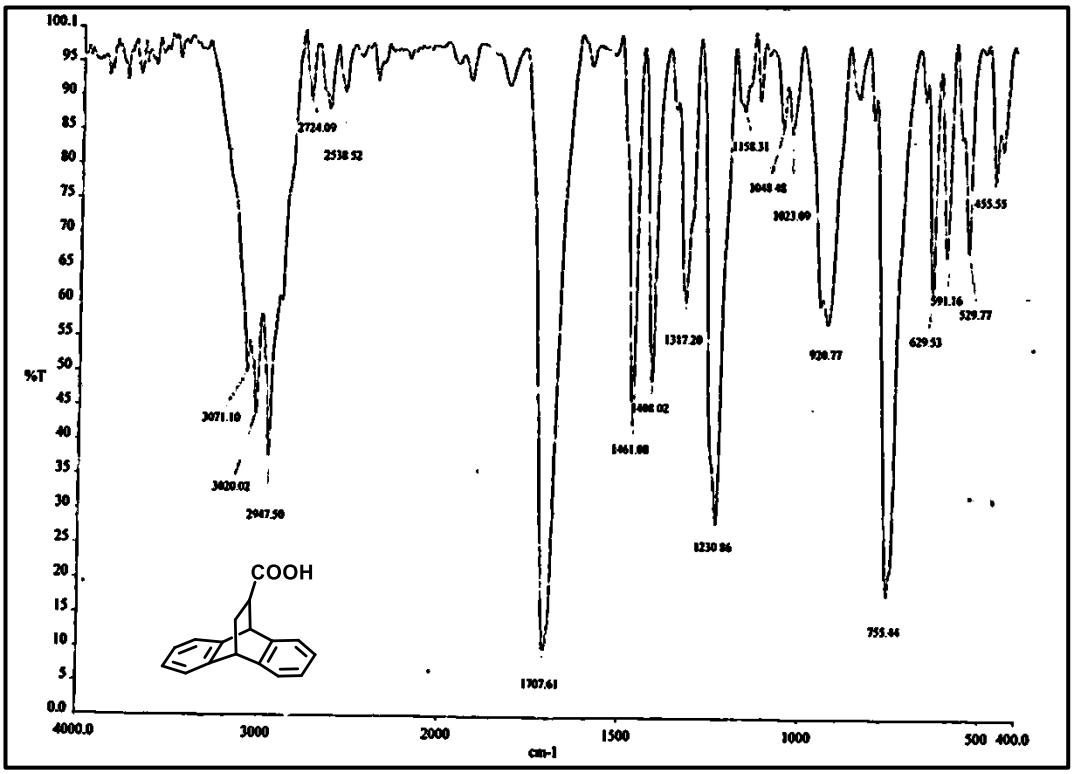

IR spectra of compound **60**

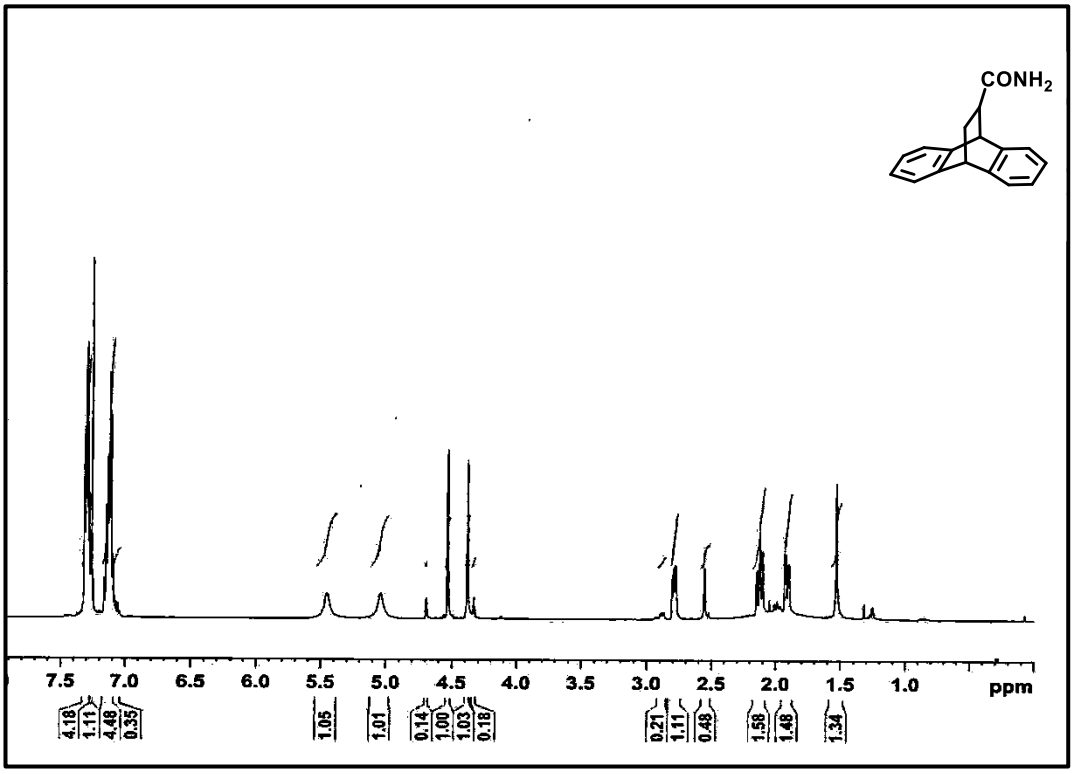

^{1}H NMR spectra of compound **61** ($CDCl_3$, 400MHz)

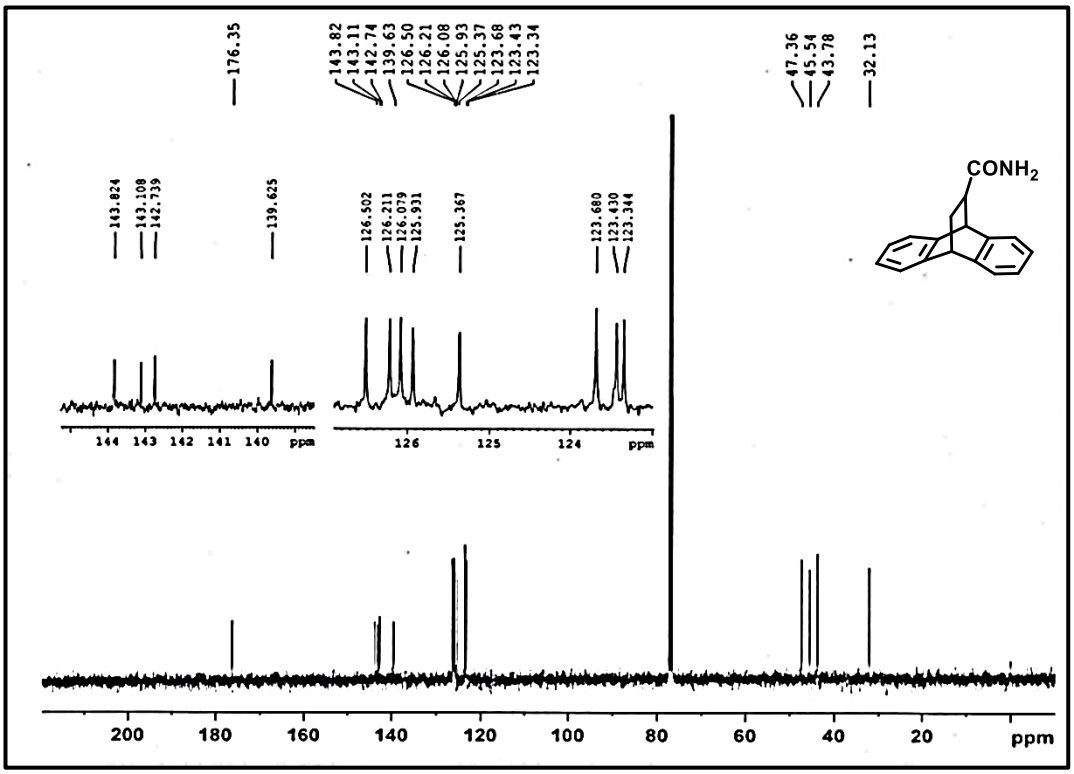

^{13}C NMR spectra of compound **61** ($CDCl_3$, 100MHz)

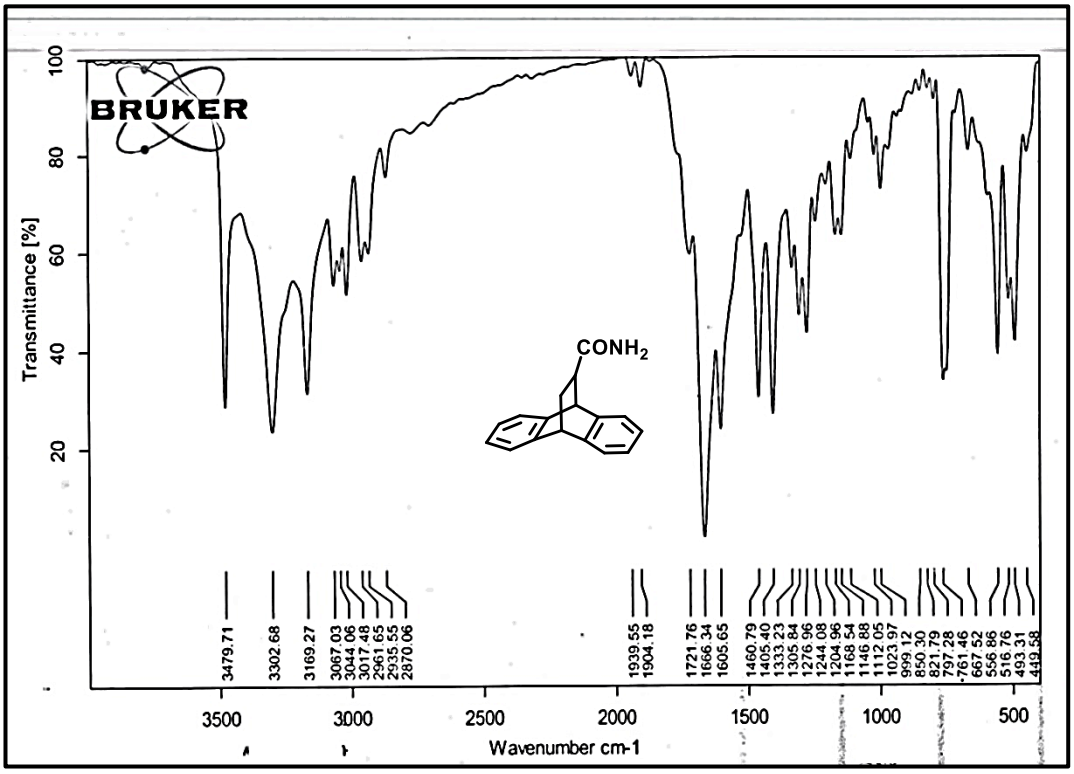

IR spectra of compound **61**

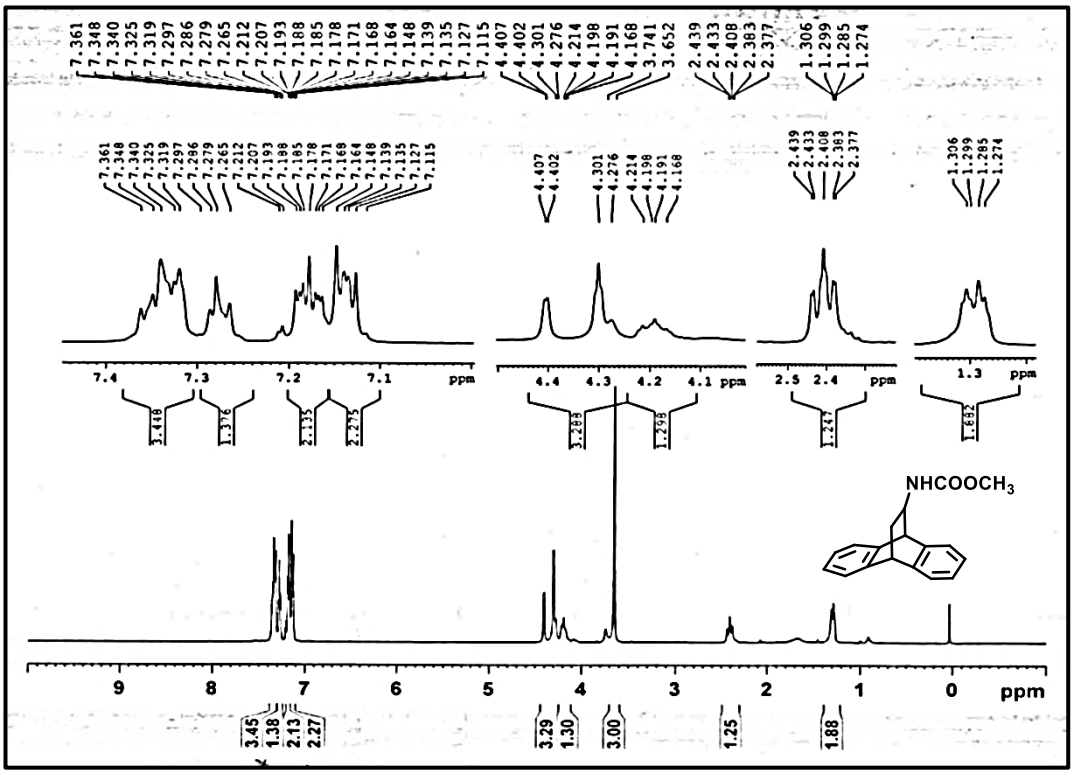

^{1}H NMR spectra of compound **62** ($CDCl_3$, 400MHz)

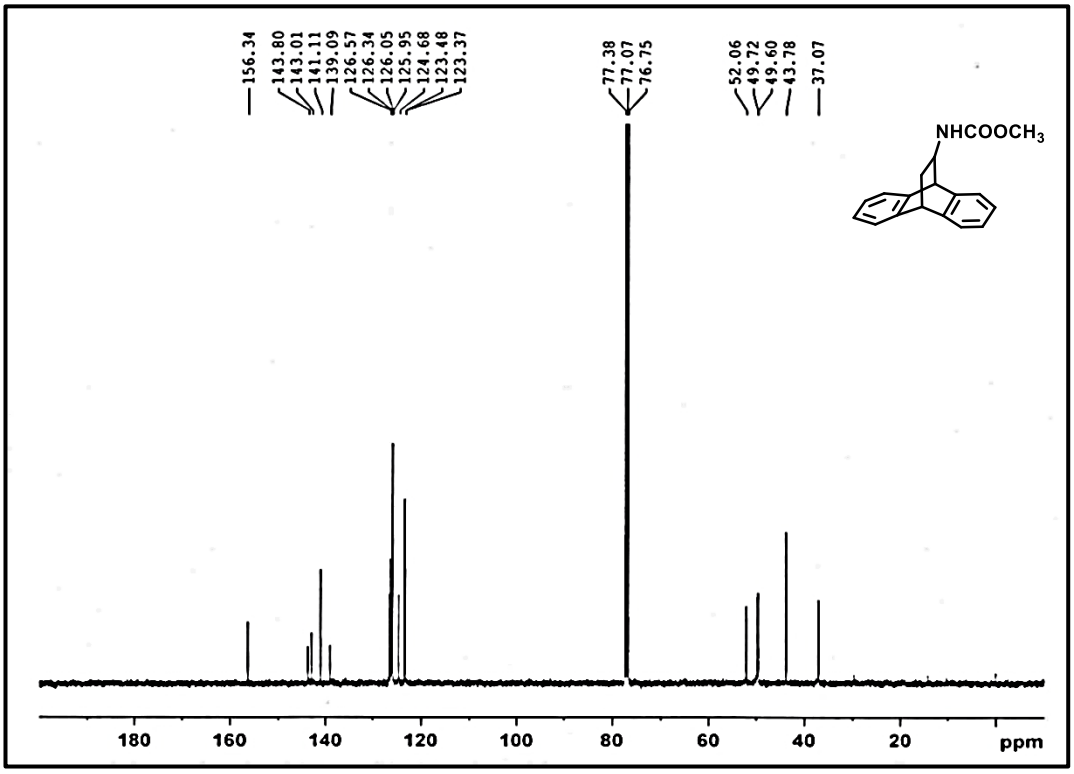

^{13}C NMR spectra of compound **62** ($CDCl_3$, 100MHz)

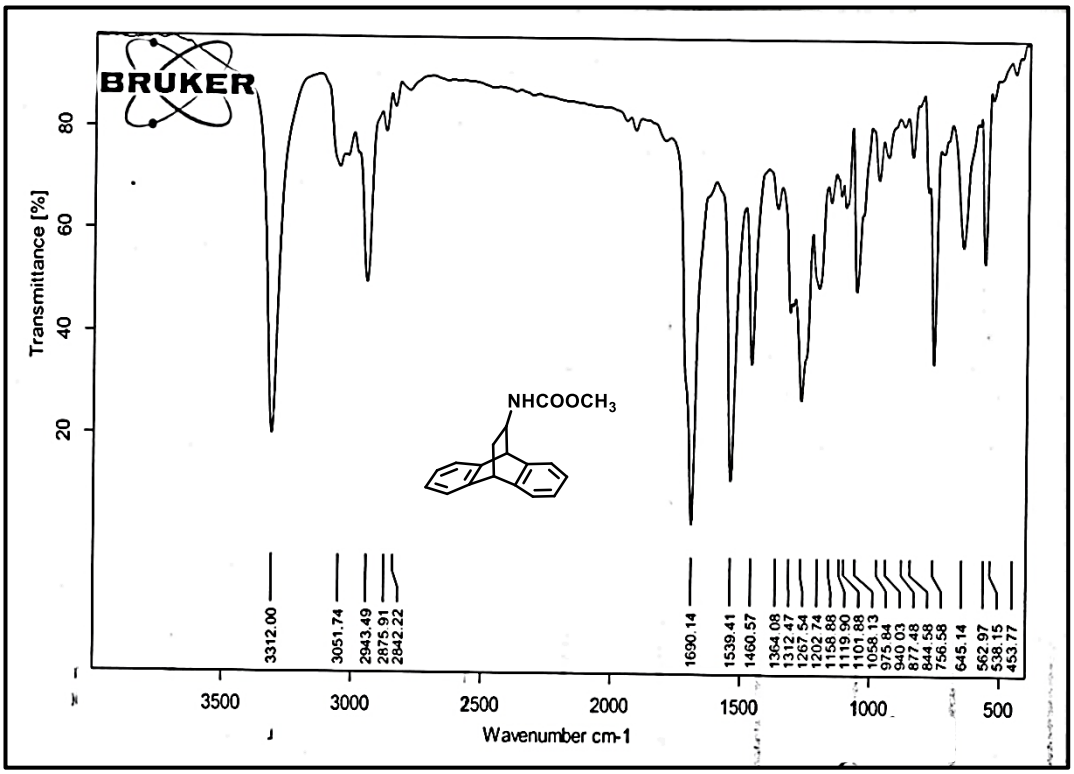

IR spectra of compound **62**

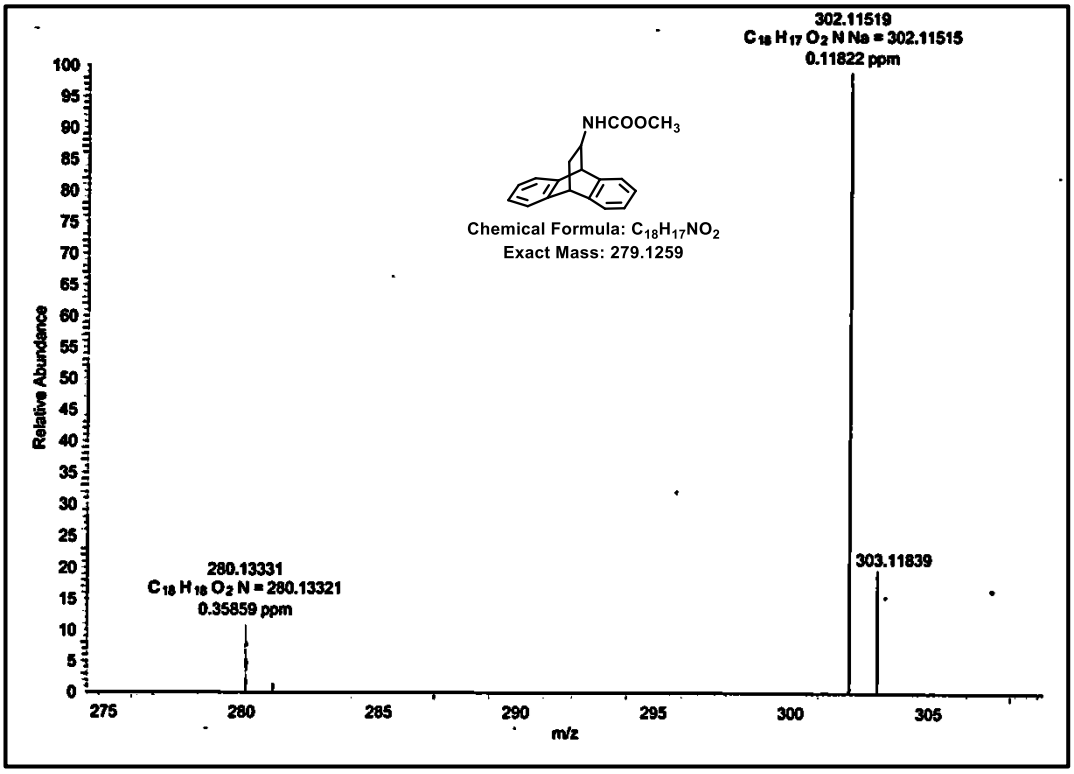

HRMS spectra of compound **62**

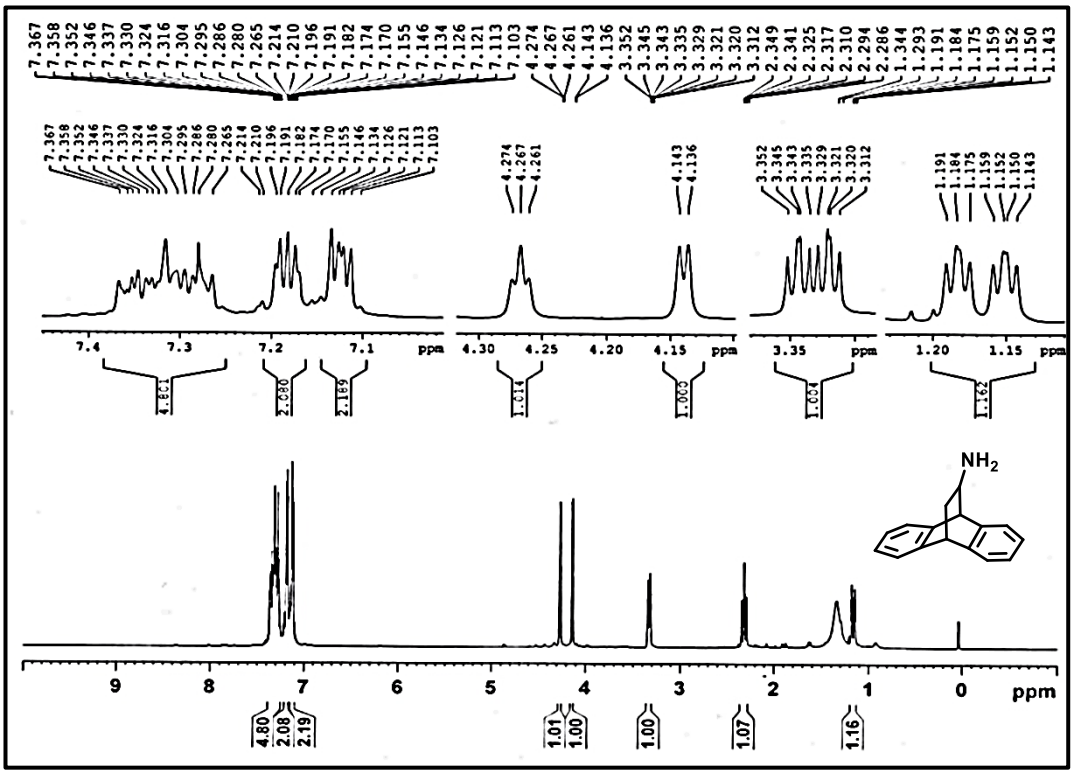

^{1}H NMR spectra of compound **63** ($CDCl_3$, 400MHz)

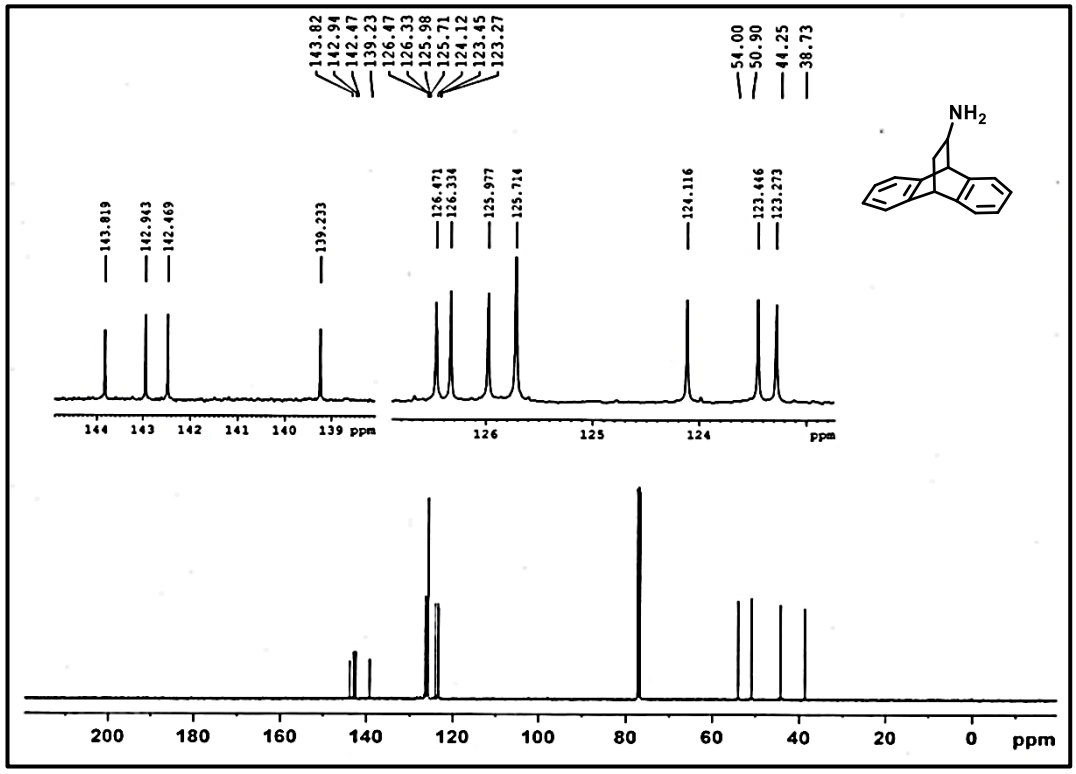

^{13}C NMR spectra of compound **63** ($CDCl_3$, 100MHz)

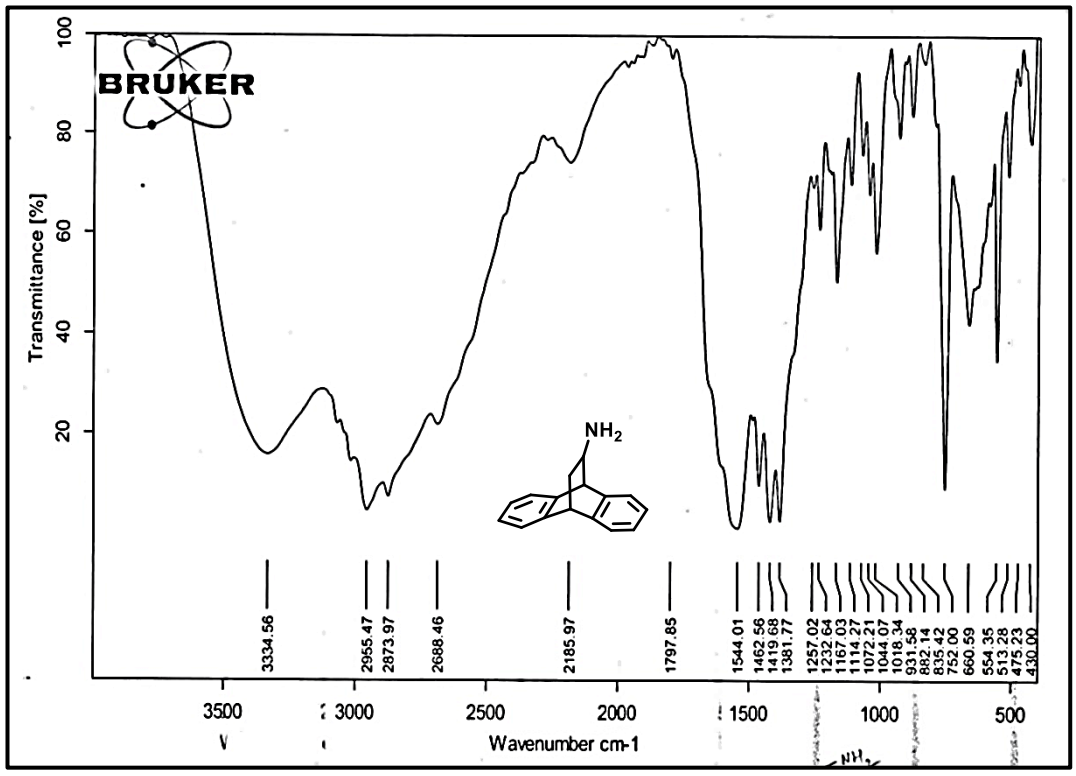

IR spectra of compound **63**

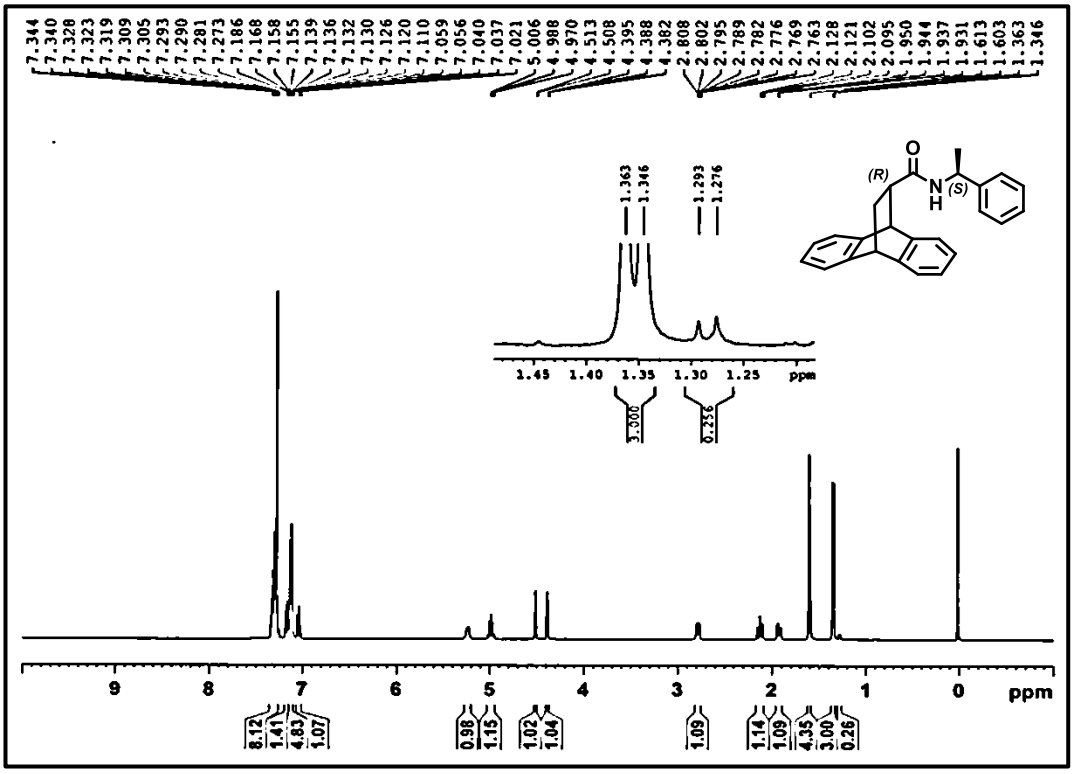

^{1}H NMR Spectra of compound **(*R,S*)-64** ($CDCl_3$, 400MHz)

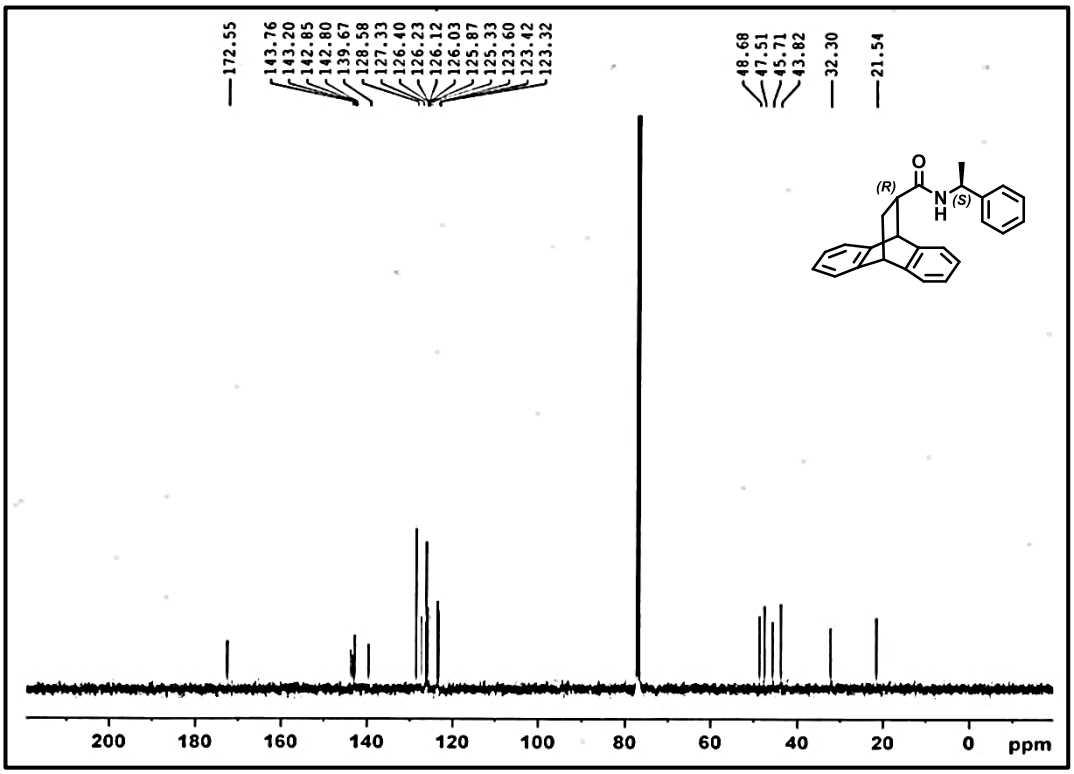

^{13}C NMR Spectra of compound **(*R,S*)-64** ($CDCl_3$, 100MHz)

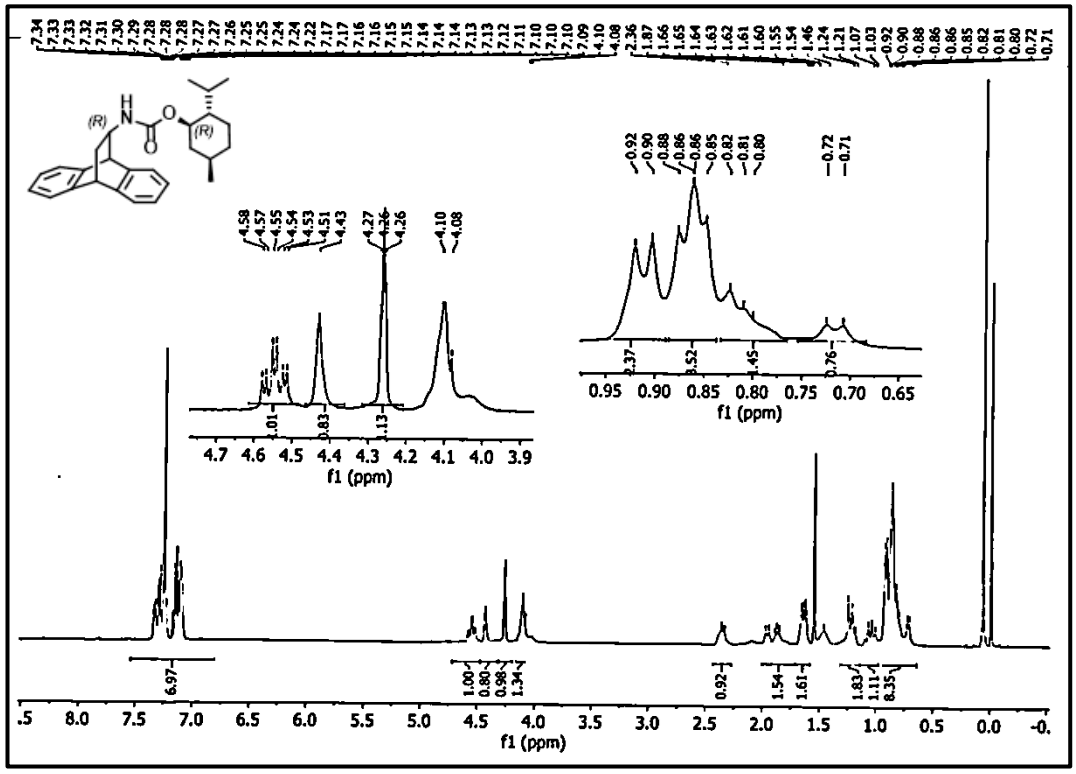

^{1}H NMR Spectra of compound **63** ($CDCl_3$, 400MHz)

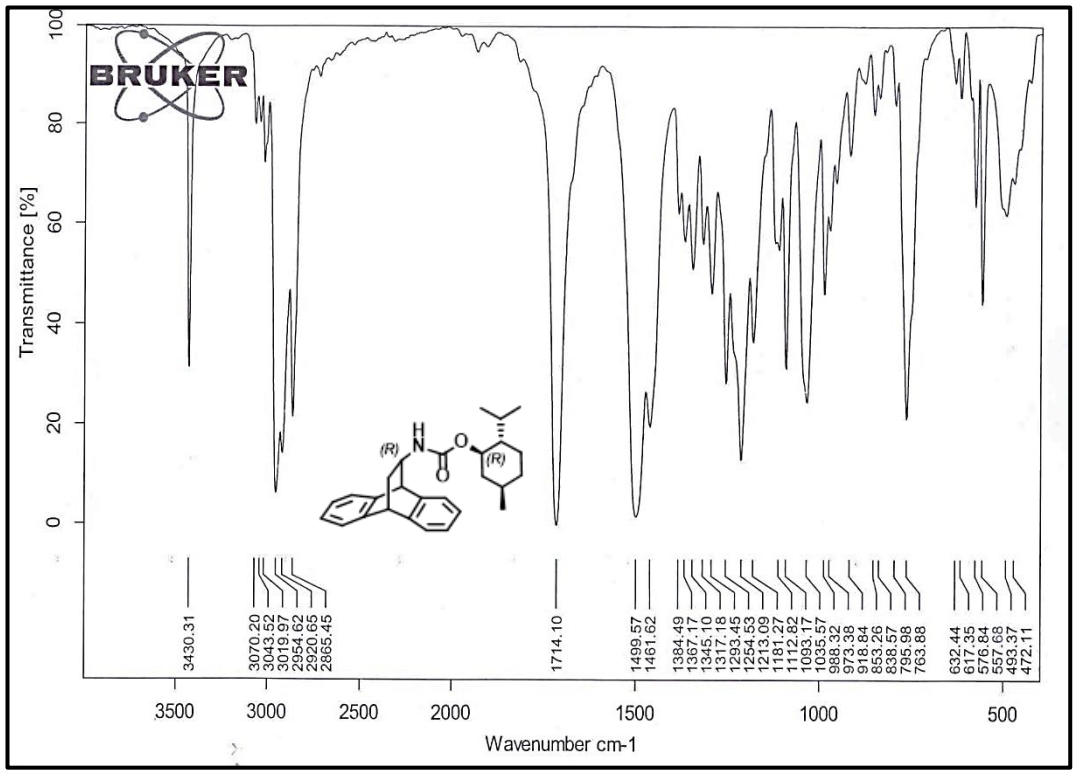

IR Spectra of compound **65**

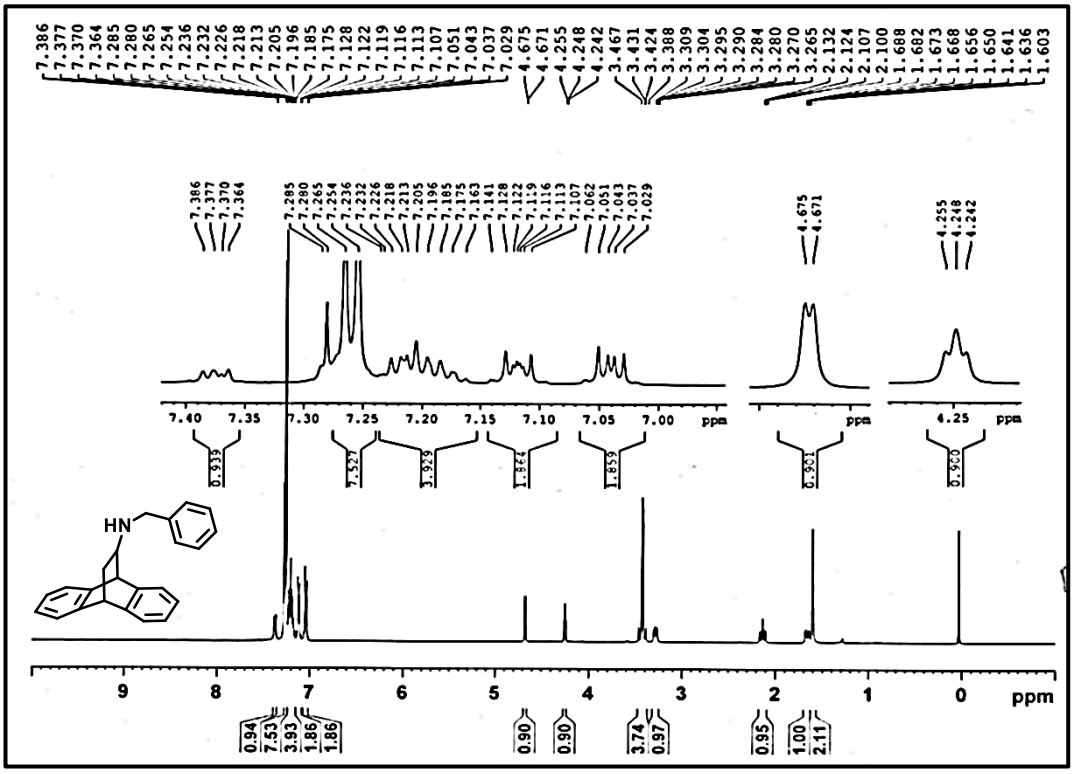

^{1}H NMR Spectra for compound **66** ($CDCl_3$, 400MHz)

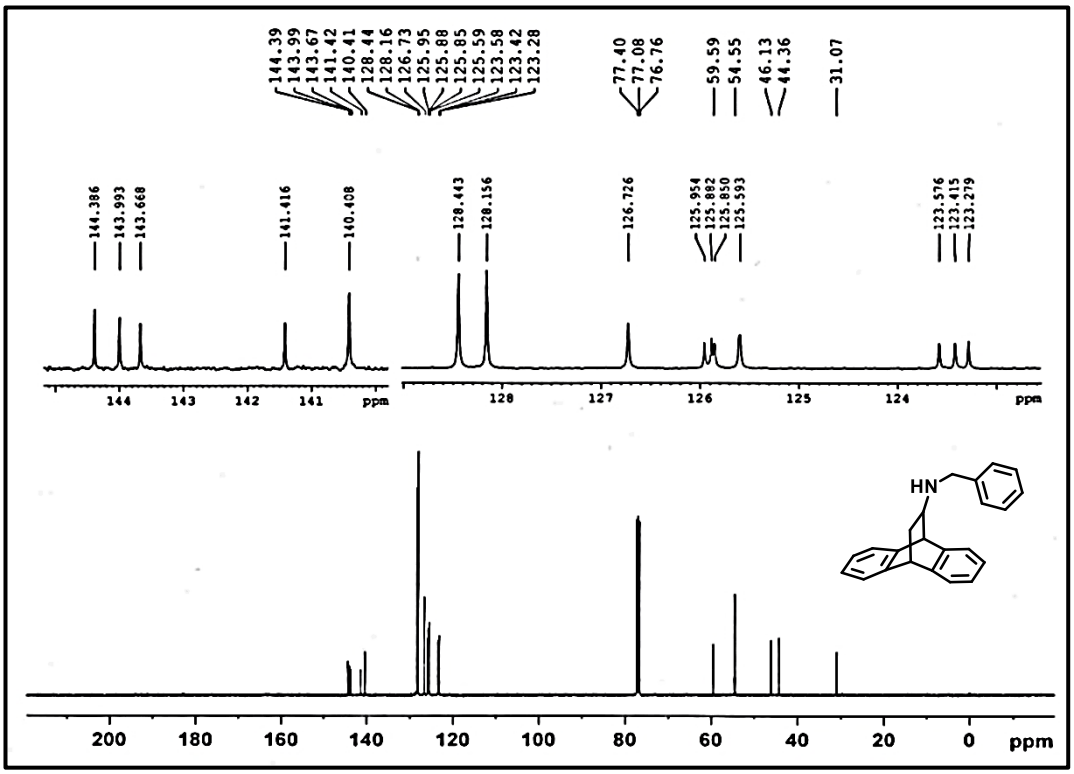

^{13}C NMR Spectra for compound **66** ($CDCl_3$, 100MHz)

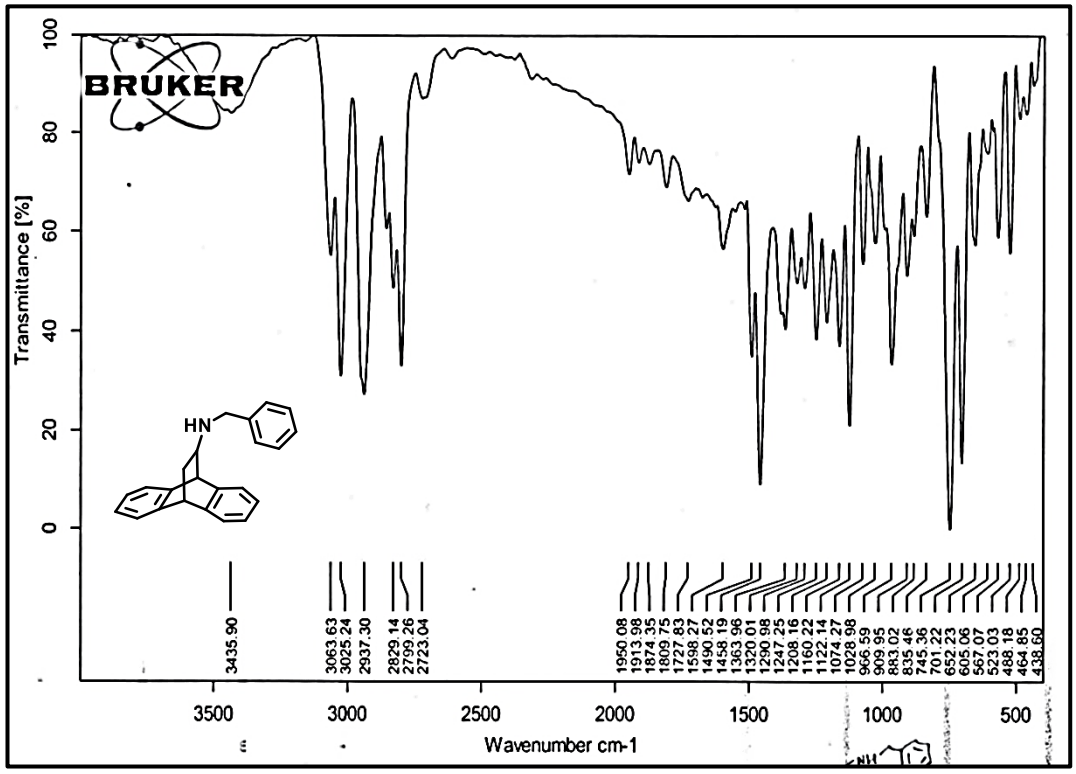

IR Spectra for compound **66**

4.6 Crystallographic Data:

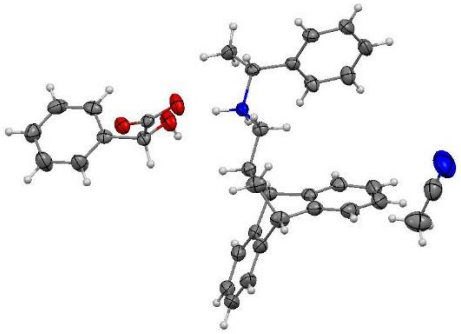

ORTEP diagram of **RR-R-MA** with ellipsoids shown at Probability level of 50%

Table 7: Crystal data and Structural Refinement of compound **RR-R-MA** (CCDC No. **: 1468129**)

Empirical formula	$C_{17.5}H_{18}NO_{1.5}$
Formula weight	266.33
Temperature/K	296(2)
Crystal system	monoclinic
Space group	P21
a/Å	10.8811(8)
b/Å	9.6564(7)
c/Å	14.0641(11)
α/°	90
β/°	97.8640(10)
γ/°	90
Volume/Å^3	1463.85(19)
Z	4
ρ_{calc}g/cm^3	1.208
μ/mm^{-1}	0.077
F(000)	568.0
Radiation	MoKα (λ = 0.71073)
2Θ range for data collection/°	3.778 to 49.992
Index ranges	-12 ≤ h ≤ 12, -11 ≤ k ≤ 11, -16 ≤ l ≤ 16
Reflections collected	15313
Independent reflections	5161 [R_{int} = 0.0283, R_{sigma} = 0.0288]
Data/restraints/parameters	5161/1/364
Goodness-of-fit on F^2	1.071
Final R indexes [I>=2σ (I)]	R_1 = 0.0368, wR_2 = 0.0873
Final R indexes [all data]	R_1 = 0.0399, wR_2 = 0.0887
Largest diff. peak/hole / e Å^{-3}	0.12/-0.17

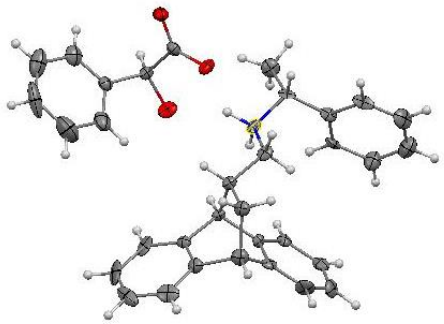

ORTEP diagram of **RR-S-MA** with ellipsoids shown at Probability level of 50%

Table 8: Crystal data and Structural Refinement of compound **RR-S-MA** (CCDC No. **1468131**)

Empirical formula	$C_{33}H_{33}NO_3$
Formula weight	491.60
Temperature/K	150(2)
Crystal system	monoclinic
Space group	$P2_1$
a/Å	9.7297(14)
b/Å	24.373(4)
c/Å	12.012(2)
α/°	90
β/°	92.421(7)
γ/°	90
Volume/Å^3	2846.1(8)
Z	4
ρ_{calc}g/cm^3	1.147
μ/mm^{-1}	0.073
F(000)	1048.0
Crystal size/mm^3	0.360 × 0.310 × 0.210
Radiation	MoKα (λ = 0.71073)
2Θ range for data collection/°	3.342 to 49.998
Index ranges	$-11 \leq h \leq 11$, $-27 \leq k \leq 28$, $-12 \leq l \leq 12$
Reflections collected	13867
Independent reflections	7860 [R_{int} = 0.0689, R_{sigma} = 0.1541]
Data/restraints/parameters	7860/181/671
Goodness-of-fit on F^2	1.075
Final R indexes [I>=2σ (I)]	R_1 = 0.0991, wR_2 = 0.1307
Final R indexes [all data]	R_1 = 0.1501, wR_2 = 0.1486
Largest diff. peak/hole / e Å^{-3}	0.28/-0.30

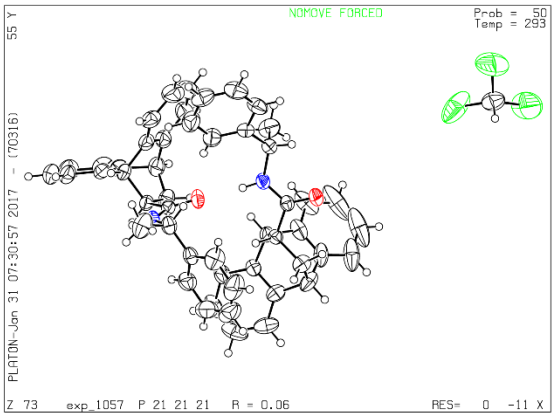

ORTEP diagram of **(*R,S*)-64** with ellipsoids shown at Probability level of 50%

Table 9: Crystal data and Structural Refinement of compound **(*R,S*)-64** (CCDC No. **1530548**)

Empirical formula	$C_{46}H_{50}N_5O_6Cl_{0.25}$
Formula weight	826.31
Temperature/K	293(2)
Crystal system	orthorhombic
Space group	$P2_12_12_1$
a/Å	12.3464(11)
b/Å	18.4020(16)
c/Å	19.3222(14)
α/°	90
β/°	90
γ/°	90
Volume/Å^3	4390.0(6)
Z	4
ρ_{calc}g/cm^3	1.2501
μ/mm^{-1}	0.251
F(000)	1738.4
Radiation	MoKα (λ = 0.71073)
2Θ range for data collection/°	6.6 to 57.98
Index ranges	$-16 \le h \le 16$, $-23 \le k \le 25$, $-24 \le l \le 23$
Reflections collected	17454
Independent reflections	11658 [R_{int} = 0.0315, R_{sigma} = 0.0554]
Data/restraints/parameters	11658/0/524
Goodness-of-fit on F^2	0.841
Final R indexes [I>=2σ (I)]	R_1 = 0.0627, wR_2 = N/A
Final R indexes [all data]	R_1 = 0.1062, wR_2 = 0.2455
Largest diff. peak/hole / e Å^{-3}	0.42/-0.56
Flack parameter	0.01(9)

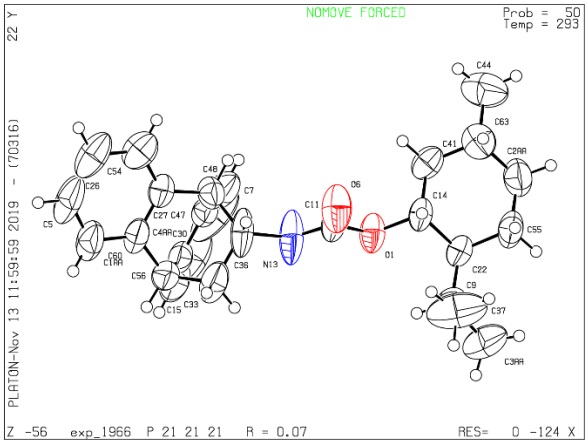

ORTEP diagram of **(*R,R*)-65** with ellipsoids shown at Probability level of 50%

Table 10: Crystal data and Structural Refinement of compound **(*R,R*)-65** (CCDC No. **1976424**)

Empirical formula	$C_{27}H_{33}NO_2$
Formula weight	403.54
Temperature/K	293(2)
Crystal system	orthorhombic
Space group	$P2_12_12_1$
a/Å	7.1380(6)
b/Å	7.5034(9)
c/Å	43.617(3)
α/°	90
β/°	90
γ/°	90
Volume/Å^3	2336.1(4)
Z	4
ρ_{calc}g/cm^3	1.147
μ/mm^{-1}	0.071
F(000)	872.0
Radiation	MoKα (λ = 0.71073)
2Θ range for data collection/°	5.784 to 58.012
Index ranges	$-9 \leq h \leq 7$, $-9 \leq k \leq 9$, $-58 \leq l \leq 58$
Reflections collected	15162
Independent reflections	5377 [R_{int} = 0.0732, R_{sigma} = 0.0984]
Data/restraints/parameters	5377/0/274
Goodness-of-fit on F^2	0.985
Final R indexes [I>=2σ (I)]	R_1 = 0.0668, wR_2 = 0.1345
Final R indexes [all data]	R_1 = 0.1787, wR_2 = 0.1856
Largest diff. peak/hole / e Å^{-3}	0.14/-0.19
Flack parameter	0.0(10)

4.7 References:

[1] E. Weber, J. Ahrendt, S. Finge, I. Csöregh, M. Czugler, *J. Org. Chem.* **1988**, *53*, 5831–5839.

[2] M. Czugler, E. Weber, J. Ahrendt, *J. Chem. Soc. Chem. Commun.* **1984**, *559*, 1632–1634.

[3] E. Weber, M. Hecker, I. Csoregh, M. Czugler, *Mol. Cryst. Liq. Cryst. Inc. Nonlinear Opt.* **1990**, *187*, 165–174.

[4] I. Csöregh, O. Gallardo, E. Weber, S. Finge, C. Reutel, *Tetrahedron: Asymmetry* **1992**, *3*, 1555–1562.

[5] I. Csoregh, M. Czugler, E. Weber, Jochen Ahrenndt, *J. Incl. Phenom. Mol. Recognit. Chem.* **1990**, 309–322.

[6] E. D. B. Barnett, N. F. Goodway, E. V. Weekes, *J. Chem. Soc.* **1938**, 1102.

[7] C. R. Ramanathan, M. Periasamy, *Tetrahedron: Asymmetry* **1998**, *9*, 2651–2656.

[8] I. Csoregh, S. Finge, E. Weber, *Bull. Chem. Soc. Jpn* **1991**, *64*, 1971–1975.

[9] S. Allenmark, U. Skogsberg, L. Thunberg, *Tetrahedron Asymmetry* **2000**, *11*, 3527–3534.

[10] E. Weber, C. Reutel, C. Foces-Foces, A. L. Llamas-Saiz, *J. Chem. Soc. Perkin Trans. 2* **1994**, *2*, 1455–1461.

[11] E. Weber, T. Hens, O. Gallardo, I. Csöregh, *J. Chem. Soc. Perkin Trans. 2* **1996**, *4*, 737–745.

[12] P. Camps, M. Font-bardia, S. Gimenez, F. Perez, X. Solans, N. Soldevilla, *Tetrahedron Asymmetry* **1999**, *10*, 3123–3138.

[13] H. Waldmann, M. Weigerding, C. Dreisbach, C. Wandrey, *Helv. Chim. Acta* **1994**, *77*, 2111–2116.

[14] S. Doherty, E. G. Robins, J. G. Knight, C. R. Newman, B. Rhodes, P. A. Champkin, W. Clegg, *J. Organomet. Chem.* **2001**, *640*, 182–196.

[15] C. Dobler, H. J. Kruenzfeld, *J. F. Prakt. Chem.* **1983**, 1021–1026.

[16] B. M. Trost, G. M. Schroeder, J. Kristensen, *An* **2002**, *41*, 3492–3495.

[17] H. J. Kreuzfeld, C. Dobler, *React. Kinet. Catal. Lett.* **1984**, *24*, 153–156.

[18] L. Thunberg, S. Allenmark, *Tetrahedron Asymmetry* **2003**, *14*, 1317–1322.

[19] H. Matsunaga, K. Kimura, T. Ishizuka, M. Karatake, T. Kunieda, *Tetrahedron Lett.* **1991**, *32*, 7715–7718.

[20] A. A. M. Abdel-Aziz, J. Okuno, S. Tanaka, T. Ishizuka, H. Matsunaga, T. Kunieda, *Tetrahedron Lett.* **2000**, *41*, 8533–8537.

[21] K. Yokoyama, T. Ishizuka, N. Ohmachi, T. Kunieda, *Tetrahedron Lett.* **1998**, *39*, 4847–4850.

[22] S. Hoshimoto, H. Matsunaga, T. Kunieda, *Chem. Pharm. Bull.* **2000**, *48*, 1541–1544.

[23] A. Sasaoka, I. Uddin, A. Shimomoto, Y. Ichikawa, *Tetrahedron Asymmetry* **2006**, *17*, 2963–2969.

[24] H. Mihara, Y. Xu, N. E. Shepherd, S. Matsunaga, M. Shibasaki, *J. Am. Chem. Soc.*

2009, *131*, 8384–8385.
[25] S. Alibert, C. Santelli-Rouvier, B. Pradines, C. Houdoin, D. Parzy, J. Karolak-Wojciechowska, J. Barbe, *J. Med. Chem.* **2002**, *45*, 3195–3209.
[26] H. B. Trzezwinska, J. Barbe, *J. Chem. Crystallogr.* **1998**, *28*, 905–911.
[27] J. Millet, M. Torrentino-Madamet, S. Alibert, C. Rogier, C. Santelli-Rouvier, J. Mosnier, E. Baret, J. Barbe, D. Parzy, B. Pradines, *Antimicrob. Agents Chemother.* **2004**, *48*, 2753–2756.
[28] N. A. Anisimova, V. M. Berestovitskaya, I. S. Bagryanskaya, M. E. Ivanova, G. A. Berkova, A. A. Kuzhaeva, *Russ. J. Gen. Chem.* **2010**, *80*, 308–315.
[29] S. Alibert, C. Santelli-Rouvier, M. Castaing, M. Berthelot, G. Spengler, J. Molnar, J. Barbe, *Eur. J. Med. Chem.* **2003**, *38*, 253–263.
[30] N. Jain, A. V. Bedekar, *Tetrahedron Asymmetry* **2011**, *22*, 1176–1179.
[31] N. Jain, M. B. Mandal, A. V. Bedekar, *Tetrahedron* **2014**, *70*, 4343–4354.
[32] N. Jain, A. V. Bedekar, *Tetrahedron Lett.* **2016**, *57*, 692–695.
[33] S. Alibert, C. Santelli-Rouvier, B. Pradines, C. Houdoin, D. Parzy, J. Karolak-Wojciechowska, J. Barbe, *J. Med. Chem.* **2002**, *45*, 3195–3209.
[34] A. Wiehe, M. O. Senge, H. Kurreck, *Liebigs Ann.* **1997**, *1997*, 1951–1963.
[35] B. Wang, X. Feng, Y. Huang, H. Liu, X. Cui, Y. Jiang, *J. Org. Chem.* **2002**, *67*, 2175–2182.
[36] Z. Zeng, G. Zhao, P. Gao, H. Tang, B. Chen, Z. Zhou, C. Tang, *Catal. Commun.* **2007**, *8*, 1443–1446.
[37] M. S. Jeletic, M. T. Jan, I. Ghiviriga, K. A. Abboud, A. S. Veige, *Dalt. Trans.* **2009**, 2764–2776.
[38] A. Sasaoka, M. I. Uddin, A. Shimomoto, Y. Ichikawa, M. Shiro, H. Kotsuki, *Tetrahedron: Asymmetry* **2006**, *17*, 2963–2969.
[39] R. Annunziata, M. Benaglia, M. Cinquini, F. Cozzi, C. R. Woods, J. S. Siegel, *European J. Org. Chem.* **2001**, *2001*, 173–180.
[40] X. Yang, G. Wang, C. Zhong, X. Wu, E. Fu, *Tetrahedron: Asymmetry* **2006**, *17*, 916–921.
[41] Č. Malavašič, J. Wagger, B. Stanovnik, J. Svete, *Tetrahedron: Asymmetry* **2008**, *19*, 1557–1567.
[42] J. M. Brunel, *Chem. Rev.* **2005**, *105*, 4233.
[43] G. Uccello-Barretta, F. Balzano, P. Salvadori, *Chirality* **2005**, *17*, S243–S248.
[44] C. Rosini, G. Uccello-Barretta, D. Pini, C. Abete, P. Salvadori, *J. Org. Chem.* **1988**, *53*, 4579–4581.
[45] A. K. Bandyopadhyaya, N. M. Sangeetha, U. Maitra, *J. Org. Chem.* **2000**, *65*, 8239–8244.
[46] M. S. Sundar, H. R. Talele, H. M. Mande, A. V Bedekar, R. C. Tovar, G. Muller, *Tetrahedron Lett.* **2014**, *55*, 1760–1764.
[47] D. Parmar, E. Sugiono, S. Raja, M. Rueping, *Chem. Rev.* **2014**, *114*, 9047–9153.
[48] M. Durmaz, M. Yilmaz, A. Sirit, *Org. Biomol. Chem.* **2011**, *9*, 571–580.
[49] S. P. Zingg, E. M. Arnett, A. T. McPhail, A. A. Bothner-By, W. R. Gilkerson, *J.*

Am. Chem. Soc. **1988**, *110*, 1565–1580.
[50] W. Wang, F. Ma, X. Shen, C. Zhang, *Tetrahedron: Asymmetry* **2007**, *18*, 832–837.
[51] A. R. Chaudhary, P. Yadav, A. V Bedekar, *Tetrahedron: Asymmetry* **2014**, *25*, 767–774.
[52] G. Li, J. Cao, W. Zong, X. Lei, R. Tan, *Org. Chem. Front.* **2016**, *3*, 96–102.
[53] N. Jain, M. B. Mandal, A. V Bedekar, *Tetrahedron* **2014**, *70*, 4343–4354.
[54] A. Port, A. Virgili, C. Jaime, *Tetrahedron: Asymmetry* **1996**, *7*, 1295–1302.
[55] G. Mignonac, *Comptes Rendus* **1921**, *172*, 223–225.
[56] V. A. Tarasevich, N. G. Kozlov, *Russ. Chem. Rev.* **1999**, *68*, 55–72.
[57] M. Kitamura, M. Tsukamoto, Y. Bessho, M. Yoshimura, U. Kobs, M. Widhalm, R. Noyori, *J. Am. Chem. Soc.* **2002**, *124*, 6649–6667.
[58] R. F. Borch, M. D. Bernstein, H. D. Durst, *J. Am. Chem. Soc.* **1971**, *93*, 2897–2904.
[59] R. F. Borch, H. D. Durst, *J. Am. Chem. Soc.* **1969**, *91*, 3996–3997.
[60] S. Kim, C. H. Oh, J. S. Ko, K. H. Ahn, Y. J. Kim, *J. Org. Chem.* **1985**, *50*, 1927–1932.
[61] M. Fondo, J. Corredoira-Vázquez, A. M. GarcíaDeibe, J. Sanmartín-Matalobos, *Proceedings* **2019**, *9*, DOI 10.3390/ecsoc-22-05697.
[62] D. Menche, J. Hassfeld, J. Li, G. Menche, A. Ritter, S. Rudolph, *Org. Lett.* **2006**, *8*, 741–744.
[63] E. I. Kim, S. Paliwal, C. S. Wilcox, *J. Am. Chem. Soc.* **1998**, *120*, 11192–11193.
[64] E. C. Lee, B. H. Hong, J. Y. Lee, J. C. Kim, D. Kim, Y. Kim, P. Tarakeshwar, K. S. Kim, *J. Am. Chem. Soc.* **2005**, *127*, 4530–4537.
[65] L. J. Riwar, N. Trapp, B. Kuhn, F. Diederich, *Angew. Chemie - Int. Ed.* **2017**, *56*, 11252–11257.
[66] A. N. Khanvilkar, A. V. Bedekar, *Chem. Commun.* **2018**, *54*, 11037–11040.
[67] Z. A. los Santos, S. MacAvaney, K. Russell, C. Wolf, *Angew. Chemie Int. Ed.* **n.d.**, doi: 10.1002/anie.201912904.
[68] Y. Kubo, S. Maeda, S. Tokita, M. Kubo, *Nature* **1996**, *382*, 522–524.
[69] W. C. Su, W. G. Zhang, S. Zhang, J. Fan, X. Yin, M. L. Luo, S. C. Ng, *Biosens. Bioelectron.* **2009**, *25*, 488–492.
[70] M. Durmaz, M. Yilmaz, A. Sirit, *Org. Biomol. Chem.* **2011**, *9*, 571–580.
[71] D. A. Spivak, J. Campbell, *Analyst* **2001**, *126*, 793–797.
[72] M. Lefoix, S. Routier, J. Me, U. Jacquemard, *Tetrahedron* **2004**, *60*, 10039–10047.
[73] N.- Labeling, J. D. Desousa, B. M. Novak, *ACS Macro Lett.* **2012**, *1*, 672–675.
[74] S. R. D. George, L. T. Scott, J. B. Harper, S. R. D. George, L. T. Scott, J. B. Harper, S. R. D. George, L. T. Scott, J. B. Harper, *Polycycl. Aromat. Compd.* **2016**, *36*, 697–715.
[75] A. A. Zagulyaeva, C. T. Banek, M. S. Yusubov, V. V Zhdankin, *Org. Lett.* **2010**, *12*, 4644–4647.
[76] X. Huang, J. W. Keillor, *Tetrahedron Lett.* **1997**, *38*, 313–316.